Kinematically consistent, elastic block model of the Eastern Mediterranean constrained by GPS measurements

by

Shawn A. Lawrence

B.A., Geophysics (1998)
University of California, Berkeley

Submitted to the Department of Earth, Atmospheric and Planetary Sciences
in partial fulfillment of the requirements for the degree of

Master of Science in Geophysics

at the

MASSACHUSETTS INSTITUTE OF TECHNOLOGY

September 2003

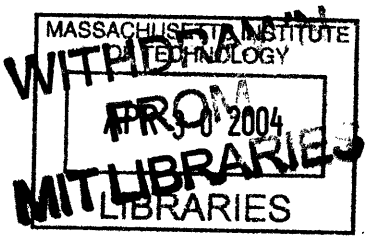

Signature of Author: _____
Department of Earth, Atmospheric and Planetary Sciences
August 8, 2003

Certified by: _____
Bradford H. Hager
Professor
Thesis Supervisor

Accepted by: _____
Maria T. Zuber
Head, Department of Earth, Atmospheric and Planetary Sciences

Kinematically consistent, elastic block model of the Eastern Mediterranean constrained by GPS measurements

by

Shawn A. Lawrence

Submitted to the Department of Earth, Atmospheric and Planetary Sciences
on August 8, 2003, in partial fulfillment of the requirements for the degree of
Master of Science in Geophysics

ABSTRACT

I use a Global Positioning System (GPS) velocity field to constrain block models of the eastern Mediterranean and surrounding regions that account for the angular velocities of constituent blocks and elastic strain accumulation on block-bounding faults in the interseismic period. Kinematically consistent fault slip rates and locking depths are estimated by this method.

Eleven blocks are considered, including the major plates, based largely on previous geodetic, seismic, and geologic studies: Eurasia (EU), Nubia (NU), Arabia (AR), Anatolia (AN), Caucasus (CA), South Aegea (AE), Central Greece (GR), North Aegea (NE), Southeast Aegea (SE), Macedonia (MA), and Adria (AD). Two models are presented, one in which the best-fitting locking depth for the entire region (~15 km) is used on all boundaries (Model A), and one in which shallower locking depths are used on the Marmara Fault, the Hellenic and Cyprus Arcs, and in the Greater Caucasus (Model B), based on a consideration of locally best-fitting locking depths. An additional block, Black Sea (BS), is postulated in a third model.

The models are in fair to good agreement with the results of previous studies of plate motion, fault slip rates, seismic moment rates and paleomagnetic rotations. Notably, some block pairs in the Aegean region have Euler poles on, or near to, their common boundaries, in qualitative agreement with so-called pinned block models, e.g., for the transfer of slip from the right-lateral North Anatolian Fault system to a set of left-lateral and normal faults in central and northern Greece (McKenzie and Jackson, 1983; Taymaz et al., 1991a; Goldsworthy et al., 2002). In addition, roughly three-quarters of the deformation in the Hellenic Arc and Greater Caucasus appears to be aseismic, in approximate agreement with previous studies (Jackson and McKenzie, 1988; Jackson, 1992). Increased data coverage will better constrain block motions, the locations of boundaries and the applicability of this method.

Thesis Supervisor: Bradford H. Hager
Title: Professor

Acknowledgments

I owe an enormous debt of gratitude to all of the people, friends, family, colleagues, and hapless bystanders, who were touched by the events leading to the completion of this thesis, only a few of whom I can mention here. This work would not have been possible without their concrete contributions, good advice, sense of humor and, especially, their patience. I, first of all, thank Brendan Meade for making available his block modeling software and cheerfully answering my many questions about its application. I thank Simon McClusky for sharing his scrupulously produced interseismic GPS velocity field, which is the basis for this study. I jointly thank my advisors Brad Hager and Rob Reilinger for their inspiring expeditionary spirit and for trying to help me to the most direct route to my goals, sometimes successfully. My work also benefited from discussions on sundry topics at sundry times with Kurt Feigl, Bob King, Clark Burchfiel, Kelin Whipple, Ming Fang, Roland Bürgmann, Eric Hetland and Monica Aponte. I am extremely grateful to my friends and family for their long unwavering support and especially to my father to whom I dedicate this work. I also wish to extend thanks to the large international cast of researchers who assisted in the collection of GPS data from Europe, Africa and the Middle East. I am solely responsible for any errors herein. Figures 1, 2, 3, 4, 5, 6, 8, 10, 11, 12, 13 and 14 were generated with Generic Mapping Tools (Wessel and Smith, 1995). My research was supported in part by a Grace B. Kerr Fellowship and NSF grant 6890454.

Table of Contents

Figures

1. Introduction and tectonic setting

Earthquakes on active faults in the eastern Mediterranean and Near East have played a signal role in the fate of the people of the region, from the earthquake which precipitated the Peloponnesian War (Sparta, 464 BCE) to the recent Turkish earthquakes which resulted in tragic loss of life (M_W 7.5, Izmit, 1999; M_W 7.2, Düzce, 1999) (Ambraseys and Jackson, 1998, 2000). In the modern theory of plate tectonics, most earthquakes are explained as the result of episodic slip on faults constituting the boundaries between large, slowly moving plates of the earth's surface (Isacks et al., 1968). Early in the history of the theory, the eastern Mediterranean region was identified to be within the zone of interaction of three major plates, underlying the continents of Eurasia, Africa and Arabia, respectively (e.g., McKenzie, 1970, 1972; Dewey et al., 1973).

Plate tectonics theory was largely developed from data of the ocean basins where the relative motions of the plates could be quantified and where the plate boundaries are usually well defined by the network of seismically active ridges, trenches and connecting faults (e.g., Morgan, 1968; Le Pichon, 1968). In continental regions, earthquakes are distributed over much broader areas (~100 km) than at most oceanic plate boundaries (~10 km), and data on crustal movements have been relatively tenuous until recently. Convergence of continental plates is also observed to be accommodated by crustal thickening and mountain building rather than subduction, which is attributed to the greater buoyancy and lower integrated strength of continental lithosphere compared to oceanic lithosphere. Thus the application of plate tectonics to continental regions is contentious, with some authors finding a micro-plate or block description useful (e.g., Avouac and Tapponnier, 1993) while others prefer a continuum description of continental tectonics (e.g., England and McKenzie, 1982; Houseman and England, 1993), depending on the features of the deformation to be explained and their spatial and temporal scale (e.g., Molnar, 1988; Thatcher, 1995).

In recent years, analysis of data from repeated surveys of points using the Global Positioning System (GPS) has made it possible to determine contemporary horizontal

surface velocities to ~2 mm/yr precision (e.g., Dixon, 1991; Hager et al., 1991). Relatively dense, GPS velocity fields are now available for vast areas of continental deformation in the period of steady motion between large earthquakes, i.e., the interseismic period (e.g., Bennett et al., 1999; McClusky et al., 2000; Wang et al., 2001), as well as for the transient motions during and subsequent to individual earthquakes (e.g., Reilinger et al., 2000; Agnew et al., 2002). These astounding data sets should help to resolve some of the long-standing debates in continental tectonics, or, perhaps as likely, engender new ones. The details of plate interaction in the eastern Mediterranean region are the subject of this thesis, as revealed by models based on newly available GPS measurements.

Reviews of the active tectonics of the eastern Mediterranean region include McKenzie (1972, 1978), Dewey and Sengör (1979), Jackson and McKenzie (1984, 1988), Jackson (1994), Westaway (1994), Barka and Reilinger (1997), and Ambraseys and Jackson (1998). The reader is urged to consult the references cited by these and other authors mentioned herein for a fuller account of the many studies which have contributed to our knowledge of this vast region. Figure 1 is a generalized tectonic map of the eastern Mediterranean and Near East (after McClusky et al., 2000).

Global plate motion models, based on analysis of sea-floor magnetic anomalies, fault orientations and earthquake slip vectors (e.g., NUVEL-1A: DeMets et al., 1990, 1994) or based on GPS data (e.g., Sella et al., 2002), show that Africa and Arabia move approximately north with respect to Eurasia. The African plate, including the eastern Mediterranean Sea basin, moves toward a subduction zone south of the Aegean Sea, while the Arabian plate moves away from a spreading ridge in the Red Sea toward a belt of seismically active, mountainous terrain in eastern Turkey and Iran. North of the Red Sea, the African-Arabian plate boundary is evidently the Dead Sea Fault (DSF) which lies inland of the Levantine coast. The plate motion model NUVEL-1A gives a velocity relative to Eurasia for the northern Arabian plate of 25 ± 1 mm/yr oriented N21° ± 7° W (at 37.25° N, 40.65° E), averaged over 3 Myr. GPS measurements at the same location give a lower velocity relative to Eurasia of 18 ± 2 mm/yr oriented N24° ± 5° W

(McClusky et al., 2000). Likewise, NUVEL-1A gives a velocity relative to Eurasia for northeastern Africa of 10 ± 1 mm/yr oriented N0° ± 4° (at 29.85° N, 31.35° E), averaged over 3 Myr. GPS measurements at the same location give a much lower velocity relative to Eurasia of 5 ± 2 mm/yr oriented N20° ± 5° W (McClusky et al., 2003). NUVEL-1A estimates of African motion may be significantly in error since it does not divide Africa into separate plates at the East African rift, i.e., Nubia and Somalia, a west and east African plate, respectively (Chu and Gordon, 1999). A detailed study of spreading rates in the Red Sea (Chu and Gordon, 1998) gives estimates of relative Arabia-Nubia motion which are in good agreement with GPS results (McClusky et al., 2003).

Seismic activity north of the African and Arabian plates is broadly distributed and complex (Figures 2 and 3). A remarkably robust picture for the tectonics of this domain was obtained more than three decades ago, with subsequent refinements, from seismological focal mechanisms and studies of surface faulting by McKenzie (1970, 1972, 1978) and Jackson and McKenzie (1984, 1988). They proposed that convergence between Arabia and Eurasia is accommodated in seismic belts surrounding the relatively aseismic regions of central Iran and central Turkey (i.e., Anatolia) which move laterally away from the apex of the collision in eastern Turkey and the Caucasus toward oceanic-type subduction zones. Motion across the northeastern boundary of the Arabian plate varies from shortening in the Zagros fold-and-thrust belt north of the Persian Gulf to right-lateral strike-slip faulting in northwestern Iran and eastern Turkey. Presumably, motion between the Arabian plate and central Turkey is primarily taken up by left-lateral strike-slip faulting on the East Anatolian Fault (EAF) which has shown little activity in the last century. The aseismic regions of central Iran and central Turkey have northern boundaries which respectively lie inland of the Caspian Sea and Black Sea basins, apparent remnants of oceanic crust caught up in the early stages of continental collision. The North Anatolian Fault (NAF), the latter boundary, was the source of many of the region's most destructive earthquakes in the last century (i.e., eleven events with $M_W \geq 6.8$ between 1939 and 1999, including the 1999 Izmit and Düzce events). The North Anatolian Fault extends from an intersection with the East Anatolian Fault in eastern Turkey near Karliova (at about 39° N, 41° E) to the Marmara Sea in western

Turkey where it evidently branches into a number of fault strands that cross the northern Aegean Sea. Surface faulting on the North Anatolian Fault consistently shows right-lateral offsets which led researchers to conclude early on that central Turkey is a plate that moves westward with respect to Eurasia (e.g., McKenzie, 1970, 1972). The Aegean Sea region is one of the most seismically active on the continents. Earthquake focal mechanisms and surface faulting in western Turkey and mainland Greece show mostly north-south directed normal faulting, while northeast-southwest directed low-angle thrust faulting predominate south of the Aegean Sea, i.e., south of Crete and southwest of the Peloponnesos. Intermediate depth earthquakes also define north-dipping Wadati-Benioff zones beneath the Aegean Sea and southern Turkey. In contrast, the crust of the southern central Aegean Sea is relatively aseismic. These observations led McKenzie (1970, 1972, 1978) to conclude that the southern Aegean is a separate plate which moves southwestward relative to Eurasia, resulting in extension around its northern boundary and subduction of the African plate beneath its southern boundary, i.e., the Hellenic Arc.

McKenzie and Jackson in the aforementioned references attempted to quantify the relative motion of central Iran, central Turkey and the southern Aegean with respect to the adjacent plates using simple velocity triangles, earthquake slip vectors and seismic moment rates. However, these estimates are necessarily very uncertain, e.g., 25-80 mm/yr slip rate on the North Anatolian Fault with a preferred rate of ~30 mm/yr and 30-110 mm/yr extension rate between the Aegean and Eurasia with a preferred rate of ~60 mm/yr (Jackson and McKenzie, 1984, 1988). Another early attempt to quantify the motion of the southern Aegean by Le Pichon and Angelier (1979) found a rate relative to Eurasia that varies from about 20 to 40 mm/yr across the Aegean, although this rate is based on a 13 Ma age of the subducting slab which is probably much underestimated (Wortel and Spakman, 2000). GPS measurements in central Turkey and the southern Aegean confirm that there is little internal deformation in these regions (<2 mm/yr) and constrain the relative plate motions precisely: 24 ± 1 mm/yr upper bound on the NAF slip rate and 30 ± 1 mm/yr oriented southwest motion of the southern Aegean relative to Eurasia (McClusky et al., 2000).

The present-day tectonics of the Mediterranean region are the latest phase in the overall process of plate convergence between Eurasia and Africa that has persisted for more than the last 65 Myr (e.g., Dercourt et al., 1986). This complex history includes subduction of oceanic crust, basin formation, accretion of crustal material, and continental collision. Continental collision between Eurasia and the Adriatic continental fragment was underway in the Alps by the late Cretaceous-early Eocene (~65 Ma) (e.g., Dercourt et al., 1986). Rifting of the Red Sea between Africa and Arabia began in the early Miocene (~35 Ma), and left-lateral movement on the Dead Sea Fault was underway by the middle Miocene (~15 Ma) (e.g., Dercourt et al., 1986; Westaway, 1994). Continental collision between Eurasia and Arabia began in the middle to late Miocene (~10 Ma) along the Bitlis-Zagros fold-and-thrust belt in eastern Turkey and Iran (e.g., Sengör et al., 1985). Shortening and crustal thickening proceeded north of the Bitlis suture, eventually closing a marginal sea basin between the Lesser and Greater Caucasus in the Pliocene (~5 Ma) (e.g., Philip et al., 1989). The latest tectonic phase probably began at about 5 Ma when the North and East Anatolian faults began to accommodate the westward movement of the Anatolian plate at something like the present rate (e.g., Westaway, 1994; Hubert-Ferrari et al., 2002). Extension in the Aegean may have also intensified at about 5 Ma, although extension throughout the Aegean, including the presently aseismic area, is thought to have begun in the Miocene (~15 Ma) (e.g., Mercier et al, 1989; Taymaz et al., 1991; Armijo et al., 1996).

In this thesis, I use a new GPS velocity field of the eastern Mediterranean and surrounding regions provided by S.C. McClusky (personal communication, 2003; Figures, 4, 5 and 6) to construct a plate (or block) model in which surface velocities are the result of the effectively rigid-body motion of plates over the long-term and elastic deformation caused by friction on plate boundaries in the interseismic period (e.g., Meade et al., 2002). (For the purposes of this work, the terms "plate" and "block" are synonymous.) The relative, rigid-body motion of two blocks constrained to move over the approximately spherical surface of the earth is described by an angular velocity vector, or equivalently an Euler vector, that is, a point on the surface of the earth about which the blocks rotate (i.e., an Euler pole) and a rotation rate (McKenzie and Parker,

1967). Model angular velocity vectors are estimated in a weighted least-squares inversion given the GPS velocity data and the block boundary geometry, specified *a priori*. A large number of block boundary geometries are tried to arrive at a preferred model. Fault slip rates and, to some extent, the depth to which faults are frictionally locked can be estimated by this method, both of which are important to considerations of seismic potential.

I find that a relatively small number of blocks (eleven), bounded by mostly recognized fault zones, explain the bulk of the GPS velocity data. The model is preliminary; fuller data sets, particularly near block boundaries, will permit improvements to the model and test early conclusions. I also find fair to good agreement with previous studies of plate motion, fault slip rates, seismic moment rates and paleomagnetic rotations. Notably, some block pairs in the Aegean region have Euler poles on, or near to, their common boundaries, in qualitative agreement with so-called pinned block models, e.g., for the transfer of slip from the right-lateral North Anatolian Fault system to a set of left-lateral and normal faults in central and northern Greece (McKenzie and Jackson, 1983; Taymaz et al., 1991; Goldsworthy et al., 2002). In addition, roughly three-quarters of the deformation in the Hellenic Arc and Greater Caucasus appears to be aseismic, in approximate agreement with previous studies (Jackson and McKenzie, 1988; Jackson, 1992). Thus the contemporary kinematics of the eastern Mediterranean is adequately explained essentially within a plate tectonic framework. However, contemporary kinematics merely provides a condition to be met for other models of the dynamics and long-term evolution of the region, which may in turn help to decide leading questions in continental tectonics.

2. Models

2.1. Block modeling method

The elastic block method of modeling interseismic surface motions has been employed in various forms by several authors, e.g., Matsu'ura et al., 1986; Bennett et al., 1996; Souter, 1998; McClusky et al., 2001; Murray and Segall, 2001; McCaffrey, 2002; Meade et al., 2002. The block modeling approach used here was developed by B.J. Souter and B.J. Meade of the Massachusetts Institute of Technology; for a fuller account of it, refer to the forth-coming Ph.D. thesis of B.J. Meade, MIT.

In the classic model of the earthquake cycle (Savage and Burford, 1973), the total surface displacement of a point near an active fault is the sum of its interseismic displacement and coseismic displacement. During the interseismic period, the shallow portion of the fault is frictionally locked to a certain depth, D, below which the blocks on either side of the fault slide past each other at a steady rate equal to the long-term (i.e., geologic) surface slip rate, s. The blocks strain elastically around the locked portion of the fault until that portion of the fault slips in an earthquake. The model assumes that coseismic displacement completely removes the interseismic elastic strain so that the total surface displacement averaged over the duration of the earthquake cycle equals the long-term slip rate. Thus, over the long-term, displacements are effectively those of rigid blocks. The slipping portion of a strike-slip fault can be represented by a vertical, infinitely extended dislocation in an elastic half-space, giving an interseismic surface velocity in the strike direction of $v = (s/\pi)\arctan(x/D)$ for a point a perpendicular distance x from the fault. The surface displacement fields that would result over an earthquake cycle for such a model are illustrated in Figure 7a. In continental crust, the locking depth of faults is thought to be about 15 km below which earthquake foci are rare and below which rock mechanics experiments suggest that brittle-elastic deformation in the upper crust gives way to ductile deformation (e.g., Chen and Molnar, 1983).

In the approach used here, the earth's surface is divided into blocks whose boundaries are a connected network of faults. The rigid-body motion of the blocks in some frame of reference is described by angular velocity vectors (i.e., equivalent to Euler vectors), $\boldsymbol{\omega}$. The long-term slip rate, $\mathbf{s}_f$, on each fault segment, f, is simply the relative rigid-body block velocity at the segment midpoint projected into the fault plane; there are two components of slip rate for each fault, strike-slip and dip-slip, or strike-slip and tensile slip for vertical faults. Interseismic surface velocities on a given block are modeled by subtracting from the rigid block motion the elastic deformation that would be caused by steady slip at the long-term rate on the locked portion of each fault. This is equivalent to subtracting coseismic displacements from total displacements (e.g., subtracting the middle panel from the final panel in Figure 7a) and averaging over the duration of the earthquake cycle. Slip below the locked portions of faults is not explicitly modeled. Thus the interseismic surface velocity of a point in geocentric coordinates, $\mathbf{r}$, can be written

$$\mathbf{v}(\mathbf{r}) = \boldsymbol{\omega}(\mathbf{r}) \times \mathbf{r} - \sum_{f=1}^{F} \mathbf{G} \cdot \mathbf{s}_f \qquad (1)$$

where $\mathbf{G}$ contains Okada's (1985) Green's functions for the deformation caused by an arbitrarily oriented rectangular dislocation in an elastic half-space and F is the total number of fault segments. Since the Green's functions only apply to a flat surface, they are calculated after transforming the point position and fault segment geometry to a flat surface using an oblique Mercator projection for each fault segment; in equation (1), these projection operations are implicit in $\mathbf{G}$.

Equation (1) can be written as the linear matrix equation $\mathbf{v} = \mathbf{J}\boldsymbol{\omega}$, since $\mathbf{s}_f$ is a linear function of $\boldsymbol{\omega}$, where $\mathbf{J}$ is the data kernel relating the model parameters, $\boldsymbol{\omega}$, to a set of model predictions, $\mathbf{v}$. To relate observed GPS velocities to block models, we treat $\mathbf{v}$ as the matrix of GPS velocity data and estimate the angular velocity vectors by a weighted least squares inversion

$$\boldsymbol{\omega}^{est} = \left[\mathbf{J}^T \mathbf{W} \mathbf{J}\right]^{-1} \mathbf{J}^T \mathbf{W} \mathbf{v} \qquad (2)$$

where the weighting matrix, $\mathbf{W}$, is the inverse of the data covariance matrix. *A priori* slip rates and angular velocity vectors can be incorporated in inversions by including them

among the data. Relative angular velocity vectors between blocks are derived from $\boldsymbol{\omega}^{est}$ by linear composition and transformed to the equivalent Euler vectors (i.e., Euler pole and rotation rate). Euler vector 1-σ uncertainties are estimated by Monte Carlo sampling, since the transformation from Cartesian coordinates to spherical coordinates is non-linear.

The disposition of residual (observed - model) velocities is used to evaluate the goodness of fit between the model and data. A good fit is indicated by randomly oriented residual velocities that lie within the 95% confidence regions of the observations, which typically have radii of ~2 mm/yr. A measure of model misfit is chi-square per degree of freedom,

$$\chi_n^2 = \frac{\sum_{i=1}^{N} (r_i / f\sigma_i)^2}{N - P} \tag{3}$$

where r_i is the residual, σ_i is the 1-σ data uncertainty, N is the number of observations, P is the number of free parameters in the inversion, and f is the data uncertainty scaling factor, assumed here to be 1. Since N is usually much larger than P, if the residuals are well matched with the data uncertainties, the expected value of χ_n^2 is ~1.

It is well known that geodetic observations sample complex time-dependent deformation, particularly after the perturbation of a large earthquake, which the classic model of the earthquake cycle does not explain. More sophisticated models include the effects of time-varying aseismic slip on faults and visco-elastic relaxation of the lower crust, although it is difficult to discriminate between these two mechanisms (e.g., Savage and Lisowski, 1998). For a model of an elastic layer over a visco-elastic half-space with characteristic relaxation time τ (i.e., the ratio of viscosity to shear modulus), surface velocities significantly depart from those of the classic model if the ratio of τ to the characteristic repeat time of earthquakes is less than 0.2 (Savage and Lisowski, 1998). A considerable effort has been made to exclude time-dependent surface deformation from the GPS velocity data; if it remains, the estimates of model parameters may be inaccurate. Similarly, although many small ($M_W < 6$) earthquakes occurred during the period

represented by the data, only large magnitude earthquakes are assumed to contribute significantly to seismic strain (e.g., Molnar, 1979).

The block modeling method outlined above implicitly enforces the path integral constraint that the relative velocity between points does not depend on the summation path between them (Figure 7b). Estimated slip-rates are thus internally consistent. Unlike other methods of modeling surface kinematics (e.g., Haines and Holt, 1993), this method seamlessly integrates small-scale and large-scale features of the deformation field (e.g., faults and plates). The block modeling method has the additional advantages that it is conceptually elegant and explanatory.

2.2. GPS velocity field

Several recent studies have presented and interpreted GPS velocity fields of interseismic deformation for parts of the eastern Mediterranean region, including Reilinger et al. (1997a), Straub et al. (1997), Clarke et al. (1998), Cocard et al. (1999), McClusky et al. (2000), Kahle et al. (2000), Briole et al. (2000), Ayhan et al. (2002), Meade et al. (2002), and McClusky et al. (2003). These studies are typically based on GPS data collected since the late 1980s. They are complemented by other space geodetic methods such as satellite laser ranging (SLR) and by terrestrial geodetic methods, including triangulation networks initiated as early as the 1890s in Greece (e.g., Le Pichon et al., 1995; Davies et al., 1997).

The GPS data set that forms the basis of this study is a global velocity field provided by S.C. McClusky (personal communication, 2003) which includes data spanning the years 1988 to 2002 from 185 stations. The global velocity field draws from previously presented survey mode GPS data in the eastern Mediterranean region (McClusky et al., 2000) and globally distributed, continuous GPS data acquired by the International GPS Service (IGS) (McClusky et al., 2000; McClusky et al., 2003). The global velocity field also includes new data for the Caucasus region and southwestern Turkey. The following synopsis of the data analysis is from McClusky et al. (2003). The data is analyzed with the GAMIT/GLOBK software (King and Bock, 1999; Herring, 1999) in a two-step approach (Dong et al., 1998). In the first step, GPS phase observations from each day are used to estimate station coordinates, zenith delay of the atmosphere at each station, and orbital and Earth orientation parameters (EOP). In the second step, loosely constrained estimates of station coordinates, orbits, and EOP and their covariances from each day are used as quasi-observations in a Kalman filter to estimate a consistent set of coordinates and velocities.

Additional GPS velocity fields presented by Clarke et al. (1998) and Meade et al. (2002) are incorporated in the data set to augment coverage in central Greece and the Marmara Sea region in northwestern Turkey, respectively. The velocity fields are transformed to

the same Eurasia-fixed reference frame using the VELROT 1.01 software (R.W. King, personal communication, 2002). A six-parameter transformation (six components of rate of change of translation and rotation) for each velocity field is estimated by minimizing the horizontal velocity residuals between co-located stations in the global velocity field provided by S.C. McClusky (personal communication, 2003). Table 1 reports the number of stations used to estimate the transformation parameters and the RMS fit between co-located stations.

I exclude stations with uncertainties greater than 3 mm/yr in either their north or east components; the mean 1-σ uncertainty per component of the final velocity field is 1.14 mm/yr. I also exclude obvious outliers and stations which are possibly affected by deformation related to the 1995 Egion earthquake in the western Gulf of Corinth (Clarke et al., 1998) and the 1991 Racha earthquake in the Caucasus (Reilinger et al., 1997b). A total of 288 stations remain in the final velocity field (Figures, 4, 5 and 6). Most stations are concentrated in the eastern Mediterranean region (i.e., 25-45° N, 20-50° E); outside of this region, only the stations used by McClusky et al. (2003) to estimate the relative motion of Nubia, Arabia and Eurasia are included. Table 2 lists the GPS velocities used in this study in a Eurasia-fixed reference frame, their sources and their block assignments.

2.3. Blocks and block boundaries

I choose blocks and block boundaries for the models on the basis of geodetic data available for this study and previous geodetic, seismic, and geologic studies. The density of GPS data is not sufficient to include every important complexity of the major fault zones. Even where well known, the surface expression of faults is discontinuous and without clear connections to other faults, especially between zones with different styles of faulting (e.g., Barka and Kadinsky-Cade, 1988). With a few exceptions such as the North Anatolian Fault, the positions of the most active faults in the eastern Mediterranean region are not precisely known, particularly submarine faults. Thus the block boundaries are necessarily schematic; the locations of the block boundaries that I have chosen may be misplaced by as much as 100 km. At some scale, all of the block boundaries probably represent multiple fault strands. Boundary slip rate estimates are thus an upper bound on the actual slip rate of any individual fault.

The preferred model geometry includes eleven blocks: Eurasia (EU), Nubia (NU), Arabia (AR), Anatolia (AN), Caucasus (CA), South Aegea (AE), Central Greece (GR), North Aegea (NE), Southeast Aegea (SE), Macedonia (MA), and Adria (AD) (Figure 8). All of the blocks have been previously recognized as domains of distinct motion on the basis of GPS data (e.g., McClusky et al., 2000; Kahle et al., 2000; Meade et al., 2002; Goldsworthy et al., 2002). The block boundaries are approximately co-located with recognized fault zones and the epicenters of moderate and large earthquakes (Figures 1, 2, and 3). Several authors have presented fault maps that were useful to this study, including McClusky et al. (2000), Sengör et al. (1985), Barka and Kadinsky-Cade (1988), Philip et al. (1989), Seber et al. (1997), Avanessian and Balassanian (1998), Kahle et al. (2000), Le Pichon et al. (2000), and Goldsworthy et al. (2002).

The boundary of the Anatolian block with Eurasia is the ~1000 km section of the North Anatolian Fault which lies between Karliova and the Mudurnu valley near the eastern end of the Marmara Sea. The North Anatolian Fault is perhaps the best-studied fault in the region (e.g., Ambraseys, 1970; Sengör, 1979; Jackson and McKenzie 1984, 1988;

Westaway 1994; Barka and Kadinsky-Cade, 1988; Hubert-Ferrari et al., 2002). A sequence of eleven events with $M_W \geq 6.8$ ruptured this section of the North Anatolian Fault between 1939 and 1999 (e.g., Stein et al., 1997); the fault has also experienced several large ($M_S \geq 7$) historical earthquakes including the very large 1668 M_S 7.9 Amasya event (Ambraseys and Jackson, 1998). The NAF primarily accommodates right-lateral slip, although the nearby 1968 M_W 6.8 Bartin thrust event on the southwest margin of the Black Sea indicates that a component of shortening is accommodated in this part of the Anatolia-Eurasia boundary. The most recent geological and geomorphological studies have constrained the age of the fault to be ~13 Ma in the east and ~5 Ma in the west with a total right-lateral offset of 80-100 km and find a Holocene slip rate of 18 ± 5 mm/yr (e.g., Hubert-Ferrari et al., 2002). Slip rate estimates from seismic moment rates are higher, ~30 mm/yr, perhaps due in part to the unusual number of large events in the last century (e.g., Jackson and McKenzie 1988). Both slip rate estimates are consistent with the 24 ± 1 mm/yr upper bound on the slip rate from GPS (McClusky et al., 2000) and with the slip rate estimate from interferometric synthetic aperture radar (INSAR), 17-32 mm/yr (Wright et al., 2001). The concave to the south trace of the fault and earthquake slip-vectors along it also strongly suggest that the Euler pole between Eurasia and the Anatolian block is located south of the fault along longitude ~33° E (Jackson and McKenzie 1984; Westaway 1994); the GPS derived Anatolia-Eurasia Euler pole (30.7° ± 0.8° N, 32.6° ± 0.4° E) confirms this suggestion (McClusky et al., 2000). The boundary I have chosen corresponds fairly well to the surface trace of the NAF except near the Niksar Basin step-over (at about 37° E) where it could be improved.

The boundary of the Anatolian block with Arabia is the northeast-southwest striking East Anatolian Fault, which lies between Karliova and an uncertain intersection with the Dead Sea Fault and the Cyprus Arc near the Gulf of Iskenderun. The East Anatolian Fault was a postulated left-lateral feature needed to accommodate the relative motion of Anatolia and Arabia (e.g., McKenzie, 1972). Field studies later confirmed the existence of a complex northeast-southwest striking fault zone with left-lateral displacements (e.g., Barka and Kadinsky-Cade, 1988; Westaway, 1994). Seismicity associated with the EAF

has been sparse over the last century; earthquakes typically have focal mechanisms with a northeast-southwest striking (063° ± 10°) nodal plane, but locally show strike-slip (1971 M_S 6.9 Bingöl), reverse slip (1975 M_S 6.7 Lice), and normal slip (1964 M_S 5.7 Malatya) (Taymaz et al., 1991b). Several large ($M_S \geq 7$) historical earthquakes can be attributed to the EAF as located in this study, including a very large ($M_S \geq 7.9$) earthquake in 1114, which implies that seismicity on the EAF in the last century is not representative of seismic activity on the fault (Ambraseys and Jackson, 1998). Geologic constraints on the total displacement and age of the EAF place them at ~25 km and ~5 Ma, respectively, (e.g., Westaway, 1994) giving a slip rate of ~5 mm/yr; a slip rate estimate from the historical seismic moment rate is 7 mm/yr with a range of 3-20 mm/yr (Taymaz et al., 1991b). These slip rate estimates are roughly consistent with the approximately 9 ± 1 mm/yr upper bound on the slip rate from GPS (McClusky et al., 2000). However, GPS derived Anatolia-Arabia Euler vectors (McClusky et al., 2000; McClusky et al., 2003) predict a component of extension on the EAF, increasing toward the northeast, which is contrary to the interpretation that this boundary zone has accommodated a component post-Miocene shortening up to the present (e.g., Lyberis et al., 1992). I have chosen the intersection of the EAF, DSF and the Cyprus Arc boundaries to be south of the Gulf of Iskenderun at the junction of the Karasu and Gharb fault zones (~36.6° N). This configuration is consistent with the notable velocity difference between adjacent GPS stations SENK (on NU) and ULUC (on AN), and it is consistent with a component of extension across the Karasu fault zone (between AN and AR) as indicated by focal mechanisms and geology (e.g., Jackson and McKenzie, 1984; Karig and Kozlu, 1990).

The boundary between Nubia and Arabia north of the Red Sea is the Dead Sea Fault, a north-south striking left-lateral fault with a prominent restraining bend in Lebanon. Like the East Anatolian Fault, seismicity on the DSF has been sparse over the last century, although several large ($M_S \geq 7$) historical earthquakes have occurred on the fault including a very large ($M_S \geq 7.9$) event in 1157 (Ambraseys and Jackson, 1998). Geologic constraints on the total displacement of the DSF since ~5 Ma place it at 30-40

km giving a slip rate of ~6-8 mm/yr since that time (e.g., Westaway, 1994); a slip rate from the historical seismic moment rate is ~5 mm/yr (Westaway, 1994). These slip rate estimates are consistent with the GPS derived Arabia-Nubia Euler vector which predicts that the total DSF slip rate increases from 5.6 ± 1 mm/yr in the south to 7.5 ± 1 mm/yr in the north where it is partitioned between 6 ± 1 mm/yr strike-slip and 4 ± 1 mm/yr fault-normal motion (McClusky et al., 2003).

West of the Mudurnu valley, the North Anatolian Fault branches into northern and southern strands that traverse the Marmara Sea region and enter the northern Aegean Sea (e.g., Barka and Kadinsky-Cade, 1988). The northern strand, which lies near major population centers such as Istanbul, evidently carries about as much slip as the NAF in the east and is referred to here with the same name (e.g., Straub et al., 1997). Following the 1999 M_W 7.5 Izmit earthquake, this region has been the subject of intensive study (e.g., Ambraseys and Jackson, 2000; Le Pichon et al., 2000; Hubert-Ferrari et al., 2000; Parsons et al., 2000; Meade et al., 2002). Like Meade et al. (2002), I assume that the northern and southern strands bound a block called here the North Aegean block (NE), and I adopt approximately the same boundary geometry they use. The NAF (i.e., the boundary between EU and NE) enters the Marmara Sea at the Gulf of Izmit and probably crosses the submarine basin along a single throughgoing fault (e.g., Le Pichon et al., 2000) before changing strike from east-west to southwest at the Ganos Dagh-Gelibolu Peninsula and entering the northern Aegean Sea at the Gulf of Saros. The NAF appears to step around the north side of the Çinarcik basin in the eastern Marmara Sea (Le Pichon et al., 2000); this relatively small-scale feature is not included in the boundary geometry since it does not much affect the model results, however, in a detailed study of seismic hazard, it should probably be included. The southern strand (i.e., the boundary between NE and AN) lies along the southern margin of the Marmara Sea, changing strike at ~28° E from east-west to southwest and entering the northern Aegean Sea at the Gulf of Edremit. Both strands produce large ($M_S \geq 7$) earthquakes, although the NAF does so much more frequently (Ambraseys and Jackson, 2000). Geologic reconstructions of the Marmara region find about 85 km displacement beginning at ~5 Ma on the northern strand as on other parts of the NAF and little resolvable slip on the southern strand

(Armijo et al., 1999). Slip rate estimates from instrumental and historical seismic moment data are ~24 mm/yr on the northern strand (Eyidoğan, 1988; Ambraseys and Jackson, 2000) and ~12 mm/yr oriented northeast-southwest on the southern strand (Eyidoğan, 1988). These rates are in good agreement with the GPS-derived block model of Meade et al. (2000) in which the northern strand carries ~24.5 ± 2 mm/yr right-lateral slip with a small amounts (1-5 mm/yr) of extension and contraction on the submarine and subaerial sections, respectively, and in which the total right-lateral transtensional motion on the southern strand varies from ~13 to ~7 ± 4 mm/yr between the Mudurnu valley and the Gulf of Edremit. In the northern Aegean Sea, strike-slip faulting corresponding to the North Anatolian Fault Zone (NAFZ) is indicated by focal mechanisms and bathymetric deeps such as the North Aegean Trough (e.g., Taymaz et al., 1991a) which terminate near the obliquely oriented coastline of central Greece.

Central Greece has an extensive record of instrumental and historical seismicity which indicates north-south directed normal faulting on east-west to west-northwest striking fault zones (e.g., Hatzfeld et al., 1999; Goldsworthy et al., 2002). In a recent study of seismicity and surface faulting, Goldsworthy et al. (2002) identify several narrow fault zones which they conclude bound relatively rigid blocks. The fault zones radiate away from the Ionian coast in the west to the Aegean coast in the east; from south to north, they are the Gulf of Corinth, the North Gulf of Evia (west of Evia), and the Volos region in Thessaly. Seismicity and faulting in the Gulf of Corinth, the most active zone in Greece, changes from distinct to diffuse from west to east, while the other fault zones show the opposite pattern. Throughout mainland Greece, paleomagnetism of rocks since ~5 Ma shows large clockwise rotations relative to Eurasia (25° to 50°) (e.g., Kissel and Laj, 1988). Such observations led some authors to conclude that mainland Greece consists of a set of clockwise rotating blocks which both accommodate oblique right-lateral shear between the Aegean block and Eurasia and accommodate east-west shortening between western Turkey and the convergent boundary along the Ionian coast (McKenzie and Jackson, 1983; Taymaz et al., 1991a). The same authors explain the observations with simple kinematic models, so-called pinned block models, in which blocks in Greece are pinned (or hinged) to Eurasia near the Ionian coast, pinned to blocks

in the North Anatolian Fault Zone near the Aegean coast, and in which the southernmost block in central Greece is pinned to the Aegean block near the eastern Gulf of Corinth. The pins (or hinges) represent Euler poles between adjacent blocks so that, near the poles, rates of relative motion are small and faulting is diffuse. Geodetic observations (triangulation and GPS) confirm some aspects of these models (e.g., Le Pichon et al., 1995; Clarke et al., 1997), including the clockwise rotation of central Greece with respect to Eurasia about a pole near the Ionian coast and high slip rates on the Gulf of Corinth, increasing from east to west, i.e., ~15 mm/yr from GPS in the central gulf (e.g., Clarke et al., 1997) in good agreement with the geologic estimate 11 ± 3 mm/yr (Armijo et al., 1996). I locate the northern and southern boundaries of the Central Greece block (GR) respectively along the Volos and Gulf of Corinth fault zones of Goldsworthy et al. (2002), connecting them directly to the western ends of the northern and southern strands of the NAFZ in the northern Aegean Sea. I locate the GR-NE boundary along the east coast of Evia, which, although relatively quiescent seismically, recently experienced a moderate left-lateral strike-slip earthquake on a northwest-southeast striking fault, the 2001 M_W 6.4 Skyros event (e.g., Kiratzi, 2002).

North of the central Greece block (GR), I define a Macedonian block (MA) on the basis of three available GPS stations (KRNA, SOXO, STHN) that show significant velocities with respect to Eurasia (~5-10 mm/yr oriented to the south) compared to velocities to the north which are smaller (e.g., Kotzev et al., 2001). The northeastern boundary of the Macedonian block lies along the east coast of the Chalkidiki Peninsula where seismicity and surface faulting suggest a northwest-southeast striking zone of left-lateral transtensional deformation (e.g., Voidomatis et al., 1990; Goldsworthy et al., 2002). The northwestern boundary of the Macedonian block lies along the Konitsa-Aridea fault zone, a northeast-southwest trending zone of normal faulting near the Greek-Albanian border (e.g., Burchfiel et al., 2000; Goldsworthy et al., 2002). One other GPS station is located on the Macedonian block, KRTS, the only station available for this study near the Ionian coast. The velocity of KRTS is small (~2 mm/yr) which is consistent with the rotation of blocks in mainland Greece around Euler poles near the Ionian coast. Other more dense GPS velocity fields for western Greece confirm that velocities near the Ionian coast are

small (Cocard et al., 1999). However, since for this study only four relatively small velocities are located on the Macedonia block, estimates of the block's motion will be very uncertain.

West of GR and MA lies the Adriatic block (AD), a continental fragment underlying the Adriatic Sea which collided with Eurasia in the Cretaceous (e.g., Dercourt et al., 1986). Moderate seismicity around the Adriatic Sea indicates primarily shortening along the coast of the Balkans and extension along the Apennines in Italy (e.g., Anderson and Jackson, 1987). GPS velocities relative to Eurasia on the Adriatic block available for this study are approximately oriented to the northeast and decrease from about ~10 mm/yr on the heel of Italy to ~2 mm/yr in the Po plain. This is consistent with the counter-clockwise rotation of the Adria block with respect to Eurasia about an Euler pole northwest of the block as suggested by the slip-vectors of earthquakes (Anderson and Jackson, 1987). However, more complex models have been suggested (e.g., Oldow et al., 2002). Similarly to the Macedonian block, only five relatively small velocities are located on the Adriatic block, thus estimates of the block's motion will be very uncertain. I choose the AD-NU boundary in the Ionian Sea to be simply the along-strike continuation of the boundary in the Apennines to the western end of the Hellenic Arc; there is little indication of tectonic activity at this location, however, it does correspond to a bathymetric escarpment. I locate the AD-AE boundary along the Kephalonia Fault Zone, a seismically active northeast trending right-lateral fault zone in the Ionian islands (e.g., Baker et al., 1997) across which GPS measurements indicate a slip rate ~40 mm/yr (Cocard et al., 1999).

South of the North Anatolian Fault Zone in western Turkey, seismicity and surface faulting indicate that the boundary between the Anatolian and Aegean blocks is characterized by north-south directed extension on east-west and west-northwest striking faults (e.g., McKenzie, 1978; Sengör et al., 1985; Eyidoğan, 1988). Extension in western Turkey is thought to have begun in the Miocene (~15 Ma), although it may have intensified throughout the Aegean at about 5 Ma (e.g., Mercier et al, 1989; Armijo et al., 1996). By summing seismic moment tensors, Eyidoğan (1988) estimated a 13.5 mm/yr

rate of extension in southwest Turkey oriented north-south. This estimate agrees well with the total relative motion between Anatolia and the Aegean based on the GPS-derived Euler vector for those blocks: 10-15 mm/yr oriented north-south (McClusky et al., 2000). Normal focal mechanisms and surface faulting in western Turkey appear to cover a large area west of ~31° E, including from north to south the Eskişehir, Simav, Gediz, Buyuk Menderes, and Gokova faults. However, north of a west-northwest oriented line between the island of Lesvos (~ 39° N, 26° E) and the northeastern end of the Fethye-Burdur fault zone (~ 37° N, 30° E), the available GPS velocities show little difference with the GPS-derived estimate of Anatolian block motion (McClusky et al., 2000). Thus I choose this approximate line as the western boundary of the Anatolian block, running it through the prominent Buyuk Menderes graben, into the Aegean Sea at Izmir and along the southern coast of Lesvos to an intersection with the southern strand of the North Anatolian Fault Zone. South of the Buyuk Menderes graben, this boundary separates the Anatolian block from the Southeast Aegean block (SE), a block with more southerly oriented GPS velocities relative to Eurasia than the main Aegean block (AE) (McClusky et al., 2000). The western boundary of the Southeast Aegean block with AE is the east-northeast trending Gokova graben and a north-south trending bathymetric trough between Rhodes and Crete that is associated with east-west directed normal focal mechanisms. North of the Gokova graben, the SE-AE boundary is less clear, apparently since the relative motion of the two blocks is small in this area; I chose a boundary approximating a coastal northeast oriented fault that intersects the western end of the Buyuk Menderes graben, however I now think the northwest or northeast oriented faults emanating from the eastern Gulf of Gokova (probably the latter) would be preferable boundaries (e.g., Sengör et al., 1985).

The southern boundary of the Aegean block and Southeast Aegean block with NU is the Hellenic Arc, a north-dipping subduction zone indicated by intermediate depth seismicity and a high seismic velocity slab imaged to at least 600 km depth, implying continuous subduction since at least the middle Miocene (e.g., Mueller and Kahle, 1993; Wortel and Spakman, 2000). I locate the Hellenic Arc boundary along the Hellenic Trench, a series of northwest trending bathymetric troughs south of the Ionian islands, the Peloponnesos,

and Crete. East of Crete, I locate the Hellenic Arc boundary along the northeast trending Pliny-Strabo Trench which has an uncertain intersection with the Fethye-Burdur fault zone and the Cyprus Arc between Rhodes and the southwest coast of Turkey. I give the Hellenic Trench section a dip to the north of 30° and the Pliny-Strabo Trench section a dip to the north of 45° consistent with the geometry of the Wadati-Benioff zones (e.g., Hatzfeld et al., 1993; Papazachos et al., 2000). The epicenters of most shallow earthquakes south of the Aegean Sea lie along the Hellenic Trench, however, some authors claim that slip in the Hellenic Arc is partitioned into arc-normal shortening along the Mediterranean Ridge accretionary complex, right-lateral strike-slip faulting parallel to the Hellenic Trench and left-lateral strike-slip faulting parallel to the Pliny-Strabo Trench (e.g., Le Pichon et al., 1995); the motion of the fore-arc sliver proposed by the latter authors cannot be constrained with GPS measurements since it is completely submarine. Thus the configuration of the Hellenic Arc boundary is doubtful.

The southern boundary of the Anatolia block with NU is the Cyprus Arc, a north dipping subduction zone indicated by intermediate seismicity northwest of Cyprus (e.g., Jackson and McKenzie, 1984). The surface trace of the boundary between the Hellenic Arc and Cyprus is uncertain; I locate this section of the boundary approximately on the Florence Rise and shallow epicenters, and I give a it a dip to the north of 30°. East of Cyprus, the boundary evidently lies along northeast trending submarine lineaments, connecting to the East Anatolian Fault and Dead Sea Fault near the Gulf of Iskenderun where normal-slip focal mechanisms prevail. There has been relatively little seismicity the Cyprus Arc in the last century, and $M_S > 7.3$ historical events on it are not known (e.g., McKenzie and Jackson, 1988).

East of the Anatolian block, convergence between Arabia and Eurasia is accommodated in the Caucasus region and Iran. Since GPS data in Iran is not available for this study, only the Caucasus region is formally included in the block model. Continental collision in eastern Turkey began along the Bitlis suture in the middle to late Miocene (~10 Ma) (e.g., Sengör et al., 1985), eventually resulting in the consumption of a marginal sea basin between the Lesser and Greater Caucasus in the Pliocene (~5 Ma) (e.g., Philip et al.,

1989). Three wide fault zones are indicated by contemporary seismicity and surface faulting in eastern Turkey and the Caucasus region: a west-northwest trending zone of right-lateral transpressional faulting north of Lake Van in eastern Turkey ("Lake Van Fault Zone"), a northeast trending zone of left-lateral transpressional faulting between the NAF/EAF junction near Karliova and the Greater Caucasus ("Northeast Anatolian Fault Zone"), and a west-northwest trending zone of shortening in the eastern Greater Caucasus (e.g., Barka and Kadinsky-Cade, 1988; Philip et al., 1989; Westaway, 1990a; Jackson, 1992). Several moderate ($6 \leq M_S \leq 7$) earthquakes have occurred in the Greater Caucasus and the Northeast Anatolian Fault Zone (e.g., the 1991 M_S 7 Racha earthquake and the 1983 M_S 6.9 Horasan-Narman earthquake, respectively), but larger earthquakes are only known in the Lake Van Fault Zone (e.g., the 1976 M_S 7.4 Çaldiran earthquake); the historical record also reflects this pattern (Jackson, 1992; Jackson and Ambraseys, 1997). Jackson (1992) proposed that the northwest oriented motion of northern Arabia relative to Eurasia is partitioned into a component of right-lateral strike-slip motion on the Lake Van Fault Zone in eastern Turkey and a component of convergence normal to the eastern Greater Caucasus. GPS measurements generally confirm this proposal (Reilinger et al., 1997b; McClusky et al., 2000), indicating about 16 ± 1 mm/yr right-lateral strike slip across the Lake Van Fault Zone and 10 ± 2 mm/yr convergence across the Lesser and eastern Greater Caucasus. I treat the Lake Van, Northeast Anatolian and eastern Greater Caucasus fault zones as the respectively southern, western and northern boundaries of the Caucasus block (CA), where the Lake Van Fault Zone bounds Arabia and the other boundaries are with Eurasia. The CA-AR boundary is fairly well defined by the Çaldiran Fault and GPS velocities. Although seismicity is broadly distributed, a boundary located on the main Caucasus thrust with a dip to the north of 30° (e.g., Triep et al., 1995) is sufficient to account for the available GPS velocities in the eastern Greater Caucasus. The location of the western boundary of the Caucasus block (i.e., the Northeast Anatolian Fault Zone) is much more difficult to define. Seismicity and surface faulting in this area are diffuse and complex, locally showing strike-slip, thrust faulting and volcanism apparently associated with extensional faulting (e.g., Rebai et al., 1993); the main throughgoing left-lateral fault, the so-called Northeast Anatolian/Borjomi-Kazbeg

Fault (e.g., Barka and Kadinsky-Cade, 1988; Philip et al., 1989) appears to lie somewhat west of the seismic zone. GPS velocities on either side of the zone are small (~5 mm/yr oriented north-northeast) and not appreciably different. The preceding observations and occasional thrust earthquakes in the western Greater Caucasus (including perhaps the 1991 Racha event) may imply that the Black Sea basin is a separate block with a small component of northward motion relative to Eurasia on it's eastern edge. Setting aside the latter suggestion, I locate the western boundary of the Caucasus block as near as possible to the northeast trending seismic zone between the NAF/EAF junction near Karliova and the Greater Caucasus, from south to north approximately on the Horasan-Narman and Borjomi-Kazbeg faults.

The southeastern end of the CA-AR boundary is its intersection with the northwest striking Main Recent Fault near the Turkish-Iranian border northwest of Lake Rezaiyeh (e.g., Jackson and McKenzie, 1984). I continue the southern boundary of the Caucasus block along strike to the Alborz mountains south of the Caspian Sea. Estimates of relative motion on the latter boundary are not realistic since no account is made of the motion of central Iran, however, although it is recently seismically quiescent, two M_S 7.7 earthquakes near Tabriz in 1721 and 1780 are documented on this boundary (Ambraseys and Jackson, 1998). I close the Caucasus block with a north-northwest striking boundary along the seismically active Talesh mountains west of the south Caspian Sea (e.g., Philip et al., 1989; Jackson et al., 2002). No account is made of the motion of the south Caspian Sea basin, thus estimates of relative motion on the latter boundary are also not realistic.

As mentioned previously, the density of GPS data is not sufficient to include every important tectonic complexity. Given sufficient data, every block in the model could probably be divided into smaller blocks. Just a few of the unmodeled complexities include the normal faulting in the North Gulf of Evia, normal faults in the southern Peloponnesos, normal faults in western Turkey between the NAF Zone and the Buyuk Menderes graben, faulting in the Isparta Angle of southern Turkey, and complex deformation in the Greater and Lesser Caucasus. However, these complexities are probably less important to the regional kinematics than the features which are included.

2.4. Block models

The GPS velocity data are inverted with equation (2) to estimate the motion (i.e., angular velocity vectors) of the eleven blocks described above. So that it will not be affected by residual velocities near boundaries, the motion of the Eurasian block is also constrained to match an *a priori* angular velocity vector derived from 23 minimized velocities on the stable interior of the block (i.e., the 23 Eurasian stations used by McClusky et al., 2003).

To estimate the best-fitting locking depth for the entire region, all locking depths in the eastern Mediterranean region are varied to find the locking depth that minimizes model misfit (Figure 9): ~15 km, in agreement with conventional notions of crustal rheology. The model with the (best-fitting) regional locking depth, 15 km, is Model A. To obtain a second, preferred model (Model B), the best-fitting locking depths of three selected boundaries are estimated in the same manner while holding all other locking depths at 15 km (Figure 9). The three boundaries in question are the Marmara Fault (i.e., the submarine section of the NAF in the Marmara Sea), the Hellenic Arc, and the eastern Greater Caucasus Thrust, which were previously identified to have lower seismic potential than would be expected if the local locking depth was 15 km (Meade et al., 2002; Jackson and McKenzie et al., 1988; Jackson, 1992). I find a best-fitting locking depth of ~5 ± 2 km for the Marmara Fault, ~4 ± 2 km for the Hellenic Arc and ~4 ± 2 km for the eastern Greater Caucasus Thrust, although, given the uncertainties in geometry and the sparsity of stations near the latter two boundaries especially, these estimates are preliminary. In Model B these three boundaries are assigned their best-fitting locking depths, the locking depth on the relatively aseismic Cyprus Arc is also set to 4 km, and all other locking depths are set to 15 km. Also of interest, but not investigated here, is whether locking depths throughout the Aegean region are less than 15 km as suggested by focal depths and elevated heat flow (Jackson and McKenzie, 1988).

Model A and Model B fit the GPS velocity data fairly well considering the simplicity of the models (Figures 10 and 11). For both models the mean residual magnitude per station

is ~2 mm/yr. About 54% of residual component magnitudes are less than the 1-σ component uncertainties of the data. The mean residual magnitude per component is ~1.3 mm/yr, compared to the mean 1-σ component uncertainty of the data 1.17 mm/yr. The misfit, χ_n^2, of Model A and Model B is 2.63 and 2.38, respectively. By selectively excluding about 100 stations with the most anomalous residuals, it is possible to obtain, without *a priori* constraints, approximately the same model parameters within uncertainties as Model B with $\chi_n^2 \sim 1$, mean residual magnitude per station 1.3 mm/yr, and 73% of residual component magnitudes less than the 1-σ component uncertainties of the data. Thus inverting the full velocity field with the preferred model geometry is justified notwithstanding that the match between residuals and uncertainties is only fair.

Apparently coherent patterns of residuals likely indicate inadequacies of the model, e.g., mislocated boundaries, too few blocks, inaccurate locking geometry, nonsecular deformation. Coherent patterns of residuals for Model B (Figures 10 and 11) include, among others, northeast oriented residuals between the southeastern coast of the Black Sea and the western CA-EU boundary, southeast oriented residuals on the Teke Peninsula of southern Turkey, respectively west and east oriented residuals on the western and eastern Anatolian block, northwest oriented residuals south of the AN-AE boundary, and northwest oriented residuals along the AN-NE boundary. Most of the latter instances suggest the need for additional blocks.

3. Discussion

3.1. Comparison with previous geodetic, geologic and seismicity studies

The preferred model (Model B) is relatively simple, yet it has considerable explanatory value. The model is in fair to good agreement with the results of previous studies of plate motion, fault slip rates, and paleomagnetic rotations. The model also makes new predictions or suggests them. Table 3 lists the Euler vectors and their 1-σ uncertainties for Model A, Model B, and other recent studies. Figures 12, 13 and 14 show the Euler poles and their error ellipses. Euler vectors for all block pairs with Eurasia and for selected blocks with a common boundary are shown. The predicted slip rates on block boundaries are shown in Figures 15, 16, 17, and 18; slip rate formal uncertainties underestimate realistic values by perhaps a factor of 2 or more.

The relative Euler vectors of the major plates and blocks (e.g., NU-EU, AR-EU, AN-EU, AE-EU, AR-NU, AN-AR, AN-AE) agree well with Euler vectors estimated from sparser GPS velocity fields that exclude stations affected by elastic strain accumulation (e.g., McClusky et al., 2000; Reilinger and McClusky, 2001; Sella et al., 2002; McClusky et al., 2003). The CA-EU Euler vector (42.06° ± 2.53° N, 37.3° ± 2.93° E, 0.795° ± 0.035° /Myr) located in the eastern Black Sea fairly matches the north-northeast motion, increasing to the east, of the Caucasus region. Notably, several Euler poles in the Aegean region are located on, or near to, the common boundaries of their respective blocks, in qualitative agreement with so-called pinned block models (McKenzie and Jackson, 1983; Taymaz et al., 1991a; Goldsworthy et al., 2002). For instance, GR-EU (39.25° ± 2.04° N, 21.01° ± 2.03° E, -6.688° ± 0.261° /Myr) is a clockwise Euler vector located on the GR boundary near the Ionian coast where velocities relative to nearby EU are small (Cocard et al., 1999); AE-GR (38.03° ± 2.02° N, 23.8° ± 2.07° E, 6.813° ± 0.259° /Myr) is a counter-clockwise Euler vector located near the AE-GR boundary east of the Gulf of Corinth; and NE-GR (38.42° ± 1.53° N, 23.29° ± 1.52° E, 9.528° ± 0.257° /Myr) is a counter-clockwise Euler vector located in eastern Central Greece, relatively near to the albeit uncertain NE-GR boundary. NE-EU (36.29° ± 1.45° N, 28.42° ± 1.45° E, 2.854° ±

0.076° /Myr) is a counter-clockwise Euler vector located off the southwest coast of Turkey, a small-circle about which approximately follows the NAF in northwest Turkey and the northern Aegean Sea. As in the pinned block models, NE-GR motion accommodates east-west convergence across the northern Aegean Sea, while GR-EU/AE-GR motion accommodates oblique right-lateral motion between AE and EU and opens the Gulf of Corinth. In another instance, SE-AE (36.9° ± 1.65° N, 28.23° ± 1.81° E, 4.362° ± 0.136° /Myr) is a counter-clockwise Euler vector located near the eastern Gulf of Gokova. The SE-AE boundary can be run approximately through the latter Euler pole without significantly affecting the model parameters; thus SE-AE motion appears to open the Gulf of Gokova similarly to the Gulf of Corinth. The MA-EU and AD-EU Euler vectors may be further instances of poles located on the common boundary of adjacent blocks, however, these poles are very uncertain as expected.

The sense and magnitude of model slip rates displayed in Figures 15 to 18 matches the contemporary tectonic pattern based on geodesy, seismology and geology quite well as described in the foregoing discussion of block boundaries. Only a few exceptions are discussed here. Questionable slip rates occur locally on the idealized boundaries. Relative motion on the westernmost AE-GR boundary (~29 ± 2 mm/yr opening) appears too high, as it does on the southernmost SE-AE boundary (~18.5 ± 1 mm/yr opening). The uncertain relative motion of MA with respect to adjacent blocks GR and NE probably results in too much apparent shortening (too little opening) on the westernmost MA-GR boundary and on the NAF in the North Aegean Trough (MA-NE boundary); note that other authors usually locate the latter boundary along the southern margin of the North Aegean Trough to the Sporades islands (e.g., Taymaz et al., 1991a; Goldsworthy et al., 2002), rather than along the northern margin as I do.

The block model is roughly consistent with paleomagnetic evidence for, relative to Eurasia, clockwise rotations in central Greece (26° to 48° since ~5 Ma: Kissel and Laj, 1988), counter-clockwise rotations in the southeastern Aegean (18 ± 12° since ~1.8 Ma: Duermeijer et al., 2000), and negligible rotations in the southern Aegean and western Turkey since ~5 Ma (Kissel and Laj, 1988). Large counter-clockwise rotations in western

Turkey would be expected to produce right-lateral slip on east-west striking faults as on the Buyuk Menderes graben in the model (~10 ± 1 mm/yr). However, there is little or no clear geologic evidence for either such rotations or right-lateral slip (e.g., Kissel and Laj, 1988; Westaway, 1990b). Strike-slip motion on the Buyuk Menderes is negligible if the SE-AE and AN-AE boundaries are connected east of the graben as I suggest above.

One remarkable outcome of the model simply confirms earlier GPS results (McClusky et al., 2000; McClusky et al., 2003) implying that AN-AR motion along the EAF has a component of extension increasing to the northeast towards the NAF/EAF junction near Karliova (from about 3 to 10 ± 1 mm/yr). Seismicity and surface faulting do not clearly indicate the sense of fault normal motion on the EAF (e.g., Westaway, 1994); some authors conclude that the AN-AR boundary has been an oblique collisional zone since the initiation of continental collision along the nearby Bitlis suture in the middle to late Miocene (e.g., Lyberis et al., 1992). However, assuming that the easternmost AN-AR boundary is not located well to the south, the GPS results require that as much as 10 mm/yr extension must be accommodated between Anatolia and Arabia on apparently unrecognized features. Total displacements on the easternmost EAF appear to be distributed between its present-day trace and (unmodeled) faults to the northwest as far as the subparallel Ovacik Fault (~200 km to the northwest); furthermore, total displacements on the easternmost NAF appear to be less than west of its intersection with the Ovacik Fault (Westaway, 1994). The single GPS station that lies between the EAF and the Ovacik Fault, MLTY (at 38.4° N, 38.2° E), has a relatively large residual velocity of 5 mm/yr oriented due east, that is, opposite to the predicted westward slip-vector on the nearby AN-AR boundary. Thus it is possible that a number of small unmodeled blocks presently distribute Anatolia-Arabia relative motion, including a component of extension.

As mentioned above, the western Caucasus block boundary (CA-EU) is difficult to locate and a coherent pattern of north-northeast oriented residuals lie between the boundary and the southeastern coast of the Black Sea. These observations and occasional thrust earthquakes in the western Greater Caucasus may imply that the Black Sea basin is a separate block with a small component of northward motion relative to Eurasia on it's

eastern edge. In trial models, I use 16 velocities around the eastern Black Sea to estimate the motion of a Black Sea block (BS). The resulting counter-clockwise BS-EU Euler vector is located on the northern margin of the Black Sea basin, although the position of the pole is rather uncertain, while the counter-clockwise CA-BS Euler vector is located on the southeastern margin of the Black Sea basin. Slip rates on the western Caucasus block boundary are reduced from ~6.5 to 3 ± 0.5 mm/yr, and ~3.5 ± 0.5 mm/yr of convergence is predicted on the western Greater Caucasus. The estimated motion of the Black Sea basin, a counter-clockwise rotation about a pole on the northern basin margin, is also consistent with small amounts of approximately north-south extension in Bulgaria (e.g., Burchfiel et al., 2000), although the western limit of the Black Sea basin block is speculative. The Euler vectors for Model A are BS-EU (45.01° ± 7.62° N, 32.30° ± 8.17° E, 0.198° ± 0.025° /Myr) and CA-BS (41.01° ± 4.08° N, 39.15° ± 4.50° E, 0.624° ± 0.043° /Myr); the Euler vectors for Model B are BS-EU (44.61° ± 7.12° N, 32.60° ± 7.47° E, 0.215° ± 0.027° /Myr) and CA-BS (40.93° ± 4.01° N, 39.93° ± 4.10° E, 0.660° ± 0.044° /Myr); slip rates predicted by the latter Euler vectors are shown in parentheses in Figures 15 and 16.

One can speculate about the motion of Iran and the South Caspian Sea basin. The motion of northeast Iran and northwest Arabia with respect to Eurasia may be approximately parallel as it appears in a strain model based on earthquake moment tensors and kinematic constraints (Jackson et al., 1995). Supposing that the motion of northeast Iran is like that of Arabia but reduced in magnitude, I can compare AR-EU relative motion on the Main Recent Fault (~18 mm/yr right-lateral) with geologic constraints on the actual slip rate (10-17 mm/yr right-lateral: Talebian and Jackson, 2002) to estimate a reduction in magnitude of ~½ to none. Thus the Caucasus-Iran relative motion near their possible boundary at Tabriz may range from ~7 to 14 mm/yr right-lateral parallel to the AR-CA boundary. Jackson et al. (2002) use seismicity and surface faulting to estimate the motion of the South Caspian Sea Basin: ~13-17 mm/yr to the southwest relative to Iran and ~8-10 mm/yr to the northwest or north-northwest relative to Eurasia. I assume a Caucasus-South Caspian Euler vector (41° N, 49° E, 1.75° /Myr), supposing that the Caucasus-South Caspian Euler pole is located near their common boundary at the easternmost

Greater Caucasus and that their relative motion is ~10 mm/yr oriented east-west in the Talesh mountains as the northerly fall-off in thrust focal mechanisms suggests. By adding the assumed Caucasus-South Caspian Euler vector with the model CA-EU Euler vector, I obtain a South Caspian-Eurasia Euler vector (39.5° N, 57.4° E, –1° /Myr), located near the eastern South Caspian-Eurasia boundary in the Kopeh Dag, which predicts roughly the same motion found by Jackson et al. (2002).

3.2. Preliminary comparison with observed seismic moment rates

To compare the record of recent and historical seismicity with the models, I calculate observed seismic moment rates and model moment rates using the various models presented above. I calculate the scalar model moment rate for F fault segments in a given sub-region using

$$\dot{M}_0 = \mu \sum_{f=1}^{F} H_f L_f s_f \; ; \; H_f = D_f / \sin \delta_f \tag{4}$$

where $\dot{M}_0$ is moment rate, μ (3×10^{10} N m^{-2}) is shear modulus, H_f is fault width, L_f is fault length, s_f is the total slip-rate magnitude, D_f is locking depth, and δ_f is dip (e.g., Brune, 1968; Jackson and McKenzie, 1988). Model moment rates on vertical boundaries with components of shortening or extension will presumably be underestimated, since they do not account for the dips of the actual faults accommodating this motion (e.g., Anderson, 1979). For instance, model moment rates may be underestimated in the Aegean region where vertical boundaries represent rapidly slipping normal faults (e.g., in the Gulf of Corinth); on the other hand, the locking depth in the Aegean (excluding the Hellenic Arc) is assumed to be 15 km which may overestimate model moment rates if the actual locking depth is closer to 10 km (e.g., Jackson and McKenzie, 1988).

To calculate seismic moment rates, I compile published values of surface-wave magnitudes (M_S) of recent and historical earthquakes by sub-region and calculate seismic moments using both the global M_S-M_0 relations of Ekström and Dziewonski (1988) and the continental M_S-M_0 relations of Ekström (1987) (Table 4). In previous studies, the global M_S-M_0 relations were favored or found adequate in the Caucasus region and on the North Anatolian Fault (e.g., Jackson, 1992; Ambraseys and Jackson, 2000), however, Ekström and England (1989) favor the continental M_S-M_0 relations in the Aegean region where they point out anomalously high M_S values in the Harvard Centroid Moment Tensor Catalog. The sources of M_S values include Jackson and

McKenzie (1988), Taymaz et al. (1991b), Jackson (1992), Jackson et al. (1992), Westaway (1994), Ambraseys and Jackson (1998), and the Harvard CMT catalog (2003).

The eastern Mediterranean region is divided into eight sub-regions: Dead Sea Fault (28-36.6°N), East Anatolian Fault (36.6-39°N), North Anatolian Fault (31-41°E), Aegean and western Turkey (36-41°N; 21-31°E), Hellenic Arc (20-29°E), Cyprus Arc (29-36.5°E), Eastern Turkey (39-40°N; 41-44°E), and Caucasus (40-44°N; 41-48.5°E). The Caucasus sub-region corresponds to the area between the Black and Caspian Seas, north of the Lake Van Fault Zone in eastern Turkey (AR-CA boundary), and excluding seismicity near the Caspian Sea (e.g., in the Talesh mountains). The seismic moment rates of the DSF and EAF are 1000-year averages of instrumental and pre-instrumental seismic moments. The seismic moment rate of the NAF is the 330-year average of instrumental and pre-instrumental seismic moments (i.e., since the 1668 M_S 7.9 Amasya event). The seismic moment rates for the Aegean-western Turkey, Hellenic Arc, and Cyprus Arc are 94-year averages of instrumental seismic moments; and the seismic moment rates for eastern Turkey and the Caucasus are 92-year averages of instrumental seismic moments. Errors in observed seismic moment rates are difficult to estimate, but they may be considerable: pre-instrumental M_S values are only known for a fraction of earthquakes ($M_S \geq 6.0$) (Ambraseys and Jackson, 1998), the catalog of recent events may not be representative of long-term seismicity, and M_S-M_0 relations may not be reliable (Ekström and Dziewonski, 1988).

Observed seismic moment rates and model moment rates are compared in Table 5. Seismic moment rates calculated with the global M_S-M_0 relations match the model moment rates much better than those calculated with the continental M_S-M_0 relations. The five best matches (observed:model, i.e., the seismic coupling coefficient) for Model A (with all locking depths set to 15 km) are the Dead Sea Fault (82%), East Anatolian Fault (88%), North Anatolian Fault (80%), Aegean-western Turkey (77%), and Eastern Turkey (95%) using the global M_S-M_0 relations or respectively 27%, 30%, 29%, 41%, and 34% using the continental M_S-M_0 relations. The three poorest matches for Model A

are the Hellenic Arc (14%), Cyprus Arc (5%), and Caucasus (31%) using the global M_S-M_0 relations or respectively 7%, 3%, and 17% using the continental M_S-M_0 relations. Relative to the best match, approximately the same pattern emerges regardless of the M_S-M_0 relations used. Unless noted otherwise, hereafter observed seismic moment rates refer to those calculated with the global M_S-M_0 relations.

I confirm the earlier results of Jackson and McKenzie (1988) and Jackson (1992) that most of the deformation in the Hellenic Arc and Caucasus is aseismic; the Cyprus Arc may also be primarily aseismic, although there is little data on which to base this conclusion. The matches provided by Model B (with lower, best-fitting locking depths on the apparently aseismic boundaries) are better than for Model A, e.g., Hellenic Arc (57%), Cyprus Arc (12%), and Caucasus (72%). If a Black Sea block is included in Model B, the match in the Caucasus is improved again (86%). Jackson and McKenzie (1988) suggested that the size of seismogenic fault planes is limited by thick sediment piles (~10 km) in the eastern Mediterranean Sea basin and in the Caucasus (e.g., Kura basin) which are decoupled from basement faulting by salt horizons and below which basement temperatures are relatively elevated. If their suggestion is correct, the uppermost portion of the crust in these areas is effectively unlocked and may deform by aseismic folding. A low shear modulus of basinal sediments may also explain the high-strain gradients observed at these boundaries with GPS, without invoking low locking depths (e.g., Hager et al., 1999); seismic moment rate is proportional to the product of locking width and shear modulus, thus a low seismic moment rate is explained on this basis as well.

3.3. Implications for continental dynamics

Several driving forces have been proposed to explain the deformation observed in the eastern Mediterranean region including Arabian plate push (e.g., Lundgren et al., 1998), slab roll-back of the Hellenic Arc (e.g., Royden, 1993), gravitational collapse of the Aegean region (Le Pichon, 1983; Sonder and England, 1989; Martinod et al., 2000), and small-scale convection of the aesthenosphere (e.g., Wdowinski et al., 1989). The response of the lithosphere to driving forces is controlled by its rheological structure. Some authors suggest that the forces driving surface deformation on the continents are primarily transmitted through the brittle-elastic upper portion of the crust (e.g., Jackson, 2002), while others suggest that the forces are transmitted by a strong ductile layer in the mantle lithosphere (e.g., Molnar, 1988; Bourne, et al., 1998). The kinematic models presented here are probably consistent with many different combinations of driving forces and rheological structure, however, some of the most intriguing features of the models call attention to particular driving mechanisms.

There are several instances of Euler poles lying on or near the common boundaries of adjacent blocks; many of the blocks in the Aegean appear to be "hinged" in this way to at least one other adjacent block. The diffuse deformation observed near several major plate boundaries (e.g., North America-South America, North America-Eurasia, Indian-Australian) is explained in this way (Gordon, 1998). This configuration suggests that there is strong mechanical coupling between the blocks near their pole. If the present-day relative motion of "hinged" blocks adequately describes their long-term finite rotations, this may be indirect evidence that significant forces driving surface deformation in continents can be transmitted laterally through the upper brittle-elastic crust (e.g., Jackson and Molnar, 1990; Molnar and Gipson, 1994). This hypothesis has testable predictions. For example, if the "hinge" poles in the north Aegean region (GR-EU, AE-GR, NE-GR) have remained in the same positions relative to their respective blocks, then, relative to Eurasia, the South Aegean must have had a more southerly direction of motion in the past than its present southwesterly direction. Estimates of paleostress directions from fault lineations in western Turkey show that they have rotated clockwise over the past 5 Ma

(Angelier et al., 1982; Mercier et al., 1989; Meijer and Wortel, 1997) which may be interpreted as a clockwise rotation in the direction of relative motion between the Aegean and Turkey. Similarly, space geodetic studies have shown that the North America, Oregon, and Sierra Nevada blocks are presently "hinged" (e.g., Wells et al., 1998; McCaffrey et al., 2000; Dixon et al., 2000), and geologic reconstructions (e.g., Atwater and Stock, 1998) provide evidence that the present configuration may have persisted for several Myr; in this case, the Sierra Nevada had a more westerly direction of motion relative to North America in the past. However, another possibility, is that in some reference frame Euler vectors have not significantly changed in the last few Myr, and instead boundaries have migrated with respect to their blocks so that blocks remain hinged at any given time (e.g., Cohen et al., 1995; Jackson, 1999; Goldsworthy et al., 2002).

On the other hand, there seems to be kinematic evidence that edge forces are not the most important driving forces in the region. The models show that Anatolia and Arabia have a slightly transtensional boundary on the East Anatolian Fault where tensile rates increase to the Karliova triple junction to about 10 mm/yr. The Arabia-Anatolia pole or boundary would have to be drastically changed to make the boundary convergent. This would seem to preclude Arabia-push as major driving force for Anatolia. Instead, Anatolia may be primarily driven by buoyancy forces (e.g., Jones, 1996; England and Molnar, 1997) generated by crustal thickening in the collision zone between Arabia and the southeast corner of the Black Sea. The apparent transtension on the Anatolia-Arabia boundary near the Karliova triple junction may actually represent the evacuation or annexation of material in the collision zone to the Anatolian block. A similar suggestion was made by other authors (Jackson and McKenzie, 1984; Westaway, 1990a, 1994) who also noted the distributed nature of the faulting in this location.

4. Conclusions

I use a new GPS velocity field of the eastern Mediterranean and surrounding regions provided by S.C. McClusky (personal communication, 2003) to construct a block model in which surface velocities are the result of the effectively rigid-body motion of blocks over the long-term and elastic deformation caused by friction on block boundaries in the interseismic period (e.g., Meade et al., 2002). I find that a relatively small number of blocks (eleven), bounded by mostly recognized fault zones, explain the bulk of the GPS velocity data. The model is preliminary; fuller data sets, particularly near block boundaries, will permit improvements to the model and test early conclusions. I also find fair to good agreement with previous studies of plate motion, fault slip rates, seismic moment rates and paleomagnetic rotations. Notably, some block pairs in the Aegean region have Euler poles on, or near to, their common boundaries, in qualitative agreement with so-called pinned block models, e.g., for the transfer of slip from the right-lateral North Anatolian Fault system to a set of left-lateral and normal faults in central and northern Greece (McKenzie and Jackson, 1983; Taymaz et al., 1991; Goldsworthy et al., 2002). In addition, roughly three-quarters of the deformation in the Hellenic Arc and Greater Caucasus appears to be aseismic, in approximate agreement with previous studies (Jackson and McKenzie, 1988; Jackson, 1992). Thus the contemporary kinematics of the eastern Mediterranean is adequately explained essentially within a plate tectonic framework. However, contemporary kinematics merely provides a condition to be met for other models of the dynamics and long-term evolution of the region, which may in turn help to decide leading questions in continental tectonics.

References

Agnew, D. C., S. Owen, Z.-K. Shen, G. Anderson, J. Svarc, H. Johnson, K. E. Austin, and R. Reilinger, Coseismic displacement from the Hector Mine, California, earthquake; results from survey-mode Global Positioning System, Bull. Seismol. Soc. Am., 92, 1355-1364, 2002.

Ambraseys, N., Some characteristic features of the Anatolian fault zone, Earthquake mechanics, Tectonophysics, 9, 143-165, 1970.

Ambraseys, N.N., and J. A. Jackson, Faulting associated with historical and recent earthquakes in the eastern Mediterranean region, Geophys. J. Int., 133, 390-406, 1998.

Ambraseys, N., and J. Jackson, Seismicity of the Sea of Marmara (Turkey) since 1500, Geophys. J. Int., 141, F1-F6, 2000.

Anderson, H., and J. Jackson, Active tectonics of the Adriatic region, Geophys. J. R. Astr. Soc., 91, 937-983, 1987.

Anderson, J. G., Estimating the seismicity from geological structure for seismic risk studies, Bull. Seismol. Soc. Am., 69, 135-158, 1979.

Angelier, J., N. Lyberis, X. LePichon, E. Barrier, and P. Huchon, The tectonic development of the Hellenic arc and the Sea of Crete, a synthesis, Tectonophysics, 86, 159-196, 1982.

Armijo, R., B. Meyer, G.C.P. King, A. Rigo, and D. Papanastassiou, Quaternary evolution of the Gulf of Corinth rift and its implications for the Late Cenozoic evolution of the Aegean, Geophys. J. R. Astr. Soc., 126, 11-53, 1996.

Armijo, R., B. Meyers, A. Hubert, and A. Barka, Propagation of the North Anatolian fault into the northern Aegean: Timing and kinematics, Geology, 27, 11-53, 1999.

Atwater, T., and J. Stock, Pacific-North America Plate Tectonics of Neogene Southwestern United States: An Update, Int. Geol. Rev., 40, 375-402, 1998.

Avanessian, A,. and S. Balassanian, Fault Map of the Caucasus and Eastern Turkey, Proceedings of the Second International Conference on Earthquake Hazard and Seismic Risk Reduction, Yerevan, 1998.

Avouac, J. P., and P. Tapponnier, Kinematic model of active deformation in Central Asia, Geophys. Res. Lett., 20, 895–898, 1993.

Ayhan, M.E., C. Demir, O. Lenk, A. Kilicoglu, Y. Altiner, R. Reilinger, A. Barka, S. Ergintav, H. Ozener, Interseismic Strain Accumulation in the Marmara Region, Bull. Seismol. Soc. Am., 92, 216-229, 2002.

Baker, C., D. Hatzfeld, H. Lyon-Caen, E. Papadimitriou, and A. Rigo, Earthquake mechanisms of the Adriatic sea and western Greece: implications for the oceanic subduction-continental collision transition, Geophys. J. Int ., 131 , 559-594, 1997.

Barka, A., and K. Kadinsky-Cade, Strike-slip fault geometry in Turkey and its influence on earthquake activity, Tectonics, 7, 663-684, 1988.

Barka, A., and R. Reilinger, Active tectonics of the eastern Mediterranean region: Deduced from GPS, neotectonic, and seismicity data, Annali Geofisica, 40, 587-610, 1997.

Bennett, R.A., J.L. Davis, and B.P. Wernicke, Present-day pattern of Cordilleran deformation in the western United States, Geology, 27, 371-374, 1999.

Bennett, R., W. Rodi, R. Reilinger, Global Positioning System constraints on fault slip rates in Southern California and northern Baja, Mexico, J. Geophys. Res., 101, 10, 21,943-21,960, 1996.

Briole, P., A. Rigo, H. Lyon-Caen, J.-C. Ruegg, K, Papazissi, C. Mistakaki, A. Balodimou, G. Veis, D. Hatzfeld, and A. Deschamps, Active Deformation of the Gulf of Korinthos, Greece: Results from Repeated GPS Surveys between 1990 and 1995, J. Geophys. Res., 105, 25,605-25,625, 2000.

Brune, J. N., Seismic moment, seismicity, and rate of slip along major fault zones, J. Geophys. Res., 73, 777-784., 1968.

Bourne, S., P. England, and B. Parsons, The motion of crustal blocks driven by flow of the lower lithosphere: implications for slip rates of faults in the South Island of New Zealand and Southern California, Nature, 391, 655-659, 1998.

Burchfiel, B.C., R. Nakov, T., Tzankov, and L.H. Royden, Cenozoic extension in Bulgaria and Northern Greece: the northern part of the Aegean extensional regime, in Tectonics and Magmatism in Turkey and the Surrounding Area, edited by E. Bozkvet, J.A. Winchester, and J.D.A. Piper, Spec. Publ. Geol. Soc. London, 173, 325–352, 2000.

Chen, W.P., and P. Molnar, Focal depths of intracontinental and intraplate earthquakes and their implication for the thermal and mechanical properties of the lithosphere, J. Geophys. Res., 88, 4183-4214, 1983.

Chu, D., and R.G. Gordon, Current plate motions across the Red Sea, Geophys. J. Int., 135, 313-328, 1998.

Chu, D., and R.G. Gordon, Evidence for motion between Nubia and Somalia along the Southwest Indian ridge, Nature, 398, 64-67, 1999.

Clarke, P.J., R.R. Davies, P.C. England, B. Parsons, H. Billiris, D. Paradissis, G. Veis, P.A. Cross, P.H. Denys, V. Ashkenazi, R. Bingley, H.-G. Kahle, M.-V. Muller, and P. Briole, Crustal strain in central Greece from repeated GPS measurements in the interval 1989-1997, Geophys. J. Int., 134, 195-214, 1998.

Cocard, M., H.-G. Kahle, Y. Peter, A. Geiger, G. Veis, S. Felekis, D. Paradissis, and H. Billiris, New constraints on the rapid crustal motion of the Aegean region: recent results inferred from GPS measurements (1993-1998) across the West Hellenic Arc, Greece, Earth Planet. Sci. Lett., 172, 39-47, 1999.

Cohen, H.A., C.J. Dart, H.S. Akyuz, and A. Barka, Syn-rift sedimentation and structural development of the Gediz and Buyuk Menderes graben, western Turkey, J. Geol. Soc. London, 152, 629-638, 1995.

Davies, R., P. England, B. Parsons, H. Billiris, D. Paradissis, and G. Veis, Geodetic strain in Greece in the interval 1892-1992, J. Geophys. Res., 102, 24,571-24,588, 1997.

DeMets, C., R. Gordon, D.F. Argus, and S. Stein, Current plate motions, Geophys. J. Int., 101, 425-478, 1990.

DeMets, C., R. Gordon, D.F. Argus, and S. Stein, Effects of recent revisions to the geomagnetic time scale on estimates of current plate motion, Geophys. Res. Lett., 21, 2191-2194, 1994.

Dercourt, J., et al., Geological evolution of the Tethys belt from the Atlantic to the Pamirs since the Lias, Tectonophysics, 123, 241-315, 1986.

Dewey, J.F., W.C. III Pitman, W.B.F. Ryan, and J. Bonnin, Plate tectonics and the evolution of the Alpine system, Geol. Soc. Amer. Bull, 84, 3137-3180, 1973.

Dewey, J.F., and A.M.C. Sengör, Aegean and surrounding regions: Complex multiplate and continuum tectonics in a convergent zone. Geol. Soc. Am. Bull., 90, 84–92, 1979.

Dixon, T.H., An introduction to the Global Positioning System and some geological applications, Rev. Geophys., 29, 249-276, 1991.

Dixon, T.H., M. Miller, F. Farina, H.Z. Wang, and D. Johnson, Present-day motion of the Sierra Nevada block and some tectonic implications for the Basin and Range province, North American cordillera, Tectonics, 19, 1–24, 2000.

Dong, D., T.A. Herring, and R.W. King, Estimating regional deformation from a combination of space and terrestrial geodetic data, J. Geod., 72, 200-211, 1998.

Duermeijer, C.E., M. Nyst, P.Th. Meijer, C.G. Langereis, and W. Spakman, Neogene evolution of the Aegean arc: paleomagnetic and geodetic evidence for a rapid and young rotation phase, Earth Planet. Sci. Lett., 176, 509-525, 2000.

Ekström, G., A broad band method of earthquake analysis, Ph.D. thesis, Harvard Univ., Cambridge, Mass., 1987.

Ekström, G., and A.M. Dziewonski, Evidence of bias in estimation of earthquake size, Nature, 332, 319-323, 1988.

Ekström, G., and P. England, Seismic strain rates in regions of distributed continental deformation, J. Geophys. Res., 94, 10,231-10,257, 1989.

England, P.C., and D.P. McKenzie, A thin viscous sheet model for continental deformation, Geophys. J. R. Astr. Soc., 70, 295-321, 1982.

England, P., and P. Molnar, Active deformation of Asia: from kinematics to dynamics, Science, 278, 647-650, 1997.

Eyidoğan, H., Rates of crustal deformation in western Turkey as deduced from major earthquakes, Tectonophysics, 148, 83-92, 1988.

Goldsworthy, M., J. Jackson, and J. Haines, The continuity of active fault systems in Greece, Geophys. J. Int., 148, 596–618, 2002.

Gordon, R.G., The plate tectonic approximation: plate nonrigidity, diffuse plate boundaries, and global plate reconstructions, Ann. Rev. Earth Planet Sci., 26, 615-642, 1998.

Hager, B.H., R.W. King, and M.H. Murray, Measurement of crustal deformation using the Global Positioning System, Annu. Rev. Earth Planet. Sci., 19, 351-382, 1991.

Hager, B., G. Lyzenga, A. Donnellan, and D. Dong, Reconciling rapid strain accumulation with deep seismogenic fault planes in the Ventura Basin, California, J. Geophys. Res., 104, 25,207-25,219, 1999.

Haines, A.J., and W.E. Holt, A procedure for obtaining the complete horizontal motions within zones of distributed deformation from the inversion of strain rate data, J. geophys. Res., 98, 12 057-12 082, 1993.

Harvard CMT Catalog (http://www.seismology.harvard.edu/CMTsearch.html), 2003.

Hatzfeld, D., M. Besnard, K. Makropoulos, N. Voulgaris, V. Kouskouna, P. Hatzidimitriou, D. Panagiotopoulos, G. Karakaisis, A. Deschamps, and H. Lyon-Caen, Subcrustal microearthquake seismicity and fault plane solutions beneath the Hellenic arc. J. Geophys. Res., 98, 9861-9870, 1993.

Hatzfeld, D., M. Ziazia, D. Kementzetzidou, P. Hatzidimitriou, D. Panagiotopoulos, K. Makropoulos, P. Papadimitriou, and A. Deschamps, Microseismicity and focal

mechanisms at the western termination of the North Anatolian Fault, and their implications for continental tectonics, Geophys. J. Int., 137, 891-908, 1999.

Herring, T.A., GLOBK: Global kalman filter VLBI and GPS analysis program version 4.1, Mass. Inst. of Technol., Cambridge, 1999.

Houseman, G.A., and P.C. England, Crustal thickening versus lateral expulsion in the Indian-Asian continental collision, J. Geophys. Res., 98, 12,233-12,249, 1993.

Hubert-Ferrari, A., R. Armijo, G. King, B. Meyer, and A. Barka, Morphology, displacement, and slip rates along the North Anatolian Fault, Turkey, J. Geophys. Res., 107, 2235, doi:10.1029/2001JB000393, 2002.

Hubert-Ferrari, A., A. Barka, E. Jacques, S. Nalbant, B. Meyer, R. Armijo, P. Tapponier, G. King, Seismic hazard in the Marmara Sea region following the 17 August 1999 Izmit earthqauke, Nature, 404, 269–271, 2000.

Jackson, J., Partitioning of strike-slip and convergent motion between Eurasia and Arabia in eastern Turkey, J. Geophys. Res., 97, 12471-12479, 1992.

Jackson, J., Active tectonics of the Aegean region, Annu. Rev. Earth Planet. Sci., 22, 239-271, 1994.

Jackson, J.A., Fault death: a perspective from actively deforming regions, J. Struct. Geol., 21, 1003-1010, 1999.

Jackson, J., Strength of the continental lithosphere: time to abandon the jelly sandwich?, GSA Today, 12, 4-10, 2002.

Jackson, J.A., and N.N. Ambraseys, Convergence between Eurasia and Arabia in eastern Turkey and the Caucasus, in Historical and prehistorical earthquakes in the Caucasus,

edited by D. Giardini and S. Balassanian, NATO ASI Series, Environment, 28, 79-90, 1997.

Jackson, J., J. Haines, and W. Holt, The horizontal velocity field in the deforming Aegean Sea region determined from the moment tensors of earthquakes, J. Geophys. Res., 97, 17657-17684, 1992.

Jackson, J., J. Haines, and W. Holt, The accommodation of Arabia-Eurasia plate convergence in Iran, J. Geophys. Res., 100, 15,205-15,219, 1995.

Jackson, J., and D.P. McKenzie, Active tectonics of the Alpine-Himalayan Belt between western Turkey and Pakistan, Geophys. J.R. Astr. Soc., 77, 185-246, 1984.

Jackson, J., and D. McKenzie, The relationship between plate motions and seismic tremors, and the rates of active deformation in the Mediterranean and Middle East, Geophys. J. R. Astr. Soc., 93, 45-73, 1988.

Jackson, J., and P. Molnar, Active faulting and block rotations in the Western Transverse Ranges, California, J. Geophys. Res., 95, 22,073-22,087, 1990.

Jackson, J., K. Priestley, M. Allen, and M. Berberian, Active tectonics of the South Caspian Basin, Geophys. J. Int.,148, 214–245, 2002.

Jones, C.H., Unruh, J.R., and L.J. Sonder, The role of gravitational potential energy in active deformation in the southwestern United States, Nature, 381, 37-41, 1996.

Karig, D.E., and H. Kozlu, Late Palaeogene–Neogene evolution of the triple junction region near Maras, south-central Turkey., J. Geol. Soc. London, 147, 1023–1034, 1990.

Kahle, H.-G., M. Cocard, Y. Peter, A. Geiger, R. Reilinger, A. Barka, and G. Veis, GPS derived strain rate field within the boundary zones of the Eurasian, African, and Arabian plates, J. Geophys. Res., 105, 23,353-23,370, 2000.

King, R.W., and Y. Bock, Documentation for GAMIT analysis software, release 9.7, Mass. Inst. of Technol., Cambridge, 1999.

Kiratzi, A., Stress tensor inversions along the westernmost North Anatolian Fault Zone and its continuation into the North Aegean Sea., Geophys. J. Int., 151, 360-376, 2002.

Kissel, C., and C. Laj, The Tertiary geodynamic evolution of the Aegean arc: a paleomagnetic reconstruction. Tectonophysics 146, 183-201, 1988.

Kotzev, V., R. Nakov, C. Burchfiel, R. King, and R. Reilinger, GPS study of Active Tectonic in Bulgaria, J. of Geodynamics, 31, 189-200, 2001.

Le Pichon, X., Sea-floor spreading and continental drift, J. Geophys. Res., 73, 3661-3697,1968.

Le Pichon, X., Land-locked oceanic basins and continental collision: the Eastern Mediterranean as a case example, in Mountain Building Processes, edited by K.J. Hsü, pp. 201–211, Academic Press, London, 1983.

Le Pichon, X., and J. Angelier, The Hellenic arc and trench system: A key to the neotectonic evolution of the eastern Mediterranean area, Tectonophysics, 60, 1-42, 1979.

Le Pichon, X., N. Chamot-Rooke, S. Lallemant, R. Noomen, and G. Veis, Geodetic determination of the kinematics of central Greece with respect to Europe: Implications for eastern Mediterranean tectonics, J. Geophys. Res., 100, 12,675-12,690, 1995.

Le Pichon, X., A.M.C. Şengör, E. Demirbağ, C. Rangin, C. İmren, R. Armijo, N. Görür, N. Çağatay, B. Mercier de Lepinay, B. Meyer, R. Saatçilar, B. Tok, The active Main Marmara Fault, Earth Planet. Sci. Lett., 192, 595-616, 2000.

Lundgren, P., D. Giardini, and R. M . Russo, A geodynamic framework for eastern Mediterranean kinematics, Geophys. Res. Lett., 25, 4007-4010, 1998.

Lyberis, N., T. Yurur, J. Chorowicz, E. Kasapoglu, and N. Gundogdu, The East Anatolian fault: An oblique collisional belt, Tectonophysics, 204, 1-15, 1992.

Martinod, J., D. Hatzfeld, J.-P. Brun, P. Davy, and P. Gautier, Continental collision, Gravity spreading, and Kinematics of the Aegea and Anatolia, Tectonics, 19, 290-299, 2000.

Matsu'ura, M., D.D. Jackson, and A. Cheng, Dislocation model for aseismic crustal deformation at Hollister, California, J. Geophys. Res., 91, 12,661-12,674, 1986.

McCaffrey, R., Crustal block rotations and plate coupling, in Plate Boundary Zones, edited by S. Stein and J. Freymueller, AGU Geodynamics Series 30, 101-122, 2002.

McCaffrey, R., M. D. Long, C. Goldfinger, P. C. Zwick, J. L. Nabelek, C. K. Johnson, and C. Smith, Rotation and plate locking at the southern Cascadia subduction zone, Geophys. Res. Lett., 27, 3117-3120, 2000.

McClusky S., S. Balssanian, A. Barka, C. Demir, S. Ergintav, I. Georgiev, O. Gurkan, M. Hamburger, K. Hurst, H. Kahle, K. Kastens, G. Kekelidze, R. King, V. Kotzev, O. Lenk, S. Mahmoud, A. Mishin, M. Nadariya, A. Ouzounis, D. Paradissis, Y. Peter, M. Prilepin, R. Reilinger, I. Sanli, H. Seeger, A.. Tealeb, M. N. Toksöz, and G. Veis, Global positioning System constraints on plate kinematics and dynamics in the eastern Mediterranean and Caucasus, J. Geophys. Res., 105, 5695-5719, 2000.

McClusky, S.C., S. C. Bjornstad, B. H. Hager, R. W. King, B. J. Meade, M. M. Miller, F. C. Monastero, and B. J. Souter, Present day kinematics of the Eastern California Shear Zone from a geodetically constrained block model, Geophys. Res. Lett. 28, 3369-3372, 2001.

McClusky, S., R. Reilinger, S. Mahmoud, D. Ben Sari, and A. Tealeb, GPS constraints on Africa (Nubia) and Arabia plate motions, Geophys. J. Int., in press, 2003.

McKenzie, D.P., Plate tectonics of the Mediterranean region, Nature, 226, 239-243, 1970.

McKenzie, D.P., Active tectonics of the Mediterranean region, Geophys. J.R. Astr. Soc., 30, 109-185, 1972.

McKenzie, D., Active tectonics of the Alpine–Himalayan belt: the Aegean Sea and surrounding regions. Geophys. J. R. Astron. Soc. 55, 217–254, 1978.

McKenzie, D., and J. Jackson, The relationship between strain rates, crustal thickening, paleomagnetism, finite strain and fault movements within a deforming zone, Earth Planet. Sci. Lett., 65, 182-202, 1983.

McKenzie, D.P., and R.L. Parker, The North Pacific: an example of tectonics on a sphere, Nature, 216, 1276-1280, 1967.

Meade, B.J., B.H. Hager, S. C. McClusky, R.E. Reilinger, S. Ergintav, O. Lenk, A. Barka, and H. Özener, Estimates of seismic potential in the Marmara region from block models of secular deformation constrained by GPS measurements, Bull. Seismol. Soc. Am., 92, 208-215, 2002.

Meijer, P.T., and M.J.R. Wortel, Present-day dynamics of the Aegean region: a model analysis of the horizontal pattern of stress and deformation, Tectonics 16, 879–895, 1997.

Mercier, J. L., D. Sorel, P. Vergely, K. Simeakis, Extensional tectonic regimes in the Aegean basins during the Cenozoic, Basin Res., 2, 49-71, 1989.

Molnar, P., Earthquake Recurrence Intervals and Plate Tectonics, Bull. Seismol. Soc. Amer., 69, 115-133, 1979.

Molnar, P., Continental tectonics in the aftermath of plate tectonics, Nature, 335, 131-137, 1988.

Molnar, P., and J.M. Gipson, Very long baseline interferometry and active rotations of crustal blocks in the Western Transverse Ranges, California, G.S.A. Bull., 106, 594-606, 1994.

Murray, M.H., and P. Segall, Modeling broadscale deformation in northern California and Nevada from plate motions and elastic strain accumulation, Geophys. Res. Lett., 28, 4315-4318, 2001.

Muller, S., and H.-G. Kahle, Crust-mantle evolution, structures and dynamics of the Mediterranean-Alpine region, Contributions of space geodesy to geodynamics: crustal dynamics, Geodyn. Ser., vol. 23, edited by D.E. Smith and D.L. Turcotte, pp. 249-298, AGU, Washington, D.C., 1993.

Okada, Y., Surface deformation due to shear and tensile faults in a half space, Bull. Seismol. Soc. Am., 75, 1135-1154, 1985.

Oldow, J.S., L. Ferranti, D.S. Lewis, J.K. Campbell, B. D'Argenio, R. Catalano, G. Pappone, L. Carmignani, P. Conti, and C.L.V. Aiken, Active fragmentation of Adria, the north African promontory, central Mediterranean orogen, Geology, 30, 779-782, 2002.

Papazachos, B. C., V.G. Karakostas, C.B. Papazachos, and E.M. Scordilis, The geometry of the Wadati-Benioff zone and lithospheric kinematics in the Hellenic Arc, Tectonophysics, 319, 275-300, 2000.

Parsons, T., S. Toda, R. S. Stein, A. Barka, J. H. Dieterich, Heightened Odds of Large Earthquakes Near Istanbul: An Interaction-Based Probability Calculation, Science, 288, 661-665, 2000.

Peter, Y., H.-G., Kahle, M. Cocard, G. Veis, S. Felekis, and D. Paradissis, Establishment of a permanent GPS network across the Kephalonia fault zone, Ionian Islands, Greece, Tectonophysics, 294, 253-260, 1998.

Philip, H., A. Cisternas, A. Gviskiani, and A. Gorshkov, The Caucasus: An actual example of the initial stages of continental collision, Tectonophysics, 161, 1-21, 1989.

Rebai, S., H. Philip, L. Dorbath, B. Borissof, H. Haessler, and A. Cisternas, Active tectonics in the Lesser Caucasus: Coexistence of compressive and extensional structures, Tectonics, 12, 1089-1114, 1993.

Reilinger, R., and S. McClusky, GPS constraints on block motions and deformations in western Turkey and the Aegean: Implications for earthquake hazards, in, Seismotectonics of the north-western Anatolia-Aegean and recent Turkish Earthquakes, edited by T. Taymaz, Istanbul Technical University, Istanbul, Turkey, 14-20, 2001.

Reilinger, R.E., S.C. McClusky, M.B. Oral, R.W. King, M.N. Toksoz, A.A. Barka, I. Kinik, O. Lenk, and I. Sanli, Global Positioning System measurements of present-day crustal movements in the Arabia-Africa-Eurasia plate collision zone, J. Geophys. Res., 102, 9983-9999, 1997a.

Reilinger, R.E., S.C. McClusky, B.J. Souter, M.W. Hamburger, M.T. Prilepin, A. Mishin, T. Guseva, S. Balassanian, Preliminary estimates of plate convergence in the Caucasus

collision zone from global positioning system measurements, Geophys. Res. Lett., 24, 1815-1818, 1997b.

Reilinger, R.E., S. McClusky, R. Bürgmann, S. Ergintav, A. Barka, H. Meteris, O. Gurkan, K.L. Feigl, N. Yalçın, and M.N. Toksöz, GPS constraints on coseismic fault slip for the MW7.4, 17 August 1999, Izmit earthquake: Implication for future earthquakes in the Marmara seismic gap, Science, 289, 1519-1524, 2000.

Royden, L., The tectonic expression of slab pull at continental convergent boundaries, Tectonics, 12, 303-325, 1993.

Savage, J., and R. Burford, Geodetic determination of relative plate motion in central California, J. Geophys. Res., 78, 832-845, 1973.

Savage, J.C., and M. Lisowski, Viscoelastic coupling model of the San Andreas Fault along the Big Bend, Southern California, J. Geophys. Res., 103, 7281-7289, 1998.

Seber, D., M. Vallve, E. Sandvol, D. Steer, and M. Barazangi, Middle East Tectonics: Applications of Geographic Information Systems (GIS), GSA Today, 7, 1-6, 1997.

Sella, G. F., T. H. Dixon, and A. Mao, REVEL: A model for Recent plate velocities from space geodesy, J. Geophys. Res., 107, 2081, doi:10.1029/2000JB000033, 2002.

Sengör, A.M.C., The North Anatolian transform fault: its age, offset, and tectonic significance, J. Geol. Soc. London, 136, 269-282, 1979.

Sengör, A.M.C., N. Gurur, and F. Saroglu, Strike-slip faulting and related basin formation in zones of tectonic escape: Turkey as a case study, in Strike slip faulting and basin formation, edited by K.T. Biddle, and N. Christie-Blick, Spec. Publ. Econ. Paleontol. Mineral, 37, 227-264, 1985.

Sonder, L., and P. England, Effects of temperature dependent rheology on large scale continental extension, J. Geophys. Res., 94, 7603-7619, 1989.

Souter, B.J., Comparisons of geological models to GPS observations in southern California, Ph.D. Thesis, Massachusetts of Technology, Cambridge, Massachusetts.

Stein, R. S., A.A. Barka, and J.H. Dietrich, Progressive failure on the North Anatolian fault since 1939 by stress triggering, Geophys. J. Int., 128, 594-604, 1997.

Straub, C, H.-G. Kahle, and C. Schindler, GPS and geologic estimates of the tectonic activity in the Marmara sea region, NW Anatolia. J. Geophys. Res., 102, B12, 27587-27601, 1997.

Talebian, M., and J. Jackson, Offset on the Main Recent Fault of NW Iran and implications for the late Cenozoic tectonics of the Arabia–Eurasia collision zone, Geophys. J. Int., 150, 422–439, 2002.

Taymaz, T., H. Eyidoğan, and J. Jackson, Source parameters of large earthquakes in the east Anatolian fault zone (Turkey), Geophys. J. Int., 106, 537-550, 1991b.

Taymaz, T., J. Jackson, D. McKenzie, Active tectonics of the north and central Aegean Sea, Geophys. J. Int., 106, 433-490, 1991a.

Thatcher, W., Microplate versus continuum descriptions of active tectonic deformation, J. Geophys. Res., 100, 3885-3894, 1995.

Triep, E.G., G.A. Abers, A.L. Lerner-Lam, V. Mishatkin, N. Zakharchenko, O. Starovoit, Active thrust front of the Greater Caucasus: The April 29, 1991 Racha Earthquake Sequence and its tectonic implications, J. Geophys. Res., 100, 4011-4034, 1995.

Voidomatis, P., S. Pavlides, and G. Papadopoulos, Active deformation and seismic potential in the Serbomacedonian zone, North Aegean, Tectonophys., 179, 1-9, 1990.

Wang, Q., P.-Z. Zhang, J. T. Freymueller, R. Bilham, K. M. Larson, X. Lai, X. You, Z. Niu, J. Wu, Y. Li, J. Liu, Z. Yang, and Q. Chen, Present-Day Crustal Deformation in China Constrained by Global Positioning System Measurements, Science, 294, 574-577, 2001.

Wells, R.E., C.S. Weaver, and R.J. Blakely, Fore-arc migration in Cascadia and its neotectonic significance, Geology, 26, 759-762, 1998.

Wessel, P., and W.H.F. Smith, New version of the generic mapping tools released, EOS, Trans. AGU, 76, 329, 1995.

Westaway, R., Seismicity and tectonic deformation rate in Soviet Armenia: Implications for local earthquake hazard and evolution of adjacent regions, Tectonics, 9, 477-503, 1990a.

Westaway, R., Block rotation in western Turkey 1. Observational evidence, J. Geophys. Res., 95, 19,857-19,884, 1990b.

Westaway, R., Present-day kinematics of the Middle East and eastern Mediterranean, J. Geophys. Res., 99, 12,071-12,090, 1994.

Wdowinski, S., R.J. O'Connell, and P. England, A continuum model of continental deformation above subduction zones: Application to the Andes and the Aegean, J. Geophys. Res., 94, 10,331-10,346, 1989.

Wright, T., B. Parsons, and E. Fielding, Measurement of interseismic strain accumulation across the North Anatolian Fault by satellite radar interferometry, Geophys. Res. Lett., 28, 2117-2120, 2001.

Wortel, M.J.R., and W. Spakman, Subduction and slab detachment in the Mediterranean-Carpathian region, Science, 290, 1910-1917, 2000.

Table captions

Table 1. GPS velocity fields combined for this study and their sources. The velocity fields are transformed to the same Eurasia-fixed reference frame using the VELROT 1.01 software (R.W. King, pers. com., 2002). The six-parameter transformation (six components of rate of change of translation and rotation) for each velocity field is estimated by minimizing the horizontal velocity residuals between co-located sites in the global velocity field (S. McClusky, pers. com., 2003).

Table 2. GPS velocities in a Eurasia-fixed reference frame, 1-sigma uncertainties (±), correlation between the east and north components of velocity (RHO), sources of data, and block assignments, used in this study. m, S. McClusky (pers. com., 2003); m2, Meade et al. (2002); c, Clarke et al. (1998). m3, sites used to determine a Eurasia-fixed reference frame in McClusky et al. (2003). BS, Black Sea block; other block abbreviations as in Figure 8.

Table 3. Euler vectors and their 1-sigma uncertainties for Model A, Model B and other recent studies. Euler vectors for all block pairs with Eurasia and for all blocks with a common boundary are shown. The first block rotates counterclockwise relative to the second block. AF, Africa as in DeMets et al. (1994); other block abbreviations as in Figure 8.

Table 4. Earthquakes used to determine seismic moment rates for the Dead Sea Fault, East Anatolian Fault, North Anatolian Fault, Aegean-western Turkey, Hellenic Arc, Cyprus Arc, eastern Turkey and the Caucasus.

Seismic moment, M_0, is in units of 10^{17} N m. Surface-wave magnitudes, M_S, of historical and recent earthquakes are taken from the references. M_0^g and M_0^c are seismic moments calculated with the global M_S - M_0 relations of Ekström and Dziewonski (1988) and the continental M_S - M_0 relations of Ekström (1987), respectively. M_0^{CMT} are observed seismic moments in the Harvard CMT catalog (2003) from 1977 through 2002. Historical earthquakes designated very large (V), large (L), or medium (m), e.g., Ambraseys and Jackson (1998), are assigned M_S 7.9, 7.5, or 6.5, respectively. *, M_0^{CMT} used in place of M_0^g or M_0^c due to anomalously high M_S values in the Aegean region, e.g., Ekström and Dziewonski (1988).

References are abbreviated as follows: jm, Jackson and McKenzie (1988); tej, Taymaz et al. (1991b); j, Jackson (1992); jhh, Jackson et al. (1992); w, Westaway (1994); Ambraseys and Jackson (1998); cmt, Harvard CMT catalog (2003).

Table 5. Preliminary comparison of observed seismic moment rates and model moment rates by region. $\dot{M}_0$ is in units of 10^{17} N m/yr. Data used to calculate observed seismic moment rates are from Jackson and McKenzie (1988), Taymaz et al. (1991b), Jackson (1992), Jackson et al. (1992), Westaway (1994), Ambraseys and Jackson (1998), and the

Harvard CMT catalog (2003). Seismic moment rates are calculated with the global M_S-M_0 relations of Ekström and Dziewonski (1988) unless otherwise noted. c, seismic moments calculated with continental M_S-M_0 relations of Ekström (1987); b, including a Black Sea block.

In model A, all locking depths are 15 km. In model B, the locking depths on the Marmara Fault, Hellenic Arc, Cyprus Arc and in the Greater Caucasus are 5 km, 4 km, 4 km, and 4 km, respectively; all other locking depths are 15 km. An uncertainty of ± 5 km is assumed in locking depth.

The seismic moment rates of the DSF and EAF are 1000-year averages of intrumental and pre-instrumental seismic moments. The seismic moment rate of the NAF is the 330-year average of intrumental and pre-instrumental seismic moments. The seismic moment rates for the Aegean-western Turkey, Hellenic Arc, and Cyprus Arc are 94-year averages of instrumental seismic moments. The seismic moment rates for eastern Turkey and the Caucasus are 92-year averages of instrumental seismic moments.

Table 1. GPS velocity fields combined for this study and their sources.

Name	Source	Sites used in study	Sites used in transformation	RMS fit (mm/yr)
Global (m)	McClusky (pers. com., 2003)	185	-	-
Marmara Sea (m2)	Meade et al. (2002)	74	24	0.72
Central Greece (c)	Clarke et al. (1998)	29	5	1.48

The velocity fields are transformed to the same Eurasia-fixed reference frame using the VELROT 1.01 software (R.W. King, pers. com., 2002). The six-parameter transformation (six components of rate of change of translation and rotation) for each velocity field is estimated by minimizing the horizontal velocity residuals between co-located sites in the global velocity field (S.C. McClusky, pers. com., 2003).

Table 2. GPS velocities in a Eurasia-fixed reference frame, 1-sigma uncertainties (±), correlation between the east and north components of velocity (RHO), sources of data, and block assignments, used in this study. m, S. McClusky (pers. com., 2003); m2, Meade et al. (2002); c, Clarke et al. (1998). m3, sites used to determine a Eurasia-fixed reference frame in McClusky et al. (2003). BS, Black Sea block; other block abbreviations as in Figure 8.

Lon. (°E)	Lat. (°N)	E (mm/yr)	N (mm/yr)	E (±)	N (±)	RHO	SITE	Ref.	Block
-4.25	40.43	-0.35	0.11	0.64	0.62	-0.003	MADR	m, m3	EU
-3.95	40.44	0.55	0.10	0.71	0.71	0.000	VILL	m, m3	EU
1.48	43.56	0.25	0.83	1.05	1.05	0.000	TOUL	m, m3	EU
4.36	50.80	0.02	-0.56	0.71	0.71	0.000	BRUS	m, m3	EU
5.81	52.18	0.04	0.03	0.60	0.60	0.000	KOSG	m, m3	EU
6.92	43.76	0.32	-0.12	0.75	0.75	0.000	GRAS	m, m3	EU
7.47	46.88	0.00	0.37	0.67	0.67	0.000	ZIMM	m, m3	EU
11.87	78.93	-0.39	-0.25	0.53	0.53	-0.001	NYAL	m, m3	EU
11.93	57.40	-1.66	-0.14	0.58	0.57	0.024	ONSA	m, m3	EU
12.88	49.14	0.44	0.19	0.76	0.76	0.000	WTZR	m, m3	EU
13.07	52.38	0.27	-0.05	0.73	0.73	0.000	POTS	m, m3	EU
15.49	47.07	0.63	0.24	0.62	0.62	0.001	GRAZ	m, m3	EU
17.07	52.28	0.12	-0.05	0.73	0.73	-0.001	BOR1	m, m3	EU
18.94	69.66	-0.62	0.78	0.51	0.51	0.007	TROM	m, m3	EU
21.03	52.10	-0.02	0.04	0.69	0.69	0.000	JOZE	m, m3	EU
24.40	60.22	0.26	-0.67	0.65	0.65	0.000	METS	m, m3	EU
36.76	55.70	0.59	0.10	0.72	0.72	0.000	ZWEN	m, m3	EU
41.57	43.79	0.90	0.82	0.68	0.65	0.003	ZECK	m, m3	EU
58.56	56.43	-0.22	0.09	1.28	1.27	0.000	ARTU	m, m3	EU
92.79	55.99	-1.34	-0.57	0.94	0.93	0.000	KSTU	m, m3	EU
104.32	52.22	-1.42	-0.76	0.75	0.74	-0.003	IRKT	m, m3	EU
128.87	71.63	0.63	0.99	1.05	1.04	0.000	TIXI	m, m3	EU
129.68	62.03	-0.72	-0.06	0.84	0.84	0.001	YAKT	m, m3	EU
23.13	41.46	0.09	-2.22	1.61	1.58	-0.007	PETB	m	EU
23.14	43.11	-1.76	-1.48	1.65	1.59	0.001	BERK	m	EU
23.40	42.56	1.35	-2.50	0.91	0.91	0.000	SOFI	m	EU
23.43	42.48	-2.58	-1.58	1.59	1.51	0.007	PLA1	m	EU
23.57	41.82	-1.18	-3.35	1.63	1.61	-0.009	DOBR	m	EU
23.91	41.60	-0.67	-4.27	1.57	1.55	-0.003	SATO	m	EU
24.24	41.38	2.32	-0.29	1.16	1.09	0.026	SKAL	m	EU
24.63	40.59	0.06	-2.85	1.08	0.94	0.067	THAS	m	EU
24.63	43.36	0.96	0.43	1.73	1.62	-0.002	KAIL	m	EU

24.75	42.15	-1.54	-2.93	1.61	1.58	-0.008	PLO2	m	EU
25.28	42.96	1.90	0.27	1.61	1.55	0.001	GABR	m	EU
25.40	41.55	3.37	-2.95	1.68	1.57	-0.004	MOMC	m2	EU
25.51	40.47	-2.87	-4.41	1.48	1.45	-0.011	SMTK	m2	EU
25.57	40.93	-0.35	-1.81	1.44	1.37	-0.004	ASKT	m2	EU
26.13	44.46	1.23	-1.43	1.09	1.08	0.000	BUCU	m	EU
26.27	43.60	0.24	-0.70	1.65	1.61	-0.002	TSAR	m	EU
26.31	42.08	-0.50	-0.54	1.57	1.53	-0.003	TOPO	m	EU
26.71	40.74	-2.91	-2.84	1.05	1.03	0.012	DOKU	m2	EU
26.73	43.49	-0.28	-0.71	1.64	1.59	-0.001	SHUM	m	EU
27.39	40.81	-3.85	-4.85	1.08	1.11	0.057	YENB	m2	EU
27.44	42.67	0.22	-1.18	1.59	1.56	-0.006	BURG	m	EU
27.48	42.48	-2.58	-1.48	1.65	1.61	-0.003	BUTG	m	EU
27.78	41.83	0.36	-1.33	1.03	0.96	-0.014	DEMI	m2	EU
27.96	40.97	-0.62	0.13	1.11	1.02	0.003	MAER	m2	EU
28.29	41.48	0.86	-2.36	1.09	1.01	-0.010	YALI	m2	EU
28.37	41.05	-0.54	0.24	1.03	0.98	-0.005	SELP	m2	EU
29.02	41.10	-1.90	-0.31	0.94	0.92	0.001	ITAY	m2	EU
29.06	41.06	-2.64	0.46	0.78	0.74	0.005	IKAN	m2	EU
29.62	41.18	-0.90	-1.55	1.35	1.18	-0.020	SILE	m2	EU
29.64	40.80	-6.05	-0.08	1.76	1.62	0.134	YUHE	m2	EU
30.13	40.75	-8.20	-1.84	1.03	1.05	0.001	SISL	m2	EU
30.64	40.61	-12.93	-1.20	0.92	0.93	0.011	KTOP	m2	EU
30.66	40.63	-12.65	-3.82	1.55	1.53	0.118	KKAP	m2	EU
30.75	40.65	-9.55	0.16	1.86	1.85	0.189	KMAL	m2	EU
30.76	40.59	-13.07	-1.78	0.91	0.89	0.006	AGOK	m2	EU
30.83	40.74	-7.18	-1.59	1.13	1.14	0.049	KDER	m2	EU
31.44	40.94	-2.79	0.11	0.99	0.96	0.006	YIGI	m2	EU, BS
32.23	41.52	0.78	-0.23	1.11	1.08	-0.003	HALI	m2	EU, BS
32.57	40.88	-7.81	0.29	1.01	0.96	0.025	ISME	m2	EU, BS
33.99	44.41	-1.99	0.31	1.89	1.80	-0.022	SIMI	m	EU
35.21	42.02	-0.54	1.57	1.06	0.97	0.008	SINO	m	EU, BS
36.34	41.30	0.45	2.52	1.22	1.22	0.030	SAMS	m	EU, BS
38.05	44.55	-0.08	-1.00	1.67	1.61	-0.011	GELE	m	EU
39.24	44.70	0.43	-0.73	1.51	1.39	0.005	GKL_	m	EU
39.70	40.97	0.94	2.01	0.82	0.79	0.011	AKTO	m	EU, BS
40.25	39.73	-2.71	5.51	0.97	0.90	-0.011	MERC	m	EU, BS
40.27	43.68	2.28	-1.84	1.94	1.75	0.006	KRPO	m	EU
40.81	40.44	0.50	2.68	0.88	0.85	-0.004	ISPI	m	EU, BS
41.30	39.97	-0.83	5.41	0.87	0.84	0.004	ERZU	m	EU, BS
41.34	41.37	-0.18	2.70	1.14	1.14	-0.009	HOPA	m	EU, BS
41.99	40.55	1.89	4.89	1.17	1.14	0.013	OLTU	m	EU, BS

42.06	42.72	0.68	3.08	1.13	1.12	-0.005	INGU	m	EU, BS
42.13	41.65	1.25	3.80	1.20	1.21	-0.006	SHUA	m	EU, BS
42.20	43.35	-0.39	-0.10	1.10	1.09	-0.005	ULKA	m	EU
42.47	42.02	2.17	3.92	0.93	0.88	-0.022	VANI	m	EU, BS
42.67	43.74	0.42	1.90	1.08	1.08	-0.006	SHAT	m	EU
42.76	41.13	2.62	6.25	2.45	2.15	-0.023	ARDA	m	EU, BS
42.79	44.01	-0.14	1.20	1.11	1.11	-0.004	BEUG	m	EU
42.87	45.27	1.52	-1.53	1.31	1.28	0.004	SVT1	m	EU
43.14	42.47	1.07	3.83	1.05	0.88	-0.007	KHOT	m	EU, BS
43.38	42.58	0.44	-0.89	0.91	0.84	0.012	KHUR	m	EU
43.40	42.49	-0.57	2.66	1.06	0.86	0.064	SHKM	m	EU
43.54	42.49	0.66	-0.62	0.95	0.91	0.019	LESO	m	EU
43.75	42.98	1.00	0.43	1.13	1.12	-0.020	MATS	m	EU
44.49	42.45	0.65	3.67	0.78	0.77	0.009	KRES	m	EU
45.80	41.95	1.02	4.77	1.48	1.26	0.034	KUDI	m	EU
47.86	40.98	1.66	4.88	1.21	1.09	0.004	KEBE	m	EU
48.53	41.60	1.05	1.18	1.24	1.13	0.000	SAMU	m	EU
48.55	40.61	1.33	3.47	1.14	1.08	-0.001	MEDR	m	EU
49.12	41.07	0.64	1.84	1.13	1.07	0.001	SIYE	m	EU
49.43	40.03	2.98	1.33	1.20	1.10	0.012	SHIK	m	EU
-15.63	27.76	-3.63	1.10	0.68	0.67	0.001	MAS1	m	NU
-9.88	-40.35	4.35	2.28	1.09	1.05	0.003	GOUG	m	NU
20.81	-32.38	0.88	4.05	1.01	1.00	0.001	SUTH	m	NU
27.23	31.35	-2.29	4.05	1.14	1.05	0.002	MATR	m	NU
27.71	-25.89	2.19	4.96	0.50	0.49	-0.003	HART	m	NU
30.89	29.51	-2.17	4.63	1.10	1.06	-0.002	MEST	m	NU
31.34	29.86	-1.93	4.86	0.89	0.85	0.002	HELW	m	NU
34.78	32.07	-2.32	7.69	0.88	0.87	-0.001	TELA	m	NU
35.39	31.59	-2.67	7.97	1.29	1.28	0.004	DRAG	m	NU
36.13	36.05	-5.46	8.71	1.20	1.10	-0.007	SENK	m	NU
35.69	33.00	-3.37	10.75	0.90	0.90	-0.004	KATZ	m	AR
36.97	37.19	-9.13	10.98	1.16	1.13	-0.001	SAKZ	m	AR
37.57	36.90	-7.89	12.28	0.89	0.85	-0.004	GAZI	m	AR
38.23	37.75	-7.39	13.44	1.11	1.07	0.000	ADYI	m	AR
39.81	37.85	-9.23	14.76	1.01	0.99	-0.004	KRCD	m	AR
40.65	37.25	-6.72	16.12	0.98	0.93	-0.014	KIZ2	m	AR
41.79	38.75	-4.78	14.46	1.01	0.88	0.074	KRKT	m	AR
43.34	38.55	-5.09	12.67	1.11	1.10	0.007	KAL2	m	AR
50.61	26.21	3.96	20.89	0.79	0.78	-0.001	BAHR	m	AR
26.45	39.23	-21.25	-13.39	1.30	1.20	-0.006	LESV	m2	AN
26.70	39.31	-18.38	-11.40	0.96	0.89	0.007	AYKA	m2	AN
26.71	39.33	-19.62	-10.03	1.07	1.04	0.020	AYVA	m2	AN

27.11	39.24	-18.25	-11.22	2.13	2.21	0.006	D5DU	m2	AN
27.27	39.58	-19.40	-5.49	1.58	1.61	0.138	EGMI	m2	AN
27.31	38.71	-18.16	-14.85	0.93	0.92	0.005	BAYO	m	AN
27.32	39.02	-20.82	-12.82	0.96	0.90	0.018	YAYA	m2	AN
27.42	39.79	-22.92	-9.44	1.10	1.08	0.059	ALAN	m2	AN
27.59	39.30	-15.67	-11.24	2.07	2.13	-0.005	D7DU	m2	AN
27.87	39.01	-20.46	-10.39	0.88	0.86	0.021	AKGA	m2	AN
27.91	39.72	-21.59	-4.68	0.86	0.76	0.009	BALI	m2	AN
28.00	38.25	-20.73	-12.80	1.19	1.13	-0.006	ODME	m	AN
28.48	38.32	-22.50	-13.51	1.22	1.15	0.002	ALSE	m	AN
28.67	39.05	-21.14	-6.47	0.89	0.83	0.005	DMIR	m2	AN
28.92	39.93	-24.41	-2.53	1.69	1.63	0.109	GIRE	m2	AN
29.10	40.14	-23.68	-4.83	1.02	0.99	0.027	ULUD	m2	AN
29.14	37.94	-21.76	-8.09	0.90	0.87	-0.005	PAMU	m	AN
29.14	40.12	-18.76	0.18	0.94	0.90	-0.001	ULDA	m2	AN
29.26	40.20	-21.75	-3.48	1.65	1.55	0.148	CATA	m2	AN
29.44	36.72	-13.10	-10.19	1.20	1.17	-0.001	SIRA	m	AN
29.51	40.16	-21.68	-2.33	1.84	1.69	0.150	HMZA	m2	AN
29.65	36.19	-10.20	-9.33	1.06	0.92	0.004	KASO	m	AN
29.68	40.36	-20.21	-0.83	0.99	0.81	0.014	DERB	m2	AN
29.81	36.97	-20.25	-8.40	1.50	1.39	-0.024	KYBS	m	AN
29.93	40.43	-18.59	-2.04	0.91	0.87	0.001	IUCK	m2	AN
30.30	37.69	-19.38	-8.18	0.93	0.90	-0.004	BURD	m	AN
30.61	36.83	-10.66	-8.86	1.17	1.11	-0.001	ANTG	m	AN
30.64	39.66	-24.17	-2.25	1.05	0.98	0.014	ESKI	m2	AN
30.64	38.77	-21.16	-3.00	0.99	0.93	0.014	AFYO	m	AN
30.68	40.55	-15.64	-2.40	1.88	1.92	0.138	BOZT	m2	AN
30.68	40.54	-16.99	-0.43	1.00	1.02	0.003	AGUZ	m2	AN
30.80	40.39	-19.73	-3.53	0.90	0.90	0.038	TEBA	m2	AN
30.86	40.56	-15.59	-2.08	1.76	1.68	0.114	PINA	m2	AN
31.12	37.76	-16.22	-5.04	1.42	1.26	-0.043	AKSU	m	AN
31.81	39.56	-20.12	-2.83	1.14	0.92	0.030	SIVR	m2	AN
32.16	36.43	-9.91	-0.02	1.33	1.16	-0.023	SEKI	m	AN
32.73	39.87	-20.52	-2.53	1.10	1.13	-0.034	ANKA	m	AN
32.76	39.89	-21.17	-1.32	1.08	1.04	0.001	ANKR	m2	AN
33.19	37.38	-13.71	2.27	0.83	0.81	0.004	MELE	m	AN
33.40	35.14	-6.78	2.82	0.91	0.91	0.000	NICO	m	AN
34.55	36.90	-12.51	3.64	1.21	1.16	0.006	MERS	m	AN
34.80	39.11	-19.29	3.50	1.81	1.81	-0.018	ABDI	m	AN
34.81	39.80	-18.75	5.12	0.91	0.88	0.004	YOZG	m	AN
34.88	40.45	-17.50	4.48	1.17	1.15	-0.011	KKIR	m	AN
35.94	36.46	-10.18	9.56	1.35	1.31	0.002	ULUC	m	AN

36.07	37.39	-11.22	12.01	1.96	1.55	0.223	KDRL	m	AN
36.14	36.90	-12.62	9.03	1.19	1.11	-0.003	DORT	m	AN
37.00	37.52	-9.87	9.51	1.69	1.63	-0.010	MARS	m	AN
37.96	39.45	-17.90	9.86	0.89	0.84	0.009	SINC	m	AN
38.22	38.46	-11.06	11.37	1.05	1.03	-0.012	MLTY	m	AN
39.16	39.61	-18.63	9.49	1.19	1.13	-0.017	KMAH	m	AN
42.91	39.24	-2.18	9.11	0.89	0.85	-0.002	PATN	m	CA
43.03	39.72	0.85	7.81	1.17	1.15	-0.004	ARGI	m	CA
43.17	40.69	1.13	5.57	0.87	0.84	0.008	KARS	m	CA
43.77	40.97	1.19	6.38	1.14	1.10	0.002	AMAS	m	CA
43.89	41.54	1.33	4.36	0.82	0.79	0.001	NINO	m	CA
43.95	40.61	1.98	7.85	1.09	1.08	-0.010	ARTI	m	CA
44.11	40.18	2.35	7.53	1.09	1.08	-0.011	MMOR	m	CA
44.36	41.03	3.36	5.77	1.12	1.07	0.001	STEP	m	CA
44.50	40.23	1.58	8.66	0.90	0.89	-0.001	NSSP	m	CA
44.53	41.83	1.50	6.35	0.73	0.71	0.015	NICH	m	CA
44.74	40.15	2.92	9.49	0.81	0.73	0.004	GARN	m	CA
44.86	40.53	1.03	5.27	1.33	1.11	-0.003	GAGA	m	CA
45.14	40.91	3.99	7.26	0.80	0.78	-0.006	IJEV	m	CA
45.66	39.84	5.41	10.22	1.12	1.08	-0.009	JERM	m	CA
46.09	39.54	3.61	9.69	1.20	1.13	0.015	NORA	m	CA
46.37	39.51	5.25	11.36	1.09	1.08	-0.006	GORI	m	CA
46.46	39.32	3.16	12.33	2.29	1.68	0.052	KARM	m	CA
46.51	41.65	1.29	5.22	1.16	1.08	0.007	KATE	m	CA
46.76	40.18	3.67	10.91	1.18	1.11	0.008	KASP	m	CA
46.76	39.75	3.14	11.01	1.15	1.08	0.006	SHOU	m	CA
47.25	41.13	0.51	5.87	1.16	1.10	0.003	SHEK	m	CA
48.15	40.33	3.61	9.82	2.12	1.70	0.020	KURD	m	CA
48.39	38.95	5.16	12.65	1.20	1.12	0.002	YARD	m	CA
48.42	38.71	4.98	11.83	1.18	1.08	0.003	GOSM	m	CA
48.72	39.50	5.56	11.56	1.20	1.10	0.007	BILE	m	CA
21.88	36.79	-16.94	-23.32	1.03	0.89	0.119	XRIS	m	AE
22.82	37.18	-15.60	-28.00	1.04	0.87	0.105	LEON	m	AE
22.94	37.79	-14.97	-27.35	1.13	1.17	0.000	CG64	c	AE
22.98	36.31	-14.29	-25.64	1.04	0.88	0.100	KYRA	m	AE
23.09	37.80	-15.50	-27.95	1.87	1.71	0.000	CG65	c	AE
23.61	38.02	-12.89	-26.87	1.45	1.48	0.001	CG58	c	AE
23.85	38.23	-17.84	-26.64	1.06	1.09	0.001	CG53	c	AE
23.93	35.33	-14.40	-24.01	1.06	0.87	0.100	OMAL	m	AE
23.93	38.08	-14.24	-26.42	0.82	0.74	0.064	DION	m	AE
24.19	38.35	-13.36	-26.06	0.98	1.01	-0.002	CG55	c	AE
24.39	38.09	-14.21	-25.80	0.93	0.85	0.046	SEVA	m	AE

24.41	37.36	-16.22	-25.70	0.96	0.85	0.063	KYNS	m	AE
24.52	36.75	-15.18	-24.53	0.96	0.84	0.056	MILO	m	AE
24.69	35.40	-14.85	-26.82	0.95	0.85	0.050	ROML	m	AE
25.38	37.45	-15.17	-26.34	1.17	1.09	0.018	MKN2	m	AE
25.44	36.35	-15.11	-30.47	1.02	0.86	0.095	THIR	m	AE
26.09	38.44	-18.14	-22.87	1.03	0.90	0.062	HIOS	m	AE
26.21	35.13	-13.90	-27.91	1.04	0.88	0.081	ZAKR	m	AE
26.39	38.31	-17.42	-22.62	0.91	0.89	-0.002	CEIL	m	AE
26.41	36.59	-13.00	-29.98	0.99	0.86	0.068	ASTP	m	AE
26.93	36.75	-14.55	-26.50	1.02	0.87	0.065	KOSI	m	AE
26.99	37.78	-17.61	-23.81	1.00	0.86	0.065	SAMO	m	AE
27.09	38.02	-18.69	-19.24	1.14	1.10	0.002	OZDE	m	AE
27.42	37.03	-14.77	-25.28	1.04	1.03	-0.001	BODR	m	AE
27.49	37.82	-19.67	-19.24	1.17	1.13	-0.011	SOKE	m	AE
22.45	38.78	-7.01	-15.44	1.96	1.94	-0.009	CG19	c	GR
22.58	38.40	-8.96	-19.97	1.43	1.41	-0.004	CG32	c	GR
22.62	38.65	-11.67	-16.63	1.67	1.70	-0.009	CG20	c	GR
22.79	38.53	-11.73	-16.23	1.54	1.50	-0.007	CG29	c	GR
22.81	38.75	-6.24	-16.59	1.47	1.50	-0.015	CG21	c	GR
22.86	38.26	-13.09	-18.48	1.51	1.46	-0.003	CG45	c	GR
22.86	38.62	-8.84	-18.95	1.86	1.73	-0.007	CG24	c	GR
22.87	38.43	-13.05	-22.27	1.55	1.51	-0.005	CG33	c	GR
22.95	38.89	-7.31	-14.98	1.04	0.92	0.069	NEVA	m	GR
23.03	38.25	-15.90	-22.05	1.23	1.20	-0.004	CG46	c	GR
23.19	39.36	-3.09	-18.00	2.01	1.94	-0.015	CG05	c	GR
23.20	38.57	-10.33	-23.17	1.21	1.23	-0.009	CG28	c	GR
23.21	38.10	-16.57	-26.53	1.17	1.13	-0.002	CG49	c	GR
23.22	38.43	-11.15	-22.17	1.30	1.32	-0.005	CG34	c	GR
23.25	39.15	-6.06	-18.45	1.71	1.70	-0.012	CG10	c	GR
23.34	38.78	-12.34	-20.84	1.28	1.23	-0.009	CG26	c	GR
23.35	38.21	-13.50	-27.23	1.31	1.34	-0.002	CG50	c	GR
23.37	38.99	-8.56	-21.23	1.45	1.44	-0.007	CG17	c	GR
23.46	38.84	-9.09	-23.13	1.28	1.29	-0.004	CG27	c	GR
23.54	38.45	-14.45	-24.07	1.14	1.09	-0.003	CG35	c	GR
23.59	38.64	-12.09	-23.38	1.19	1.21	-0.002	CG36	c	GR
23.72	38.63	-14.98	-23.94	1.08	1.10	0.001	CG37	c	GR
23.74	38.43	-13.58	-23.85	1.44	1.37	0.000	CG41	c	GR
23.96	38.39	-14.09	-26.25	0.97	1.01	0.001	CG52	c	GR
24.11	38.66	-14.05	-25.89	1.13	1.09	0.005	CG38	c	GR
24.54	38.89	-11.27	-23.81	1.02	0.90	0.054	NSKR	m	NE
25.13	39.85	-13.84	-12.58	0.99	0.89	0.056	LIMN	m	NE
26.08	39.50	-18.61	-8.10	1.65	1.67	0.075	AMAN	m2	NE

26.16	39.73	-19.07	-8.77	1.54	1.56	0.062	KEST	m2	NE
26.17	39.97	-15.90	-9.55	0.93	0.86	-0.005	SUBA	m2	NE
26.19	39.61	-17.54	-9.16	1.53	1.55	0.062	BDER	m2	NE
26.22	39.73	-19.68	-10.13	1.62	1.64	0.099	KRKE	m2	NE
26.32	39.79	-18.47	-9.27	1.56	1.67	0.069	EZIN	m2	NE
26.87	40.60	-12.40	-4.14	1.49	1.60	0.130	KVAK	m2	NE
26.88	40.40	-16.27	-6.30	1.35	1.42	0.066	SEVK	m2	NE
26.91	40.03	-18.82	-8.52	1.55	1.57	0.121	BAHA	m2	NE
27.21	40.17	-18.80	-8.83	1.50	1.55	0.104	ARAK	m2	NE
27.22	39.90	-18.99	-8.02	0.87	0.83	0.036	KIRE	m2	NE
27.30	40.38	-17.37	-5.98	1.38	1.39	0.119	KABI	m2	NE
27.59	40.59	-15.00	-6.10	1.24	1.16	0.007	MISL	m2	NE
27.63	40.25	-17.75	-4.87	1.56	1.61	0.158	UKIR	m2	NE
27.76	40.06	-23.56	-3.72	1.52	1.52	0.095	KOCB	m2	NE
27.82	40.40	-18.73	-2.11	0.92	0.88	0.038	ERDE	m2	NE
28.37	40.40	-21.20	-3.28	1.05	0.96	-0.006	YENI	m2	NE
28.78	40.17	-20.28	-4.20	1.57	1.55	0.136	HAGA	m2	NE
29.02	40.17	-22.74	-1.57	1.57	1.54	0.130	YIGE	m2	NE
29.11	40.27	-21.58	-1.75	1.57	1.53	0.149	DTAS	m2	NE
29.11	40.17	-21.00	-2.33	1.58	1.55	0.131	ZEYA	m2	NE
29.14	40.64	-15.75	0.36	0.92	0.87	0.003	CINA	m2	NE
29.15	40.46	-20.49	0.39	1.64	1.57	0.154	GEML	m2	NE
29.59	40.67	-13.46	0.29	1.68	1.60	0.138	OLUK	m2	NE
29.91	40.44	-17.39	-2.38	0.99	0.99	-0.003	IGAZ	m2	NE
30.03	40.47	-17.22	-1.93	0.81	0.74	0.000	MEKE	m2	NE
30.13	40.69	-13.40	-0.41	0.92	0.90	0.008	SMAS	m2	NE
27.22	35.49	-9.16	-30.14	1.04	0.89	0.079	KRPT	m	SE
27.39	36.68	-9.19	-30.24	1.11	1.09	-0.004	KNID	m	SE
27.78	35.95	-6.44	-28.57	1.08	0.94	0.110	KATV	m	SE
27.84	37.20	-15.95	-25.05	1.14	1.11	0.001	CAMK	m	SE
27.96	36.77	-13.83	-25.67	0.92	0.88	0.003	MARM	m	SE
28.08	37.61	-19.83	-19.92	0.98	0.94	0.003	CINE	m	SE
28.43	37.18	-16.19	-21.77	1.26	1.16	-0.016	MULA	m	SE
28.83	36.76	-13.35	-20.72	1.64	1.43	-0.031	DLMN	m	SE
29.05	37.57	-22.68	-17.16	1.60	1.50	-0.009	TAVA	m	SE
29.39	37.45	-22.19	-12.29	1.62	1.51	-0.021	GKPN	m	SE
29.54	37.19	-20.81	-13.08	1.52	1.39	-0.036	YSFC	m	SE
20.67	39.73	-0.32	-2.39	1.02	0.90	0.054	KRTS	m	MA
22.54	39.94	2.85	-6.63	1.21	1.14	0.021	KRNA	m	MA
23.43	40.79	0.70	-5.32	1.06	0.91	0.080	SOXO	m	MA
23.92	39.99	2.07	-10.02	1.00	0.89	0.061	STHN	m	MA
11.65	44.52	3.06	1.15	0.81	0.81	-0.001	MEDI	m	AD

11.91	45.39	1.13	1.10	2.16	2.16	-0.001	VOLT	m	AD
12.58	45.48	0.42	0.48	2.19	2.21	-0.008	CAVA	m	AD
16.70	40.65	1.81	4.23	0.62	0.61	0.001	MATE	m	AD
18.46	40.06	9.26	4.93	1.53	1.54	-0.027	SPEC	m	AD

Table 3. Euler vectors and their 1-sigma uncertainties for Model A, Model B and other recent studies. Euler vectors for all block pairs with Eurasia and for all blocks with a common boundary are shown. The first block rotates counterclockwise relative to the second block. AF, Africa as in DeMets et al. (1994); other block abbreviations as in Figure 8.

Blocks	**Lat. (°N)**	**Lon. (°E)**	**Rate (°/Myr)**	**Ref.**
Pairs with EU				
NU-EU	-1.81 ± 1.5	-20.78 ± 1.88	0.058 ± 0.002	Model A
NU-EU	-1.01 ± 1.45	-23 ± 1.89	0.06 ± 0.002	Model B
NU-EU	-0.95 ± 4.8	-21.8 ± 4.3	0.06 ± 0.005	McClusky et al. (2003)
NU-EU	-17.77 ± 9.5	-20.38 ± 3.7	0.062 ± 0.005	Sella et al. (2002)
AF-EU	21 ± 4.2	-20.6 ± 0.6	0.12 ± 0.015	DeMets et al. (1994)
AR-EU	26.92 ± 1.76	17.87 ± 1.95	0.394 ± 0.013	Model A
AR-EU	26.97 ± 1.72	18.05 ± 1.94	0.396 ± 0.013	Model B
AR-EU	27.4 ± 1	18.4 ± 2.5	0.4 ± 0.04	McClusky et al. (2002)
AR-EU	25.6 ± 2.1	19.7 ± 4.1	0.5 ± 0.1	McClusky et al. (2000)
AR-EU	26.29 ± 2.1	22.82 ± 1.1	0.427 ± 0.029	Sella et al. (2002)
AR-EU	24.6 ± 1.6	13.7 ± 3.9	0.5 ± 0.05	DeMets et al. (1994)
AN-EU	30.89 ± 0.69	32.62 ± 0.67	1.315 ± 0.016	Model A
AN-EU	31.05 ± 0.66	32.53 ± 0.67	1.328 ± 0.015	Model B
AN-EU	30.7 ± 0.8	32.6 ± 0.4	1.2 ± 0.1	McClusky et al. (2000)
CA-EU	42.18 ± 2.89	36.75 ± 3.07	0.756 ± 0.036	Model A
CA-EU	42.06 ± 2.53	37.3 ± 2.93	0.795 ± 0.035	Model B
AE-EU	11.44 ± 3.41	60.26 ± 3.88	0.471 ± 0.029	Model A
AE-EU	-6.15 ± 4.46	76.18 ± 4.83	0.32 ± 0.02	Model B
AE-EU	-23 ± 12.2	89.55 ± 13.5	0.27 ± 0.008	Reilinger & McClusky (2001)
EU-GR	39.32 ± 2.19	20.83 ± 2.25	6.21 ± 0.245	Model A
EU-GR	39.25 ± 2.04	21.01 ± 2.03	6.688 ± 0.261	Model B
NE-EU	36.37 ± 1.39	28.48 ± 1.41	3.014 ± 0.077	Model A
NE-EU	36.29 ± 1.45	28.42 ± 1.45	2.854 ± 0.076	Model B
SE-EU	35.07 ± 1.53	31.88 ± 1.71	5.078 ± 0.144	Model A
SE-EU	34.87 ± 1.56	31.88 ± 1.71	4.521 ± 0.124	Model B
EU-MA	38.53 ± 8.18	18.31 ± 7.77	1.088 ± 0.161	Model A
EU-MA	38.52 ± 8.4	18.6 ± 7.86	1.083 ± 0.159	Model B
AD-EU	47.01 ± 7.59	6.21 ± 5.84	0.407 ± 0.055	Model A
AD-EU	46.97 ± 7.28	6.16 ± 5.72	0.409 ± 0.052	Model B

Remaining pairs with NU				
AR-NU	30.34 ± 1.96	24.67 ± 2.32	0.357 ± 0.014	Model A
AR-NU	30.22 ± 1.96	25.37 ± 2.21	0.359 ± 0.014	Model B
AR-NU	30.5 ± 1	25.7 ± 2.3	0.37 ± 0.04	McClusky et al. (2003)
AR-NU	31.26 ± 1.3	29.55 ± 1.8	0.4 ± 0.03	Sella et al. (2002)
AR-NU	31.5 ± 1.2	23 ± 2.7	0.4 ± 0.05	Chu and Gordon (1998)
AR-AF	24.1 ± 1.7	24 ± 3.5	0.4 ± 0.05	DeMets et al. (1994)
AN-NU	31.74 ± 0.68	35.07 ± 0.71	1.287 ± 0.016	Model A
AN-NU	31.84 ± 0.67	35.1 ± 0.72	1.301 ± 0.016	Model B
AE-NU	11.79 ± 3.48	67.51 ± 3.81	0.466 ± 0.027	Model A
AE-NU	-5.69 ± 4.28	86.46 ± 4.73	0.335 ± 0.021	Model B
SE-NU	35.32 ± 1.55	32.53 ± 1.71	5.05 ± 0.144	Model A
SE-NU	35.13 ± 1.51	32.65 ± 1.72	4.493 ± 0.132	Model B
AD-NU	52.83 ± 8.3	12.9 ± 7.64	0.376 ± 0.054	Model A
AD-NU	52.72 ± 8.02	13.54 ± 8.15	0.377 ± 0.053	Model B
Remaining pairs with AR				
AN-AR	32.04 ± 1.2	39.09 ± 1.31	0.936 ± 0.021	Model A
AN-AR	32.25 ± 1.22	38.85 ± 1.28	0.947 ± 0.02	Model B
AN-AR	32.9 ± 1.3	40.3 ± 1.3	0.8 ± 0.2	McClusky et al. (2000)
CA-AR	52.29 ± 5.55	63.25 ± 5.88	0.416 ± 0.038	Model A
CA-AR	51.35 ± 5	61.61 ± 5.37	0.452 ± 0.04	Model B
Remaining pairs with AN				
AN-AE	37.78 ± 2.42	16.04 ± 2.38	0.949 ± 0.041	Model A
AN-AE	37.6 ± 1.85	18.93 ± 1.8	1.179 ± 0.039	Model B
AN-AE	38 ± 0.5	19.6 ± 1.2	1.2 ± 0.2	McClusky et al. (2000)
NE-AN	40.46 ± 2.6	24.9 ± 2.48	1.714 ± 0.075	Model A
NE-AN	40.69 ± 2.73	24.42 ± 2.79	1.54 ± 0.074	Model B
SE-AN	36.53 ± 2.09	31.61 ± 2.31	3.768 ± 0.14	Model A
SE-AN	36.46 ± 2.21	31.6 ± 2.47	3.197 ± 0.126	Model B
Remaining pairs with AE				
AE-GR	37.93 ± 1.97	24.08 ± 2.12	6.554 ± 0.253	Model A
AE-GR	38.03 ± 2.02	23.8 ± 2.07	6.813 ± 0.259	Model B
AE-GR	38.3	23.7	6.75	Goldsworthy et al. (2002)
NE-AE	39.58 ± 1.73	21.66 ± 1.79	2.658 ± 0.084	Model A
NE-AE	39.38 ± 1.66	21.98 ± 1.68	2.716 ± 0.08	Model B
SE-AE	36.94 ± 1.7	28.54 ± 1.82	4.699 ± 0.148	Model A

SE-AE	36.9 ± 1.65	28.23 ± 1.81	4.362 ± 0.136	Model B
AE-AD	-28.64 ± 7.51	97.18 ± 8	0.426 ± 0.053	Model A
AE-AD	-44.07 ± 7.53	125.8 ± 8.3	0.479 ± 0.063	Model B
Remaining pairs with GR				
NE-GR	38.41 ± 1.59	23.39 ± 1.61	9.21 ± 0.266	Model A
NE-GR	38.42 ± 1.53	23.29 ± 1.52	9.528 ± 0.257	Model B
MA-GR	39.48 ± 3.09	21.37 ± 3.11	5.123 ± 0.296	Model A
MA-GR	39.39 ± 3.03	21.48 ± 3	5.605 ± 0.294	Model B
AD-GR	39.84 ± 2.22	20.03 ± 2.13	6.607 ± 0.254	Model A
AD-GR	39.74 ± 2.02	20.26 ± 2.02	7.086 ± 0.254	Model B
Remaining pairs with NE				
NE-MA	37.03 ± 2.4	25.84 ± 2.35	4.093 ± 0.187	Model A
NE-MA	36.98 ± 2.46	25.78 ± 2.49	3.929 ± 0.173	Model B
Remaining pairs with MA				
AD-MA	40.95 ± 6.29	15.35 ± 5.84	1.488 ± 0.17	Model A
AD-MA	40.95 ± 6.5	15.53 ± 5.91	1.485 ± 0.167	Model B

Table 4. Earthquakes used to determine seismic moment rates for the Dead Sea Fault, East Anatolian Fault, North Anatolian Fault, Aegean-western Turkey, Hellenic Arc, Cyprus Arc, eastern Turkey and the Caucasus.

Date	Lat. (°N)	Lon. (°E)	M_S	M_0^{CMT}	M_0^c	M_0^g	Ref.
			Dead Sea Fault (28-36.6°N; 995-2002 CE)				
1033/12/05	32.50	35.50	L		813	2455	aj
1157/08/12	35.00	36.50	V		3236	9772	aj
1170/06/29	35.50	36.50	L		813	2455	aj
1202/05/20	33.70	35.90	L		813	2455	aj
1404/02/22	35.90	36.30	L		813	2455	w
1407/04/29	35.70	36.30	m		55	82	w
1408/12/29	36.00	36.40	m		55	82	aj
1759/10/30	33.10	35.60	m		55	82	w
1759/11/25	33.70	35.90	7.4		575	1738	aj
1796/04/26	35.50	36.00	6.6		69	113	aj
1837/01/01	33.20	35.50	7.4		575	1738	aj
1872/04/03	36.40	36.40	7.2		288	871	aj
1927/07/11	32.00	35.50	6		17	20	jm
1993/08/03	28.62	34.40	5.7	18	9	9	cmt
1993/08/03	28.36	34.08	5.1	5	2	2	cmt
1995/11/22	29.07	34.73	7.3	721	407	1230	cmt
1995/11/23	29.31	34.48	5.2	4	3	3	cmt
totals				748	8598	25562	
			East Anatolian Fault (36.6-39°N; 995-2002 CE)				
995/--/--	38.70	40.00	L		813	2455	aj
1114/11/29	37.50	37.50	V		3236	9772	aj
1513/--/--	37.50	36.50	L		813	2455	tej
1544/01/22	38.00	37.00	m		55	82	aj
1685/11/22	39.00	41.00	m		55	82	tej
1789/05/28	38.80	39.50	L		813	2455	aj
1822/08/13	36.70	36.50	7.5		813	2455	aj
1866/05/12	39.20	41.00	7.2		288	871	aj
1874/05/03	38.50	39.50	7.1		219	617	aj
1875/03/27	38.50	39.50	6.7		87	155	aj

1893/03/02	38.00	38.30	7.1		219	617	aj
1905/12/04	38.10	38.60	6.8		110	217	aj
1945/03/20	37.00	35.60	6		17	20	jm
1971/05/22	38.83	40.52	6.8		110	217	jm, aj
1975/09/06	38.50	40.70	6.6		69	113	aj
1986/05/05	37.72	37.70	5.9	14	14	15	cmt
1986/06/06	37.36	37.99	5.6	6	7	7	cmt
1989/05/20	38.87	40.01	5.1	2	2	2	cmt
totals				22	7740	22607	

North Anatolian Fault (31-41°E; 1668-2002 CE)

1668/08/17	40.50	36.00	7.9		3236	9772	aj
1784/07/18	39.50	40.20	7.6		1148	3467	aj
1909/02/09	40.20	37.80	6.4		44	61	jm, aj
1910/06/25	40.90	34.60	6.3		35	45	jm
1916/01/24	40.10	36.60	7.2		288	871	jm, aj
1919/06/09	40.70	34.10	6		17	20	jm
1924/09/13	40.00	42.00	6.9		138	309	jm
1929/05/18	40.00	38.00	6.1		22	26	jm
1939/12/26	39.70	39.40	7.8		2291	6918	jm, aj
1942/12/20	40.70	36.40	7.1		219	617	jm
1943/11/26	41.00	33.40	7.4		575	1738	jm, aj
1944/02/01	41.10	33.20	7.3		407	1230	jm, aj
1949/08/17	39.40	40.90	6.9		138	309	jm, aj
1951/08/13	40.90	33.20	6.9		138	309	jm
1953/09/07	40.90	33.10	6		17	20	jm
1957/05/26	40.61	31.27	7		174	437	jm, aj
1957/05/26	40.61	31.27	6		17	20	jm
1966/08/19	39.17	41.56	6.8		110	217	jm
1967/07/22	40.60	30.80	7.1		219	617	jm, aj
1967/07/26	39.50	40.40	6		17	20	jm
1968/09/03	41.79	32.31	6.5		55	82	jm
1977/10/05	40.39	33.62	5.8	6	11	12	cmt
1992/03/13	39.94	39.57	6.8	116	110	217	cmt
1992/03/15	39.52	39.84	5.8	8	11	12	cmt
1996/08/14	40.52	35.02	5.6	5	7	7	cmt
1996/08/14	40.86	35.18	5.5	4	5	6	cmt
1999/11/12	40.93	31.25	7.5	665	665*	665*	cmt
2000/06/06	40.75	32.70	6.1	11	22	26	cmt
totals				815	10136	28050	

Aegean and western Turkey (36-41°N; 21-31°E; 1909-2002 CE)

1909/01/19	38.70	26.90	6	17	20	jhh
1911/02/18	41.10	20.70	6.7	87	155	jhh
1912/08/09	40.75	27.20	7.4	575	1738	jhh
1912/08/10	40.75	27.20	6.3	35	45	jhh
1912/12/13	40.10	26.80	6.9	138	309	jhh
1914/10/03	37.90	30.40	7	174	437	jhh
1914/10/17	38.20	23.50	6.2	28	34	jhh
1915/06/04	39.10	21.40	6.1	22	26	jhh
1919/11/18	39.10	27.40	6.9	138	309	jhh
1923/12/05	39.90	23.20	6.4	44	61	jhh
1924/11/20	39.08	30.14	6	17	20	jhh
1925/08/07	37.90	29.60	6	17	20	jhh
1926/08/30	36.80	23.20	6.6	69	113	jhh
1927/07/01	36.78	22.25	6.3	35	45	jhh
1928/03/31	38.20	27.40	6.5	55	82	jhh
1928/04/14	42.00	25.00	6.8	110	217	jhh
1928/04/18	42.00	24.70	7	174	437	jhh, aj
1928/04/22	38.00	23.00	6.3	35	45	jhh
1928/05/02	39.41	29.45	6.2	28	34	jhh
1930/03/01	39.60	23.20	6	17	20	jhh
1931/03/08	41.30	22.50	6.7	87	155	jhh
1932/12/26	40.50	23.90	6.9	138	309	jhh
1932/12/29	40.50	23.70	6.2	28	34	jhh
1933/04/23	36.70	27.40	6.5	55	82	jhh
1933/05/11	40.50	23.70	6.3	35	45	jhh
1935/01/04	40.70	27.60	6.4	44	61	jhh
1938/07/20	38.30	23.80	6.1	22	26	jhh
1939/12/22	39.10	27.00	6.5	55	82	jhh
1941/03/01	39.70	22.40	6.1	22	26	jhh
1941/05/23	37.20	28.20	6	17	20	jhh
1941/08/27	41.70	20.40	6	17	20	jhh
1942/11/15	39.38	28.10	6.2	28	34	jhh
1943/06/20	40.68	30.47	6.4	44	61	jhh
1944/06/25	38.90	29.26	6	17	20	jhh
1944/10/06	39.70	26.80	6.8	110	217	jhh
1947/10/06	36.80	22.00	6.9	138	309	jhh
1948/12/11	37.20	23.20	6.5	55	82	jhh
1949/07/23	38.70	26.70	6.6	69	113	jhh
1953/03/18	40.00	27.40	7.3	407	1230	jhh, aj
1954/04/30	39.30	22.20	6.7	87	155	jhh

1955/04/19	39.30	23.10	6.2		28	34	jhh
1955/07/16	37.60	27.25	6.7		87	155	jhh
1956/02/20	39.96	30.11	6.1		22	26	jhh
1956/07/09	36.70	25.80	7.2		288	871	jhh
1957/03/08	39.40	22.70	6.5		55	82	jhh
1957/03/08	39.40	22.70	6.6		69	113	jhh
1957/05/26	40.58	31.00	7		174	437	jhh
1963/12/18	40.90	29.20	6.4		44	61	jhh
1964/10/06	40.10	28.00	6.8		110	217	jhh, aj
1965/03/09	39.40	24.00	6.5		55	82	jhh
1965/07/06	38.40	22.40	6.4		44	61	jhh
1966/02/05	39.07	21.72	6.2		28	34	jhh
1967/03/04	39.20	24.60	6.8		110	217	jhh
1967/05/01	39.45	21.20	6.2		28	34	jhh
1967/07/22	40.67	30.69	7.1		219	617	jhh
1967/11/30	41.30	20.40	6.6		69	113	jhh
1968/02/19	39.40	25.00	7.3		407	1230	jhh
1969/03/03	40.08	27.50	6		17	20	jhh
1969/03/25	39.18	28.37	6.1		22	26	jhh
1969/03/28	38.59	28.45	6.5		55	82	jhh
1970/03/28	39.18	29.49	7.1		219	617	jhh
1970/04/08	38.43	22.66	6.2		28	34	jhh
1971/05/12	37.65	29.72	6.2		28	34	jhh
1975/03/27	40.42	26.14	6.7		87	155	jhh
1977/11/03	41.46	23.85	5.1	3	2	2	cmt
1978/05/23	39.85	23.19	5.6	6	7	7	cmt
1978/06/20	40.73	23.25	6.4		44	61	jhh, aj
1979/06/14	37.58	26.40	5.6	6	7	7	cmt
1979/06/16	38.46	26.77	5.1	1	2	2	cmt
1980/07/09	38.58	22.71	6.4	87	44	61	cmt
1980/07/10	39.00	23.09	5.3	3	3	3	cmt
1981/02/24	38.07	23.04	6.7	90	87	155	cmt
1981/02/25	37.87	22.91	6.4	38	44	61	cmt
1981/03/04	37.93	23.25	6.4	28	44	61	cmt
1981/03/05	37.77	23.01	5.2	2	3	3	cmt
1981/06/28	37.60	20.01	5.2	2	3	3	cmt
1981/12/19	38.81	25.27	7.2	228	288	871	cmt
1981/12/27	38.67	24.89	6.5	33	55	82	cmt
1981/12/29	38.38	25.06	5.3	1	3	3	cmt
1982/01/18	39.56	24.47	6.8	86	110	217	cmt
1982/06/22	37.44	21.41	5.4	2	4	4	cmt
1983/01/17	38.13	20.38	7	235	174	437	cmt

1983/01/19	37.88	20.90	5.6	6	7	7	cmt
1983/01/31	38.35	21.28	5	1	2	2	cmt
1983/03/23	37.92	20.48	6.2	22	28	34	cmt
1983/03/24	38.58	20.54	5	1	2	2	cmt
1983/05/14	38.06	20.55	5.3	1	3	3	cmt
1983/08/06	39.89	24.66	7.1	116	219	617	cmt
1983/10/10	40.18	25.76	5.1	1	2	2	cmt
1983/10/21	40.54	30.05	5	2	2	2	cmt
1984/02/11	38.11	21.86	5.4	3	4	4	cmt
1984/05/06	38.66	25.57	5.3	2	3	3	cmt
1984/06/17	38.86	25.72	6.1	1	22	26	cmt
1985/04/30	39.06	23.15	5.6	3	7	7	cmt
1985/09/07	37.35	21.53	5.1	2	2	2	cmt
1985/11/09	41.24	24.12	5.3	1	3	3	cmt
1986/03/25	38.54	25.14	5.4	2	4	4	cmt
1986/09/13	36.80	22.64	5.9	10	14	15	cmt
1986/10/11	37.31	28.71	5.5	4	5	6	cmt
1987/02/27	38.51	21.02	5.5	5	5	6	cmt
1988/10/16	37.95	20.90	5.8	7	11	12	cmt
1989/03/19	38.61	23.53	5.3	1	3	3	cmt
1989/04/27	36.71	27.75	5	2	2	2	cmt
1989/09/05	39.12	25.66	5	2	2	2	cmt
1990/06/16	38.70	20.44	5.4	3	4	4	cmt
1990/12/21	40.27	22.28	5.9	17	14	15	cmt
1991/06/26	38.42	21.17	5.1	1	2	2	cmt
1992/01/23	38.22	19.97	5.2	3	3	3	cmt
1992/03/20	36.85	24.16	5	1	2	2	cmt
1992/04/30	35.04	26.20	5.7	5	9	9	cmt
1992/07/23	39.88	24.68	5.1	2	2	2	cmt
1992/11/06	37.84	26.98	6	14	17	20	cmt
1992/11/18	38.09	22.60	5.7	9	9	9	cmt
1993/03/18	38.05	21.79	5.3	6	3	3	cmt
1993/03/26	37.61	21.18	5.2	2	3	3	cmt
1993/07/14	38.17	21.67	5.5	3	5	6	cmt
1993/11/04	38.12	22.03	5.2	1	3	3	cmt
1994/01/28	38.97	27.01	5.2	2	3	3	cmt
1994/02/25	38.63	20.50	5.1	1	2	2	cmt
1994/05/24	38.66	26.23	5.4	2	4	4	cmt
1994/11/13	37.12	28.02	5	1	2	2	cmt
1995/05/04	40.30	23.60	5.1	1	2	2	cmt
1995/05/13	39.89	21.90	6.5	76	55	82	cmt
1995/05/19	39.98	21.58	5	1	2	2	cmt

1995/06/15	38.10	22.46	6.5	60	55	82	cmt
1995/10/01	38.06	29.68	6.1	47	22	26	cmt
1996/04/02	37.83	26.94	5.1	2	2	2	cmt
1996/07/20	36.07	26.92	6.2	24	28	34	cmt
1996/07/26	39.92	20.77	5.2	1	3	3	cmt
1997/11/05	38.11	22.49	5.4	3	4	4	cmt
1997/11/14	38.74	25.77	5.8	7	11	12	cmt
1998/10/06	37.85	20.48	5.2	1	3	3	cmt
1999/08/17	41.01	29.97	7.8	2880	2880*	2880*	cmt
1999/09/07	37.87	23.64	5.8	11	11	12	cmt
1999/09/13	40.31	30.29	5.8	6	11	12	cmt
1999/11/11	40.95	30.10	5.5	4	5	6	cmt
2000/06/13	35.16	26.74	5	2	2	2	cmt
2000/12/15	38.40	31.35	5.8	12	11	12	cmt
2001/06/10	38.32	25.66	5.4	3	4	4	cmt
2001/07/26	38.96	24.29	6.6	56	69	113	cmt
2001/09/16	37.24	21.85	5.3	2	3	3	cmt
2002/02/03	38.62	31.21	6.4	60	44	61	cmt
2002/02/03	38.23	30.56	5.6	6	7	7	cmt
2002/12/02	37.70	21.42	5.4	3	4	4	cmt
totals				4387	10184	18864	

Hellenic Arc (20-29°E; 1909-2002 CE)

1912/01/24	38.20	20.50	6.8	110	217	jm
1914/11/27	38.50	20.50	6.2	28	34	jm
1915/01/27	38.50	20.50	6.4	44	61	jm
1915/08/07	38.50	20.50	6.6	69	113	jm
1919/02/24	36.70	21.00	6.4	44	61	jm
1922/08/11	34.90	27.20	6.5	55	82	jm
1922/08/13	35.50	27.80	6.7	87	155	jm
1926/03/18	35.90	29.90	6.9	138	309	jm
1926/06/26	36.00	28.00	7	174	437	jm
1927/07/01	36.70	22.40	6.3	35	45	jm
1937/12/16	35.00	23.50	6.3	35	45	jm
1940/02/29	35.50	25.50	6	17	20	jm
1947/08/30	35.10	23.40	6.4	44	61	jm
1947/10/06	36.80	21.80	6.8	110	217	jm
1948/02/09	35.50	27.20	7.1	219	617	jm
1948/04/22	38.70	20.40	6.6	69	113	jm
1948/06/30	38.90	20.50	6.4	44	61	jm
1948/07/24	34.60	24.50	6.3	35	45	jm

1952/12/17	24.50	24.40	6.5		55	82	jm
1953/08/09	38.10	20.70	6.2		28	34	jm
1953/08/11	38.10	20.70	6.5		55	82	jm
1953/08/12	38.10	20.70	7.1		219	617	jm
1953/08/12	38.10	20.70	6.1		22	26	jm
1953/10/21	28.30	20.80	6.1		22	26	jm
1955/09/12	32.20	29.60	6.1		22	26	jm
1957/04/24	36.10	29.00	6.5		55	82	jm
1957/04/25	36.50	28.80	7		174	437	jm
1958/08/27	37.45	20.72	6.4		44	61	jm
1959/05/14	35.00	24.80	6		17	20	jm
1959/11/15	37.83	20.47	7		174	437	jm
1965/04/05	37.70	21.80	6		17	20	jm
1969/01/14	36.18	29.20	6.2		28	34	jm
1969/06/12	34.40	25.06	6		17	20	jm
1972/09/17	38.28	20.34	6.5		55	82	jm
1976/05/11	37.56	20.35	6.4		44	61	jm
1977/08/18	35.27	24.08	5.3	4	3	3	cmt
1977/09/11	34.51	22.99	6	6	17	20	cmt
1978/03/07	34.19	25.45	5.1	2	2	2	cmt
1979/05/15	34.38	24.80	5.6	15	7	7	cmt
1979/06/15	34.82	24.42	5.2	1	3	3	cmt
1982/08/17	33.70	22.90	6.5	40	55	82	cmt
1983/07/14	36.51	21.37	5	1	2	2	cmt
1984/06/21	35.74	23.80	5.8	22	11	12	cmt
1985/04/21	35.35	22.41	5.1	1	2	2	cmt
1986/05/22	34.12	26.72	5.2	2	3	3	cmt
1988/09/05	34.51	26.65	5	1	2	2	cmt
1989/03/17	34.51	25.53	5.2	4	3	3	cmt
1989/06/14	34.30	26.10	5.1	2	2	2	cmt
1989/08/20	36.95	21.15	5.7	6	9	9	cmt
1990/07/09	34.45	26.24	5	2	2	2	cmt
1991/03/19	34.60	26.13	5.4	3	4	4	cmt
1993/03/05	36.90	21.41	5	1	2	2	cmt
1994/01/11	35.70	21.58	5.4	2	4	4	cmt
1994/04/16	36.99	19.99	5	2	2	2	cmt
1997/10/13	36.10	22.04	6.6	50	69	113	cmt
1997/11/18	37.33	20.84	6.4	90	44	61	cmt
1998/01/10	37.21	20.84	5.1	2	2	2	cmt
1998/04/29	36.03	22.01	5.3	2	3	3	cmt
1999/04/17	35.60	21.27	5	1	2	2	cmt
2000/03/10	34.13	25.98	5.1	1	2	2	cmt

2000/04/05	34.08	25.83	5.4	2	4	4	cmt
2000/05/24	35.80	21.95	5.6	4	7	7	cmt
totals				269	2673	5200	

Cyprus Arc (29-36.5°E; 1909-2002 CE)

1918/09/27	35.20	34.70	6.2		28	34	jm
1953/09/10	34.80	32.30	6.3		35	45	jm
1980/05/02	35.99	30.16	5.2	7	3	3	cmt
1993/03/22	34.74	34.41	5	1	2	2	cmt
1995/02/23	35.02	32.44	5.7	8	9	9	cmt
1995/05/29	34.89	32.63	5	1	2	2	cmt
1996/10/09	34.50	32.09	6.8	185	110	217	cmt
1996/10/10	34.58	31.34	5.6	5	7	7	cmt
1996/10/10	34.75	32.03	5	1	2	2	cmt
1997/01/13	34.09	31.74	5.4	4	4	4	cmt
1997/01/22	36.01	35.77	5.4	4	4	4	cmt
1998/06/27	36.87	35.58	6.2	30	28	34	cmt
1999/08/11	34.42	32.68	5.4	3	4	4	cmt
totals				249	238	367	

Eastern Turkey (39-40°N; 41-44°E; 1911-2002 CE)

1935/05/01	40.50	43.30	6.2		28	34	j
1952/01/03	39.90	41.60	6		17	20	j
1966/08/19	39.17	41.56	6.8		110	217	j
1976/11/24	39.12	43.92	7.4		575	1738	j
1988/06/25	38.44	43.08	5	2	2	2	cmt
totals				2	732	2011	

Caucasus (40-44°N; 41-48.5°E; 1911-2002 CE)

1911/07/07	41.00	50.80	6.2		28	34	j
1920/02/20	42.00	44.10	6.2		28	34	j
1931/10/20	42.00	50.80	6.3		35	45	j
1935/04/09	42.20	48.80	6.3		35	45	j
1940/05/07	41.70	43.80	6		17	20	j
1948/06/29	41.90	46.40	6.1		22	26	j
1963/07/16	43.10	41.50	6.5		55	82	j
1970/05/14	43.03	47.09	6.5		55	82	j
1976/07/28	43.17	45.60	6.1		22	26	j
1978/01/02	41.23	44.03	5.1	3	2	2	cmt

1978/05/26	41.29	46.56	5.2	2	3	3	cmt
1981/10/18	43.25	44.99	5.7	3	9	9	cmt
1983/10/30	40.47	42.05	6.9	87	138	309	cmt
1983/10/30	39.97	41.94	5.2	2	3	3	cmt
1984/09/18	40.62	42.39	5.6	2	7	7	cmt
1985/07/04	42.33	46.52	5.1	2	2	2	cmt
1986/05/13	41.03	43.92	5.4	5	4	4	cmt
1988/05/03	42.22	47.83	5	1	2	2	cmt
1988/12/07	41.10	44.36	6.8	162	110	217	cmt
1990/12/16	40.53	43.18	5	2	2	2	cmt
1991/04/29	42.60	43.61	7	334	174	437	cmt
1991/04/29	42.38	43.75	6.1	16	22	26	cmt
1991/05/03	42.54	42.94	5.3	3	3	3	cmt
1991/06/15	42.58	43.07	6.1	29	22	26	cmt
1992/10/23	42.67	45.01	6.5	49	55	82	cmt
1997/11/27	42.32	45.19	5.2	1	3	3	cmt
1999/01/31	43.56	47.14	5.4	4	4	4	cmt
1999/06/04	40.58	47.62	5	2	2	2	cmt
1999/12/03	40.61	42.40	5.5	4	5	6	cmt
totals				713	869	1543	

Seismic moment, M_0, is in units of 10^{17} N m. Surface-wave magnitudes, M_S, of historical and recent earthquakes are taken from the references. M_0^g and M_0^c are seismic moments calculated with the global M_S - M_0 relations of Ekström and Dziewonski (1988) and the continental M_S - M_0 relations of Ekström (1987), respectively. M_0^{CMT} are observed seismic moments in the Harvard CMT catalog (2003) from 1977 through 2002. Historical earthquakes designated very large (V), large (L), or medium (m), e.g., Ambraseys and Jackson (1998), are assigned M_S 7.9, 7.5, or 6.5, respectively. *, M_0^{CMT} used in place of M_0^g or M_0^c due to anomalously high M_S values in the Aegean region, e.g., Ekström and Dziewonski (1988).

References are abbreviated as follows: jm, Jackson and McKenzie (1988); tej, Taymaz et al. (1991b); j, Jackson (1992); jhh, Jackson et al. (1992); w, Westaway (1994); Ambraseys and Jackson (1998); cmt, Harvard CMT catalog (2003).

Table 5. Preliminary comparison of observed seismic moment rates and model moment rates by region.

Region	$\dot{M}_0$**(obs)**	$\dot{M}_0$**(A)**	$\dot{M}_0$**(obs) : $\dot{M}_0$(A)**	$\dot{M}_0$**(B)**	$\dot{M}_0$**(obs) : $\dot{M}_0$(B)**
Dead Sea Fault (28-36.6°N)	25.6 8.6[c]	31.3 ± 5	82 % 27 %[c]	29.6 ± 4.8	86 % 29 %[c]
East Anatolian Fault (36.6-39°N)	22.6 7.7[c]	25.8 ± 4.6	88 % 30 %[c]	25.1 ± 4.4	90 % 31 %[c]
North Anatolian Fault (31-41°E)	85 30.7[c]	106 ± 16	80 % 29 %[c]	105.9 ± 16	80 % 29 %[c]
Aegean and western Turkey (36-41°N; 21-31°E)	200.7 108.3[c]	261.1 ± 18	77 % 41 %[c]	231.2 ± 16.7	87 % 47 %[c]
Hellenic Arc (20-29°E)	55.3 28.4[c]	390 ± 56.6	14 % 7 %[c]	97.0 ± 52.8	57 % 29 %[c]
Cyprus Arc (29-36.5°E)	3.9 2.5[c]	76 ± 14.6	5 % 3 %[c]	32.3 ± 14.5	12 % 8 %[c]
Eastern Turkey (39-40°N; 41-44°E)	21.9 8[c]	23.1 ± 6.4	95 % 34 %[c]	23.3 ± 6.5	94 % 34 %[c]
Caucasus (40-44°N; 41-48.5°E)	16.8 9.4[c]	55 ± 8.8 60.0 ± 8.7[b]	31 % 28 %[b] 17 %[c] 16 %[b,c]	23.2 ± 8.7 19.6 ± 8.6[b]	72 % 86 %[b] 41 %[c] 48 %[b,c]

$\dot{M}_0$ is in units of 10^{17} N m/yr. Data used to calculate observed seismic moment rates are from Jackson and McKenzie (1988), Taymaz et al. (1991b), Jackson (1992), Jackson et al. (1992), Westaway (1994), Ambraseys and Jackson (1998), and the Harvard CMT catalog (2003). Seismic moment rates are calculated with the global M_S-M_0 relations of Ekström and Dziewonski (1988) unless otherwise noted. c, seismic moments calculated with continental M_S-M_0 relations of Ekström (1987); b, including a Black Sea block.

In model A, all locking depths are 15 km. In model B, the locking depths on the Marmara Fault, Hellenic Arc, Cyprus Arc and in the Greater Caucasus are 5 km, 4 km, 4 km, and 4 km, respectively; all other locking depths are 15 km. An uncertainty of ± 5 km is assumed in locking depth.

The seismic moment rates of the DSF and EAF are 1000-year averages of instrumental and pre-instrumental seismic moments. The seismic moment rate of the NAF is the 330-year average of instrumental and pre-instrumental seismic moments. The seismic moment rates for the Aegean-western Turkey, Hellenic Arc, and Cyprus Arc are 94-year averages of instrumental seismic moments. The seismic moment rates for eastern Turkey and the Caucasus are 92-year averages of instrumental seismic moments.

Figure captions

Figure 1. Tectonic, topographic and bathymetric map of the eastern Mediterranean region. Solid lines are strike-slip faults, lines with tick marks are normal faults with ticks on the upper block, and lines with triangles are thrust faults with triangles on the upper block. B, Buyuk Menderes graben; G, Gediz graben; GA, Gulf of Aqaba; GC, Gulf of Corinth; GG, Gulf of Gokova; GI, Gulf of Iskenderun; GS, Gulf of Suez; KFZ, Kephalonia fault zone; KTJ, Karliova triple junction; NAT, North Aegean Trough. After Plate 1 of McClusky et al., 2000.

Figure 2. Focal mechanisms (lower hemisphere projection; compressional quadrants shaded) for large (M_W > 6.0), shallow (depth < 50 km) earthquakes (Jackson and McKenzie, 1988; http://www.seismology.harvard.edu/CMTsearch.html). Tectonic symbols are as in Figure 1.

Figure 3. Epicenters of shallow (depth < 50 km) earthquakes (M_W > 4) (http://neic.usgs.gov/neis/epic/epic.html). Tectonic symbols are as in Figure 1.

Figure 4. GPS velocities used in this study and their 95% confidence ellipses in a Eurasia-fixed frame. Velocities are for the period 1988-2002, based on results from S. McClusky (pers. com., 2003), Meade et al. (2002), and Clarke et al. (1998). Tectonic symbols are as in Figure 1.

Figure 5. Expanded view of GPS velocities in eastern Turkey, the Caucasus and the Near East and their 95% confidence ellipses in a Eurasia-fixed frame. Tectonic symbols are as in Figure 1.

Figure 6. Expanded view of GPS velocities in the Aegean region and their 95% confidence ellipses in a Eurasia-fixed frame. Tectonic symbols are as in Figure 1.

Figure 7. (a) Diagram showing that the long-term, geologic displacement field of adjacent blocks is the sum of the interseismic and coseismic displacement fields. (b) Illustration showing that relative motion is independent of integration path. Two adjacent blocks move relative to a fixed, exterior block. Large arrows show the magnitude and direction of each block's motion. Small arrows show the relative sense of motion on block boundaries. Thick lines connecting P1 and P2 show possible integration paths. The sum of slip components on any path between P1 and P2 gives the same total (i.e., zero, in this example). From Figure 2 in Meade et al., 2002.

Figure 8. Blocks and block boundaries used in this study. EU, Eurasia; NU, Nubia; AR, Arabia; AN, Anatolia; CA, Caucasus; AE, South Aegea; NE, North Aegea; GR, Central Greece; SE, Southeast Aegea; MA, Macedonia; AD, Adria.

Figure 9. Model misfit as a function of locking depth for four independent experiments: R, varying the locking depth on all boundaries in the region; M, varying the locking depth on the Marmara Fault with all other locking depths set to 15 km; H, varying the

locking depth on the Hellenic Arc with all other locking depths set to 15 km; and C, varying the locking depth on the Greater Caucasus Thrust with all other locking depths set to 15 km.

Figure 10. Residual (observed - model) velocities for Model B in eastern Turkey, the Caucasus and the Near East and the 95% confidence ellipses of the observations in a Eurasia-fixed frame.

Figure 11. Residual (observed - model) velocities for Model B in the Aegean region and the 95% confidence ellipses of the observations in a Eurasia-fixed frame.

Figure 12. Euler poles and their error ellipses for Model B: global scale. All Euler poles relative to Eurasia and other selected Euler poles for block pairs with a common boundary are shown. The first block rotates counterclockwise relative to the second block. The Euler poles are as in Table 3.

Figure 13. Euler poles and their error ellipses for Model B: regional scale. Selected Euler poles relative to Eurasia and other selected Euler poles for block pairs with a common boundary are shown. The first block rotates counterclockwise relative to the second block. The Euler poles are as in Table 3.

Figure 14. Euler poles and their error ellipses for Model B: Aegean region. Selected Euler poles relative to Eurasia and other selected Euler poles for block pairs with a common

boundary are shown. The first block rotates counterclockwise relative to the second block. Euler poles are as in Table 3.

Figure 15. Strike-slip rates (mm/yr) for Model B in eastern Turkey, the Caucasus and the Near East. Positive rates are for left-lateral motion, and negative rates are for right-lateral motion. Slip rates shown in parentheses are for a model including a Black Sea block. The symbol "EU" emphasizes that Iran is unrealistically treated as part the Eurasian block.

Figure 16. Horizontal strike-normal slip rates (mm/yr) for Model B in eastern Turkey, the Caucasus and the Near East. Positive rates are for shortening, and negative rates are for extension. Slip rates shown in parentheses are for a model including a Black Sea block. The symbol "EU" is as in Figure 15.

Figure 17. Strike-slip rates (mm/yr) for Model B in the Aegean region. Positive rates are for left-lateral motion, and negative rates are for right-lateral motion.

Figure 18. Horizontal strike-normal slip rates (mm/yr) for Model B in the Aegean region. Positive rates are for shortening, and negative rates are for extension.

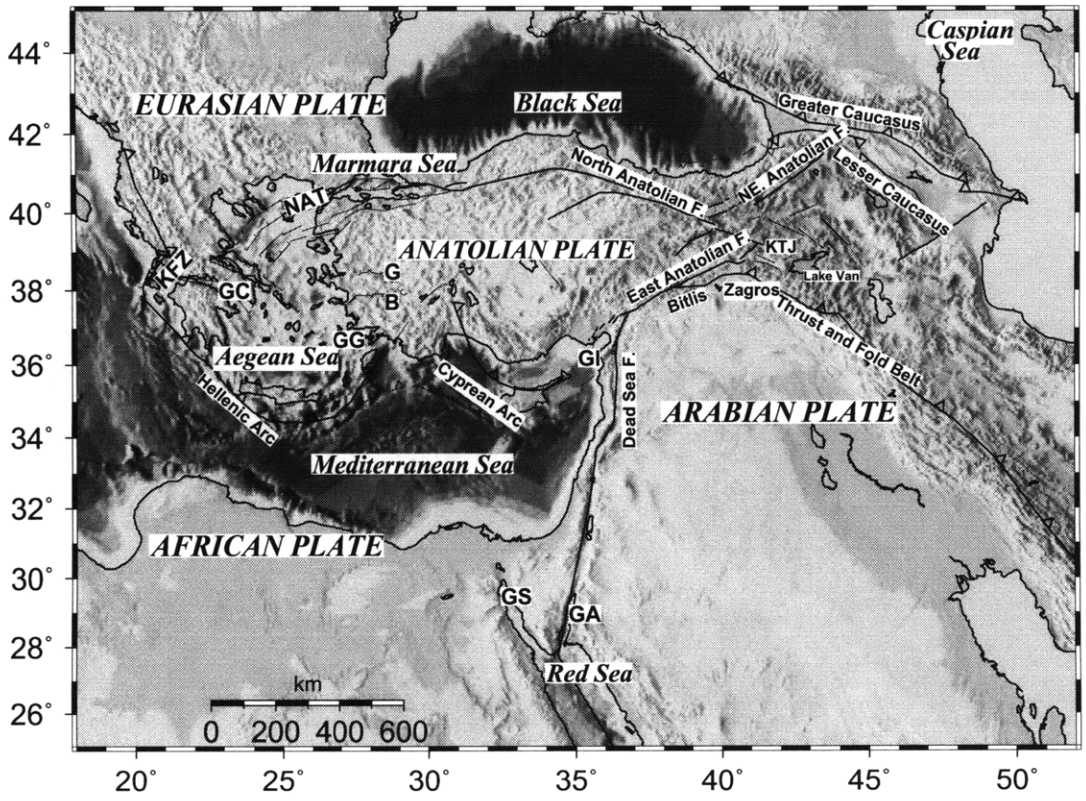
Caspian Sea
EURASIAN PLATE
Black Sea
Greater Caucasus
Marmara Sea
North Anatolian F.
NE. Anatolian F.
Lesser Caucasus
NAT
ANATOLIAN PLATE
KTJ
Lake Van
East Anatolian F.
KFZ
GC
G
B
Bitlis
Zagros
Thrust and Fold Belt
GG
Aegean Sea
GI
Cyprean Arc
Hellenic Arc
Dead Sea F.
ARABIAN PLATE
Mediterranean Sea
AFRICAN PLATE
GS
GA
Red Sea
km
0 200 400 600
44°
42°
40°
38°
36°
34°
32°
30°
28°
26°
20°
25°
30°
35°
40°
45°
50°

Figure 1

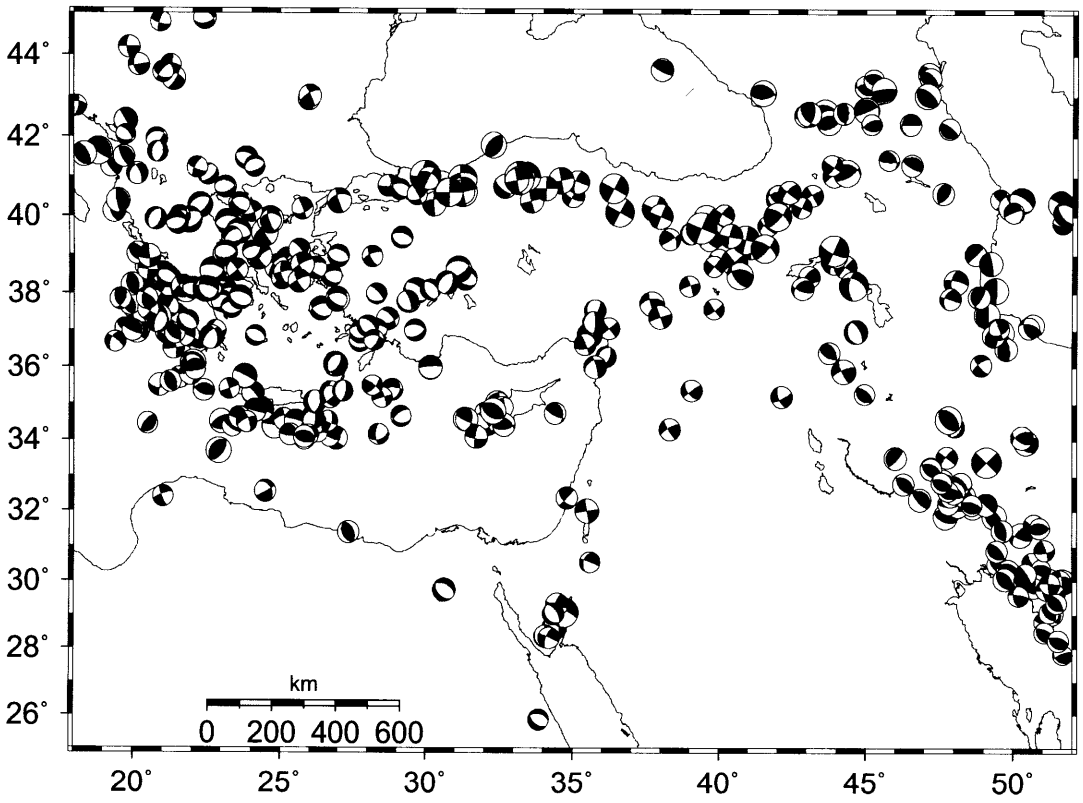

Figure 2

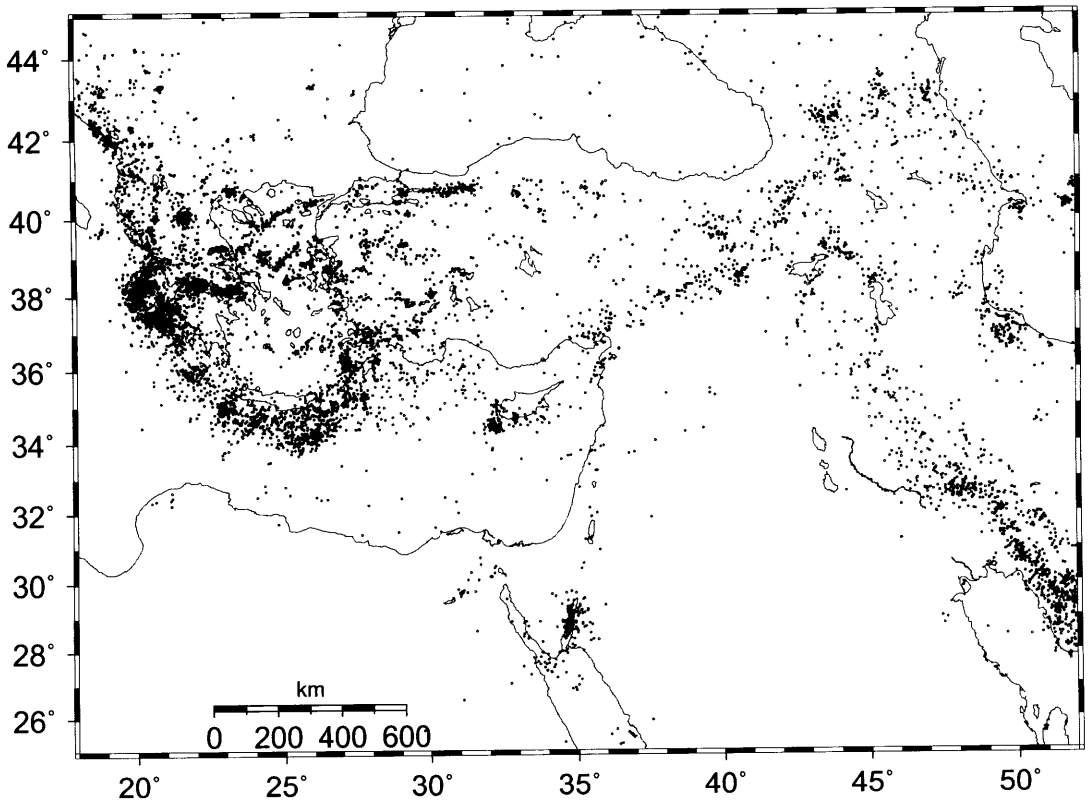

Figure 3

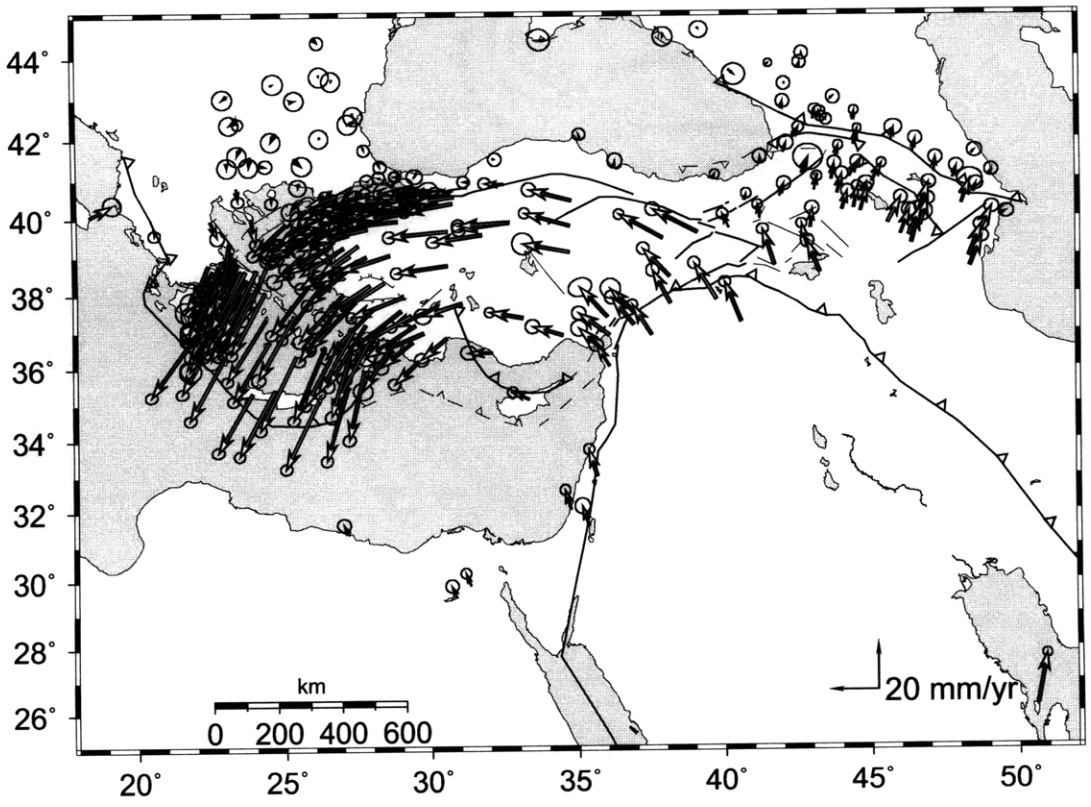
44°
42°
40°
38°
36°
34°
32°
30°
28°
26°
20°
25°
30°
35°
40°
45°
50°
km
0 200 400 600
20 mm/yr

Figure 4

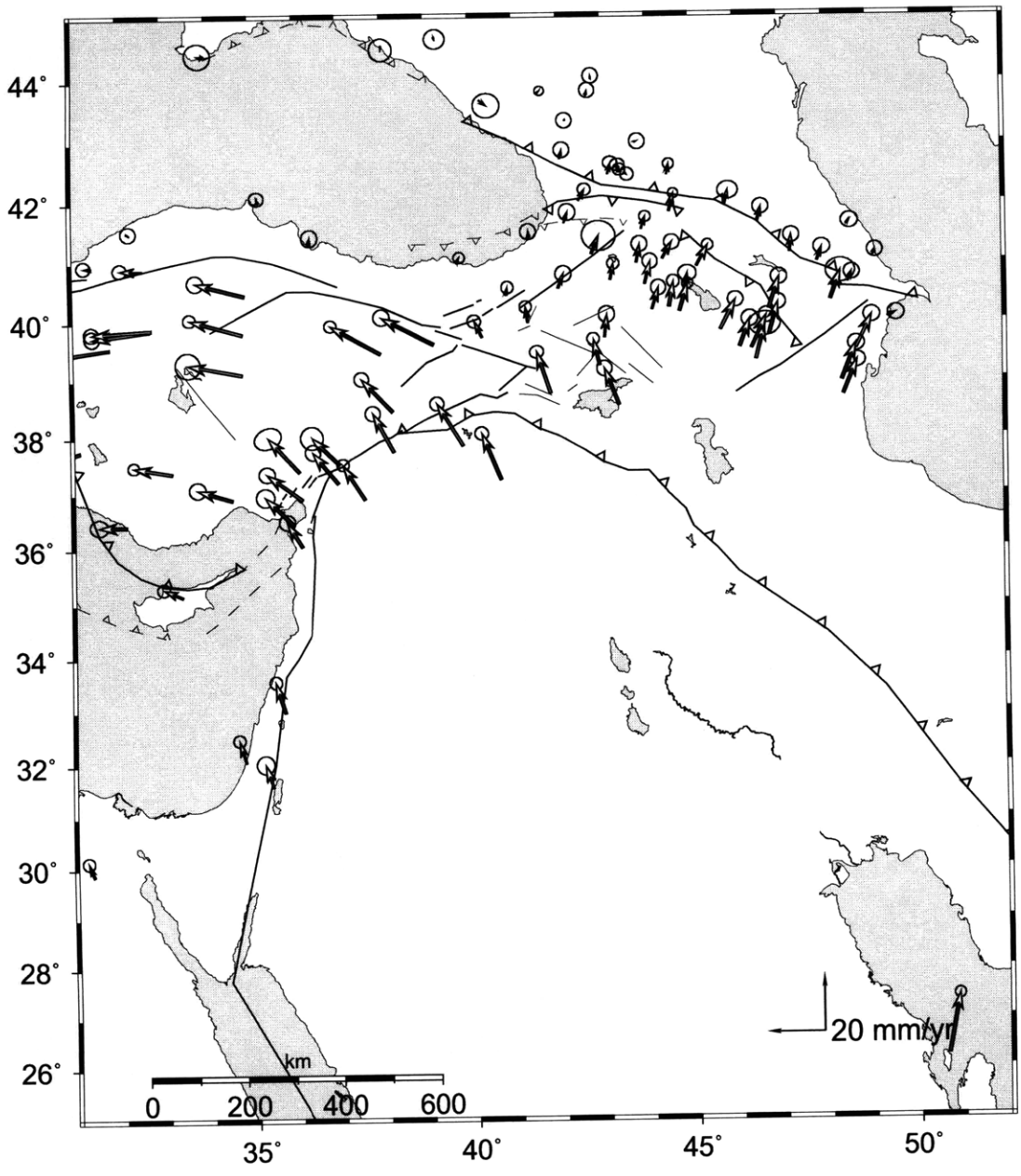

Figure 5

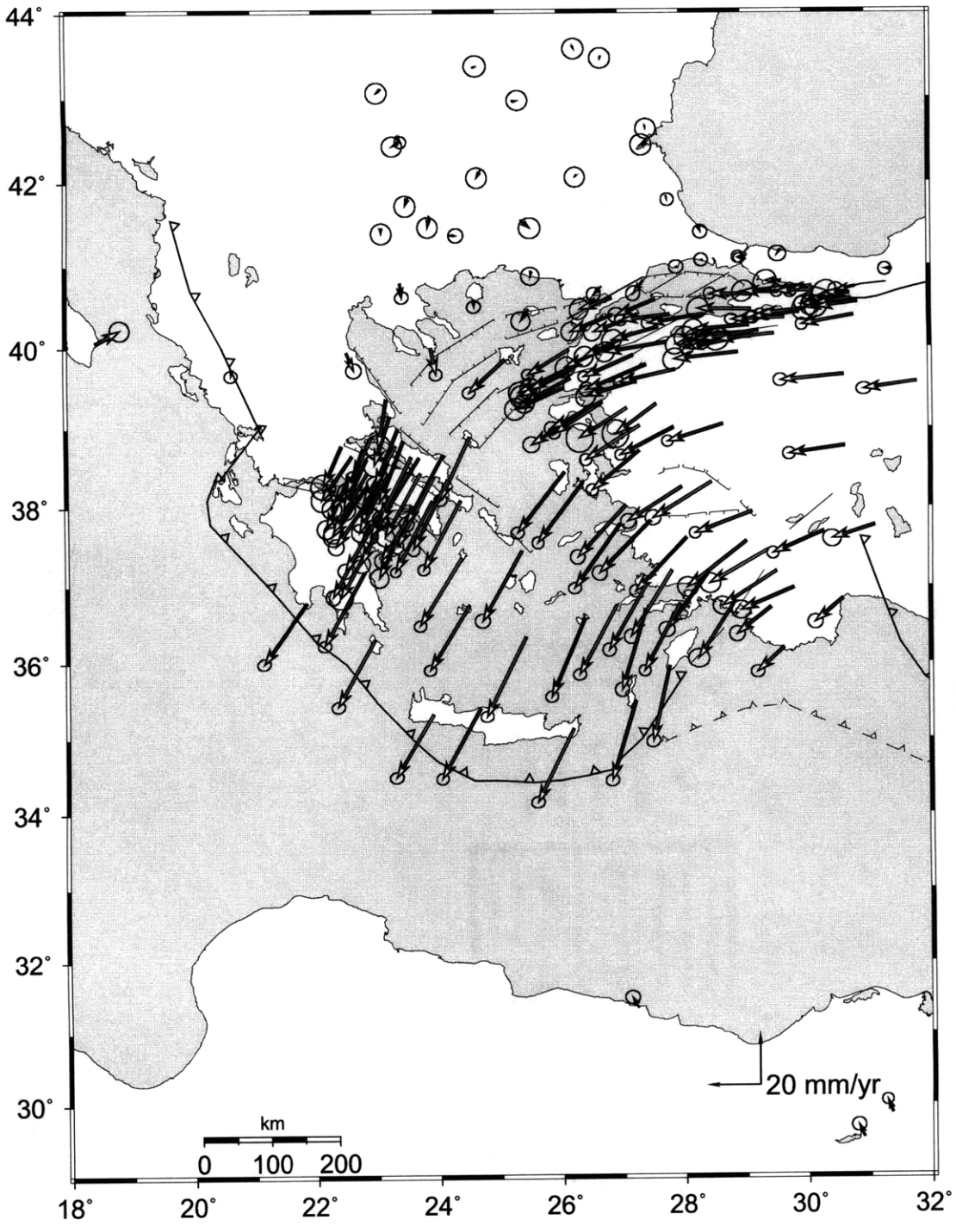

Figure 6

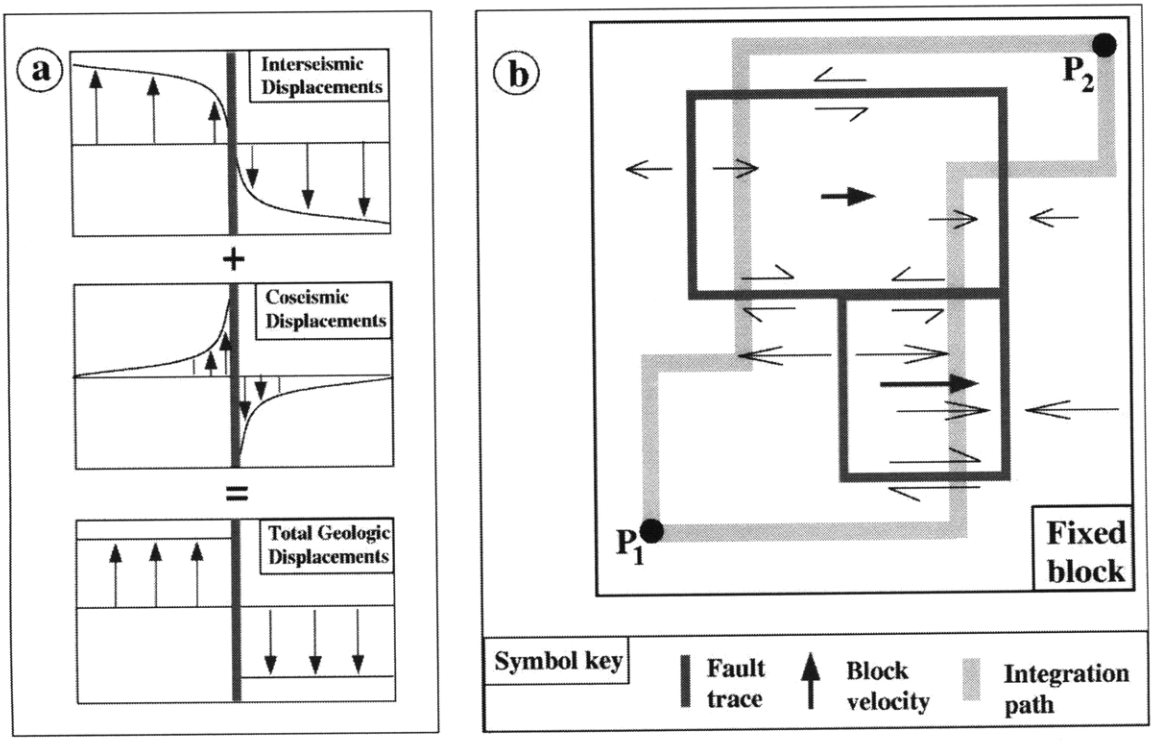
a
Interseismic Displacements
+
Coseismic Displacements
=
Total Geologic Displacements
b
P2
P1
Fixed block
Symbol key
Fault trace
Block velocity
Integration path

Figure 7

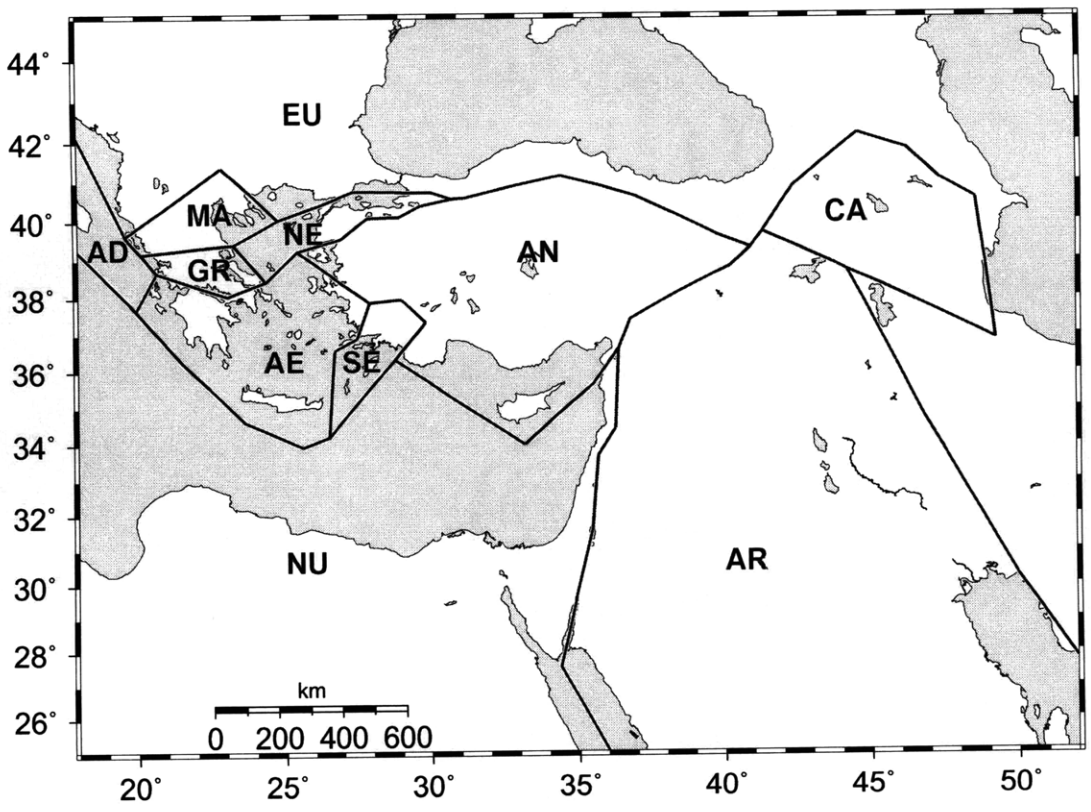
EU
MA
NE
AD
GR
AN
CA
AE
SE
NU
AR
km
0 200 400 600
44°
42°
40°
38°
36°
34°
32°
30°
28°
26°
20°
25°
30°
35°
40°
45°
50°

Figure 8

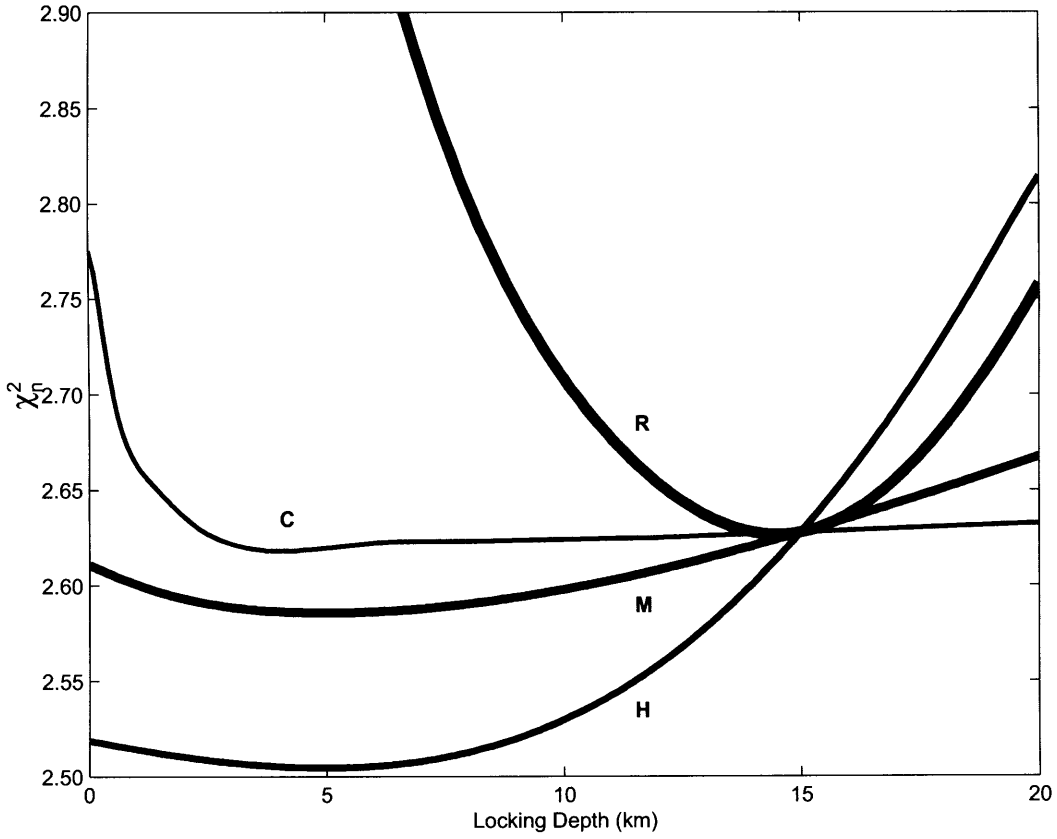
2.90
2.85
2.80
2.75
2.70
2.65
2.60
2.55
2.50
χ^2_{51}
0
5
10
15
20
Locking Depth (km)
R
C
M
H

Figure 9

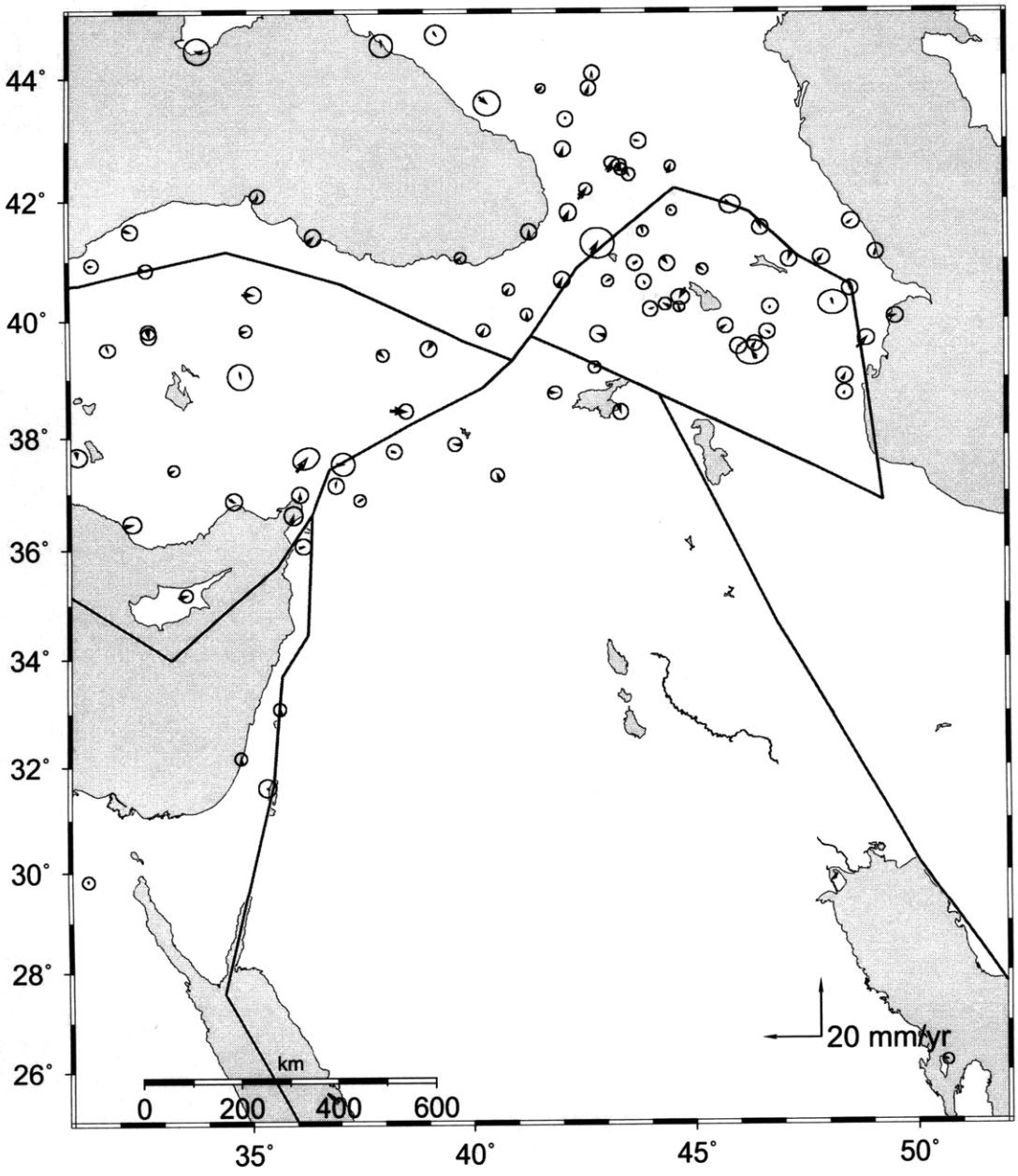

Figure 10

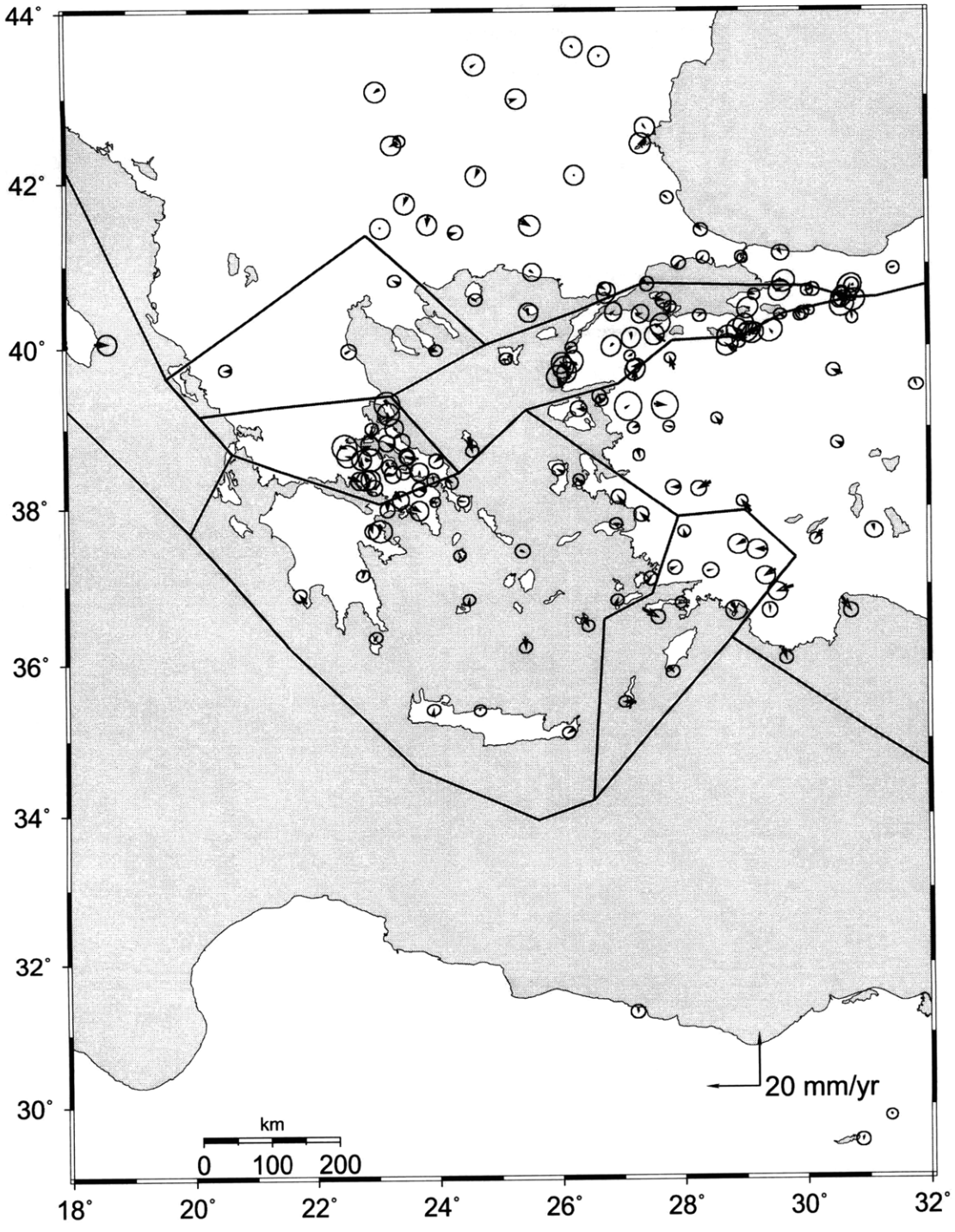

Figure 11

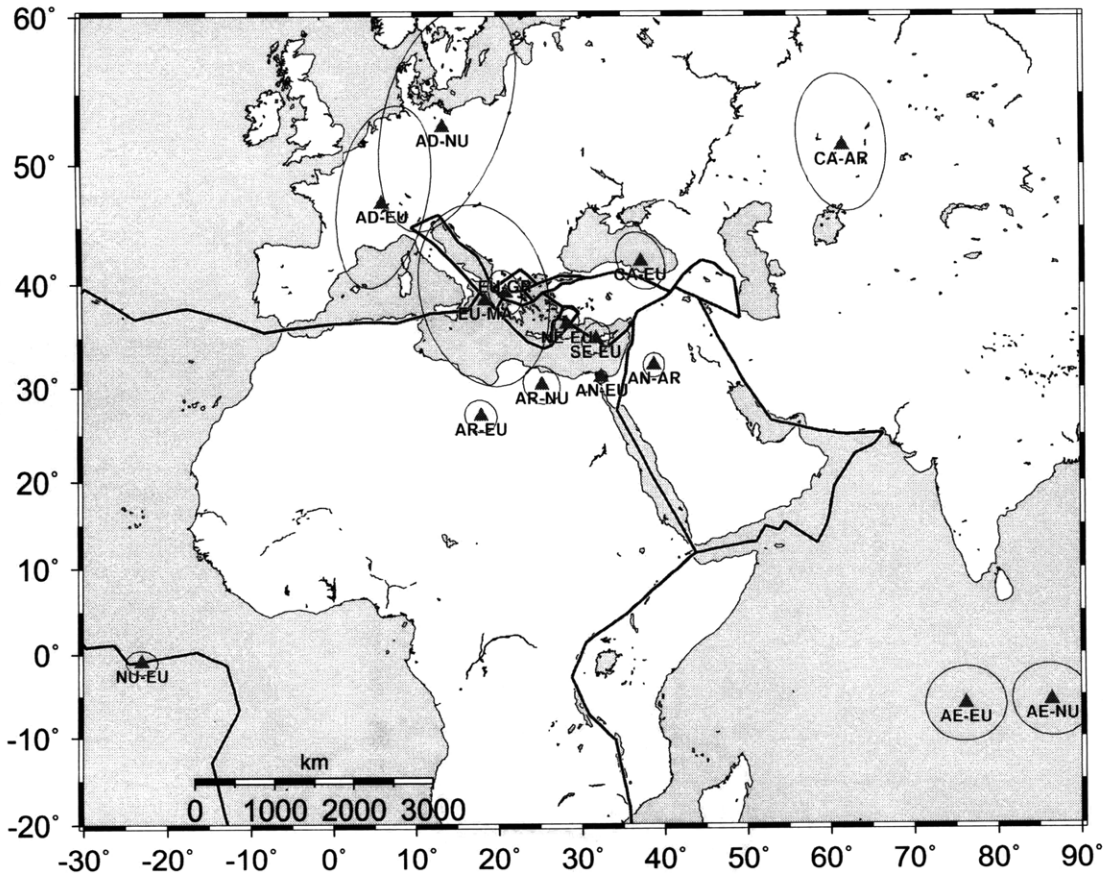
60°
50°
40°
30°
20°
10°
0°
-10°
-20°
-30°
-20°
-10°
0°
10°
20°
30°
40°
50°
60°
70°
80°
90°
AD-NU
AD-EU
CA-AR
CA-EU
EU-MI
NE-EU
SE-EU
AN-AR
AN-EU
AR-NU
AR-EU
NU-EU
AE-EU
AE-NU
km
0 1000 2000 3000

Figure 12

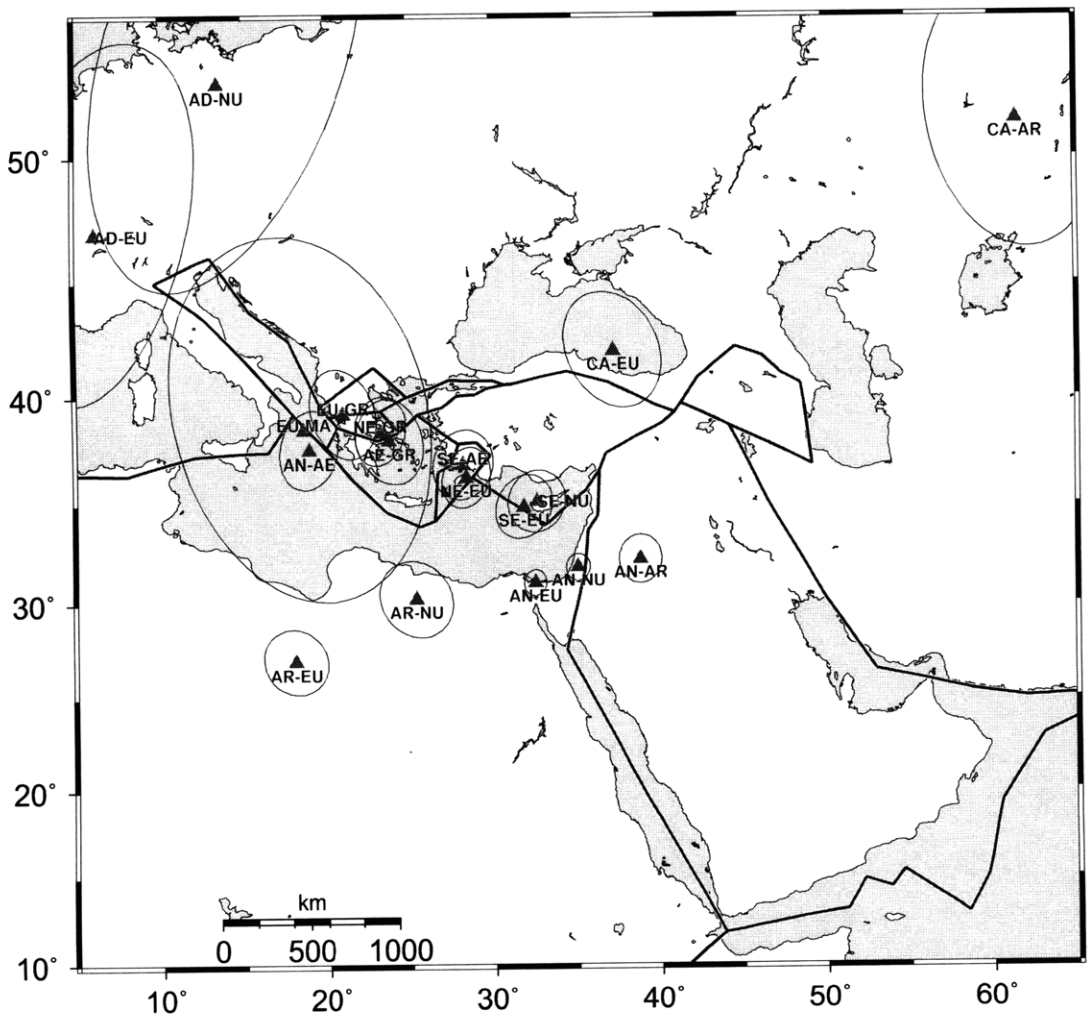
AD-NU
CA-AR
AD-EU
CA-EU
EU-GR
EU-MA
NE-OR
AN-AE
AE-GR
SE-AR
NE-EU
SE-NU
SE-EU
AN-NU
AN-AR
AN-EU
AR-NU
AR-EU
km
0 500 1000
50°
40°
30°
20°
10°
10°
20°
30°
40°
50°
60°

Figure 13

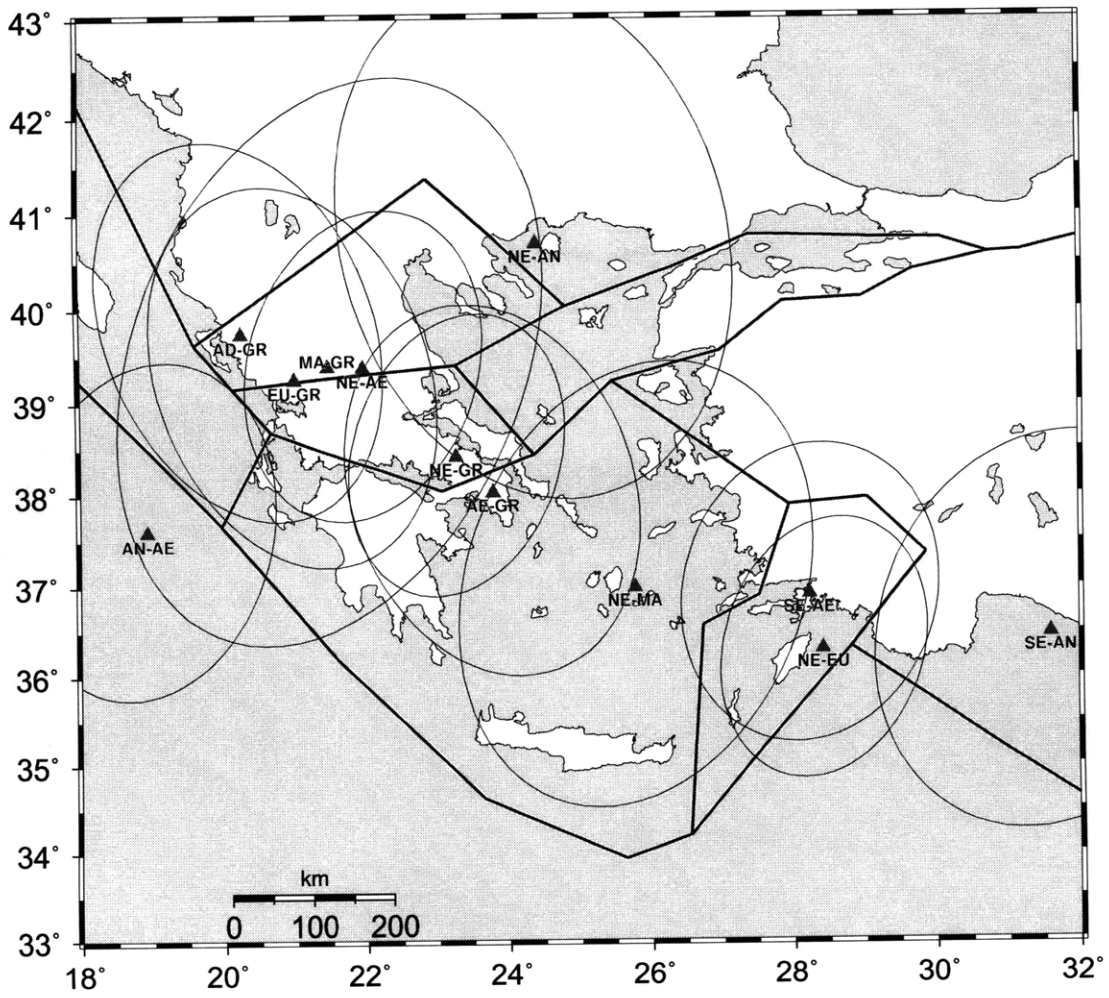
43°
42°
41°
40°
39°
38°
37°
36°
35°
34°
33°
18°
20°
22°
24°
26°
28°
30°
32°
NE-AN
AD-GR
MA-GR
NE-AE
EU-GR
NE-GR
AE-GR
AN-AE
NE-MA
SE-AE
NE-EU
SE-AN
km
0 100 200

Figure 14

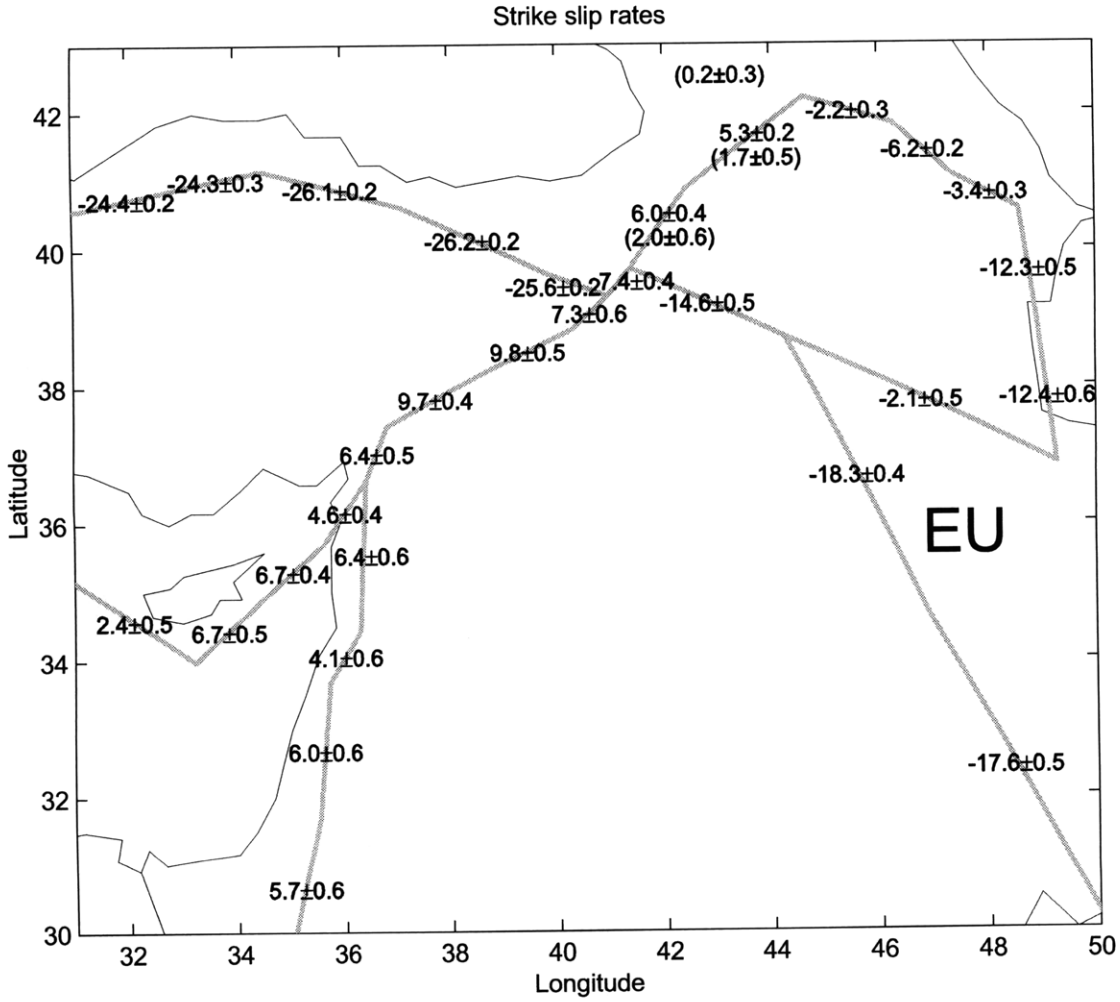
Strike slip rates
(0.2±0.3)
-2.2±0.3
5.3±0.2
(1.7±0.5)
-6.2±0.2
-3.4±0.3
-24.3±0.3
-24.4±0.2
-26.1±0.2
6.0±0.4
(2.0±0.6)
-26.2±0.2
-12.3±0.5
-25.6±0.2
7.4±0.4
-14.6±0.5
7.3±0.6
9.8±0.5
9.7±0.4
-2.1±0.5
-12.4±0.6
6.4±0.5
-18.3±0.4
EU
4.6±0.4
6.4±0.6
6.7±0.4
2.4±0.5
6.7±0.5
4.1±0.6
6.0±0.6
-17.6±0.5
5.7±0.6
Latitude
Longitude
30
32
34
36
38
40
42
44
46
48
50

Figure 15

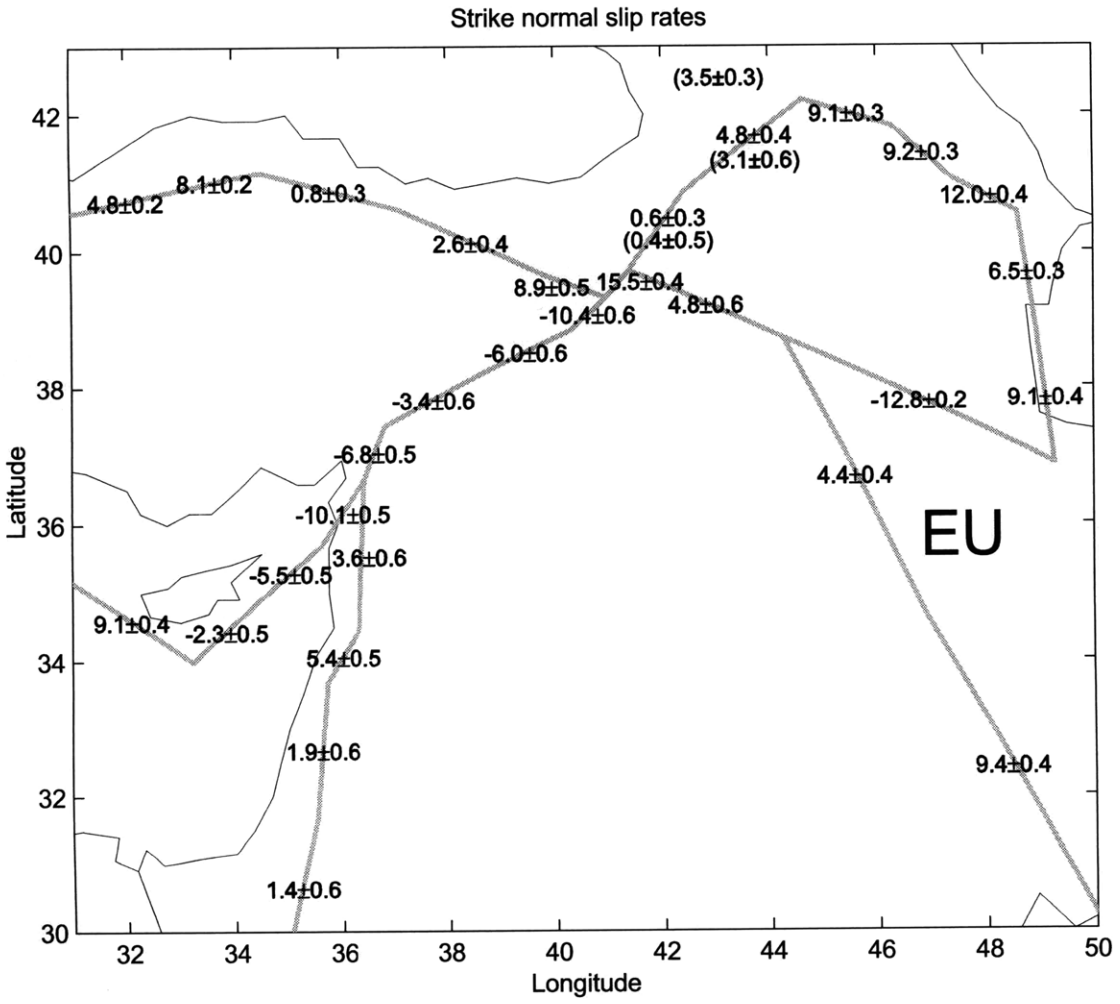
Strike normal slip rates
(3.5±0.3)
9.1±0.3
4.8±0.4
(3.1±0.6)
9.2±0.3
12.0±0.4
4.8±0.2
8.1±0.2
0.8±0.3
0.6±0.3
(0.4±0.5)
2.6±0.4
6.5±0.3
8.9±0.5
15.5±0.4
4.8±0.6
-10.4±0.6
-6.0±0.6
-3.4±0.6
-12.8±0.2
9.1±0.4
-6.8±0.5
4.4±0.4
EU
-10.1±0.5
3.6±0.6
-5.5±0.5
9.1±0.4
-2.3±0.5
5.4±0.5
1.9±0.6
9.4±0.4
1.4±0.6
Latitude
Longitude
30
32
34
36
38
40
42
44
46
48
50

Figure 16

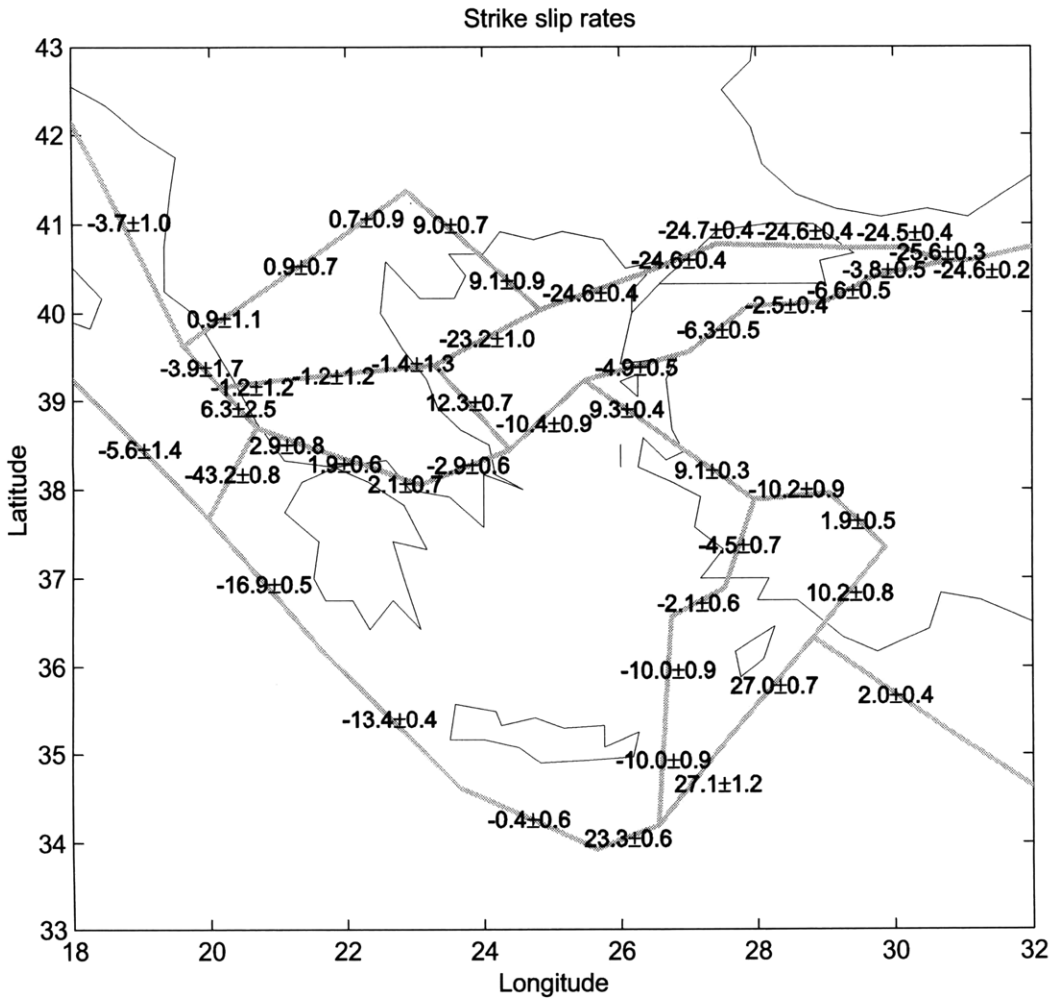
Strike slip rates
Latitude
Longitude
43
42
41
40
39
38
37
36
35
34
33
18
20
22
24
26
28
30
32
-3.7±1.0
0.7±0.9
9.0±0.7
-24.7±0.4
-24.6±0.4
-24.5±0.4
-25.6±0.3
0.9±0.7
-24.6±0.4
-3.8±0.5
-24.6±0.2
9.1±0.9
-24.6±0.4
-6.6±0.5
-2.5±0.4
0.9±1.1
-6.3±0.5
-23.2±1.0
-3.9±1.7
-1.4±1.3
-4.9±0.5
-1.2±1.2
-1.2±1.2
12.3±0.7
6.3±2.5
9.3±0.4
-10.4±0.9
-5.6±1.4
2.9±0.8
-43.2±0.8
1.9±0.6
-2.9±0.6
2.1±0.7
9.1±0.3
-10.2±0.9
1.9±0.5
-4.5±0.7
-16.9±0.5
10.2±0.8
-2.1±0.6
-10.0±0.9
27.0±0.7
2.0±0.4
-13.4±0.4
-10.0±0.9
27.1±1.2
-0.4±0.6
23.3±0.6

Figure 17

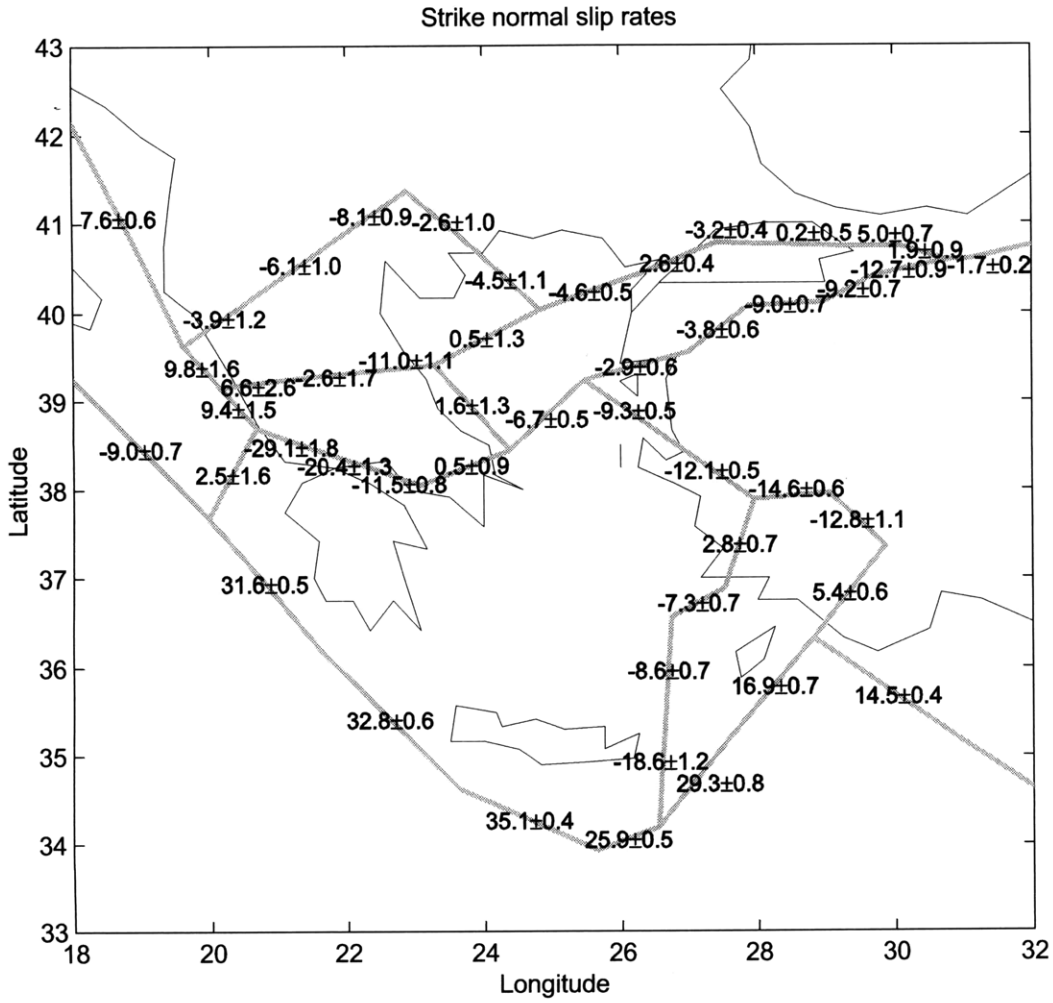
Strike normal slip rates
Latitude
Longitude
43
42
41
40
39
38
37
36
35
34
33
18
20
22
24
26
28
30
32
-7.6±0.6
-8.1±0.9
-2.6±1.0
-6.1±1.0
-4.5±1.1
-4.6±0.5
-3.2±0.4
0.2±0.5
5.0±0.7
1.9±0.9
2.6±0.4
-12.7±0.9
-1.7±0.2
-9.2±0.7
-9.0±0.7
-3.9±1.2
0.5±1.3
-3.8±0.6
9.8±1.6
-11.0±1.1
-2.9±0.6
6.6±2.6
-2.6±1.7
9.4±1.5
1.6±1.3
-6.7±0.5
-9.3±0.5
-9.0±0.7
-29.1±1.8
-20.4±1.3
0.5±0.9
2.5±1.6
-11.5±0.8
-12.1±0.5
-14.6±0.6
-12.8±1.1
2.8±0.7
31.6±0.5
-7.3±0.7
5.4±0.6
-8.6±0.7
16.9±0.7
14.5±0.4
32.8±0.6
-18.6±1.2
29.3±0.8
35.1±0.4
25.9±0.5

Figure 18